Nuclear Magnetic Resonance of Nucleic Acids In The Solid State

JOSEPH ANTHONY DIVERDI

A DISSERTATION

in

CHEMISTRY

Presented to the Graduate Faculties of the University of Pennsylvania in Partial Fulfillment of the Requirements for the Degree of Doctor of Philosophy.

1981

Supervisor of Dissertation

Committee Chairman

Reader

Graduate Group Chairman

Reader

Acknowledgements

I would like to thank all of the members of the Opella group for all of their help and support without which you would not be reading this. Also, I would like to thank Drs. David White and Neville Kallenbach for many helpful arguments.

The Chemistry Department of the University of Pennsylvania is gratefully acknowledged for generous financial support as is the Busch Foundation.

I would also like to thank Dr. Jerry Donohue for many helpful discussions and acknowledge the careful x-ray diffraction work of Dr. Pat Carroll.

Of course, no acknowledgement would be complete without reference to the thesis supervisor. I am most grateful to Dr. Stanley J. Opella for the opportunity of studying under him. The time that I have spent in his laboratory has been both enlightening and rewarding.

"...Every scientific struggle is a serious war, in which I cannot say when peace will arrive. Thus, we ought to conquer when we are able, since the advantage is always to the first comer."

Farkas Bolyai

1823

TABLE OF CONTENTS

ACKNOWLEDGEMENTS ii

LIST OF TABLES viii

LIST OF FIGURES ix

LIST OF ABBREVIATIONS xi

I. INTRODUCTION 1

II. SPECTROSCOPIC TECHNIQUES 7

II.1. Nuclear Magnetic Resonance of Solids 7

II.2. Cross Polarization 11

II.3. Proton Decoupling 14

II.4. Pulse Sequences 15

II.4.1. Short Time Behavior 15

II.4.2. Selection of Non-Protonated Resonances 20

II.4.3. Selective Averaging 22

III. ^{31}P NMR OF SOLID DNA 25

IV. DNA DYNAMICS IN SOLUTION 29

IV.1. Introduction 29

IV.2. Sample Preparation 32

IV.3. Results 33
IV.3.1. Analysis of ^{31}P NMR Line Width 33
IV.3.2. Effective Rotational Correlation time of Phosphate Motion 41
IV.3.3. Activation Energy of Phosphate Motion 42
IV.4. Discussion 45

V. DNA IN A PROKARYOTIC VIRUS 53
V.1. The fd Virus 53
V.2. Sample Preparation 56
V.3. Results and Discussion 58

VI. DNA IN EUKARYOTIC CHROMATIN 71
VI.1. Introduction 71
VI.2. Sample Preparation 73
VI.3. Results and Discussion 74

VII. DYNAMICS OF B-FORM DNA IN THE SOLID STATE 80
VII.1. Introduction 80
VII.2. Sample Preparation 82
VII.3. Results and Discussion 83

VIII. STRUCTURAL PARAMETERS FROM ^{31}P-^{31}P DIPOLAR COUPLINGS 89
VIII.1. Introduction 89

VIII.2. Sample Preparation 92
VIII.3. Results and Discussion 93
VIII.4. Application to Filamentous Viruses 95

IX. CHEMICAL SHIFT SCALING IN NMR OF ROTATING SOLIDS 101

X. ANALYSIS OF THE ^{31}P LINEWIDTH IN ROTATING SOLIDS 108

XI. ^{15}N NMR OF DNA 114
XI.1. Introduction 114
XI.2. ^{15}N Labelling of DNA 115
XI.3. Assignment of Resonances 116

XII. ^{1}H-^{15}N SEPARATED LOCAL FIELD SPECTROSCOPY OF DNA 120
XII.1. The Method 120
XII.2. Configuration of DNA 125
XII.3. Measurement of N-H Bond Lengths in DNA 126

XIII. CONCLUSION 131

APPENDIX A. CALCULATION OF ZERO ORDER AVERAGE HAMILTONIAN FOR CHAPTER IX 137

APPENDIX B. ^{31}P CHEMICAL SHIFT TENSOR IN DNA 142

APPENDIX C. PROBE RF DESIGN 151

C.1. Rationale 151
C.2. L-Match Circuitry 154
C.3. Probe Breakdonw 159
C.4. Double Resonance Tuning 162

APPENDIX D. SPECTROMETER CONSTRUCTION 165
D.1. Design Factors 165
D.2. Receivers 168
D.3. Transmitters 170
D.4. Spinners 174

APPENDIX E. CRYSTAL STRUCTURE OF $MePO_3H_2$ 177

INDEX 180

REFERENCES 183

LIST OF TABLES

VIII-1 STRUCTURAL PARAMETERS OF FILAMENTOUS VIRUSES 100

XI-1 ^{15}N DNA CHEMICAL SHIFTS 119

LIST OF FIGURES

II-1	Cross polarization schemes	12
II-2	Pulse sequences	16
III-1	^{31}P NMR of solid DNA	26
IV-1	^{31}P NMR of ds DNA is solution	37
IV-2	Field dependence of ds DNA linewidth	39
IV-3	Temperature dependence of linewidth	43
V-1	^{31}P NMR of solid fd	59
V-2	^{31}P NMR of fd solution	62
V-3	Mass of fd solution (209 mg/ml)	64
V-4	Mass of fd solution (50 mg/ml)	66
V-5	Field dependence of fd linewidth	68
V-6	T_2 measurement of fd	70
VI-1	^{31}P NMR of chromatin	75
VI-2	Mass of chromatin	77
VII-1	^{31}P NMR of B-DNA	84
VII-2	^{2}H NMR of B-DNA	86
VIII-1	M_2 of sodium pyrophosphate	94
VIII-2	M_2 of filamentous viruses	96
VIII-3	Helix parameters	97
IX-1	CS scaling factor of H_3PO_4	102
IX-2	CS scaling spectra	104
IX-3	CS scaling factor of solid $MePO_3H_2$	107
X-1	Multiple pulse experiments	109

X-2 Linewidth scaling 111
X-3 Linewidth scaling 112
XI-1 ^{15}N NMR of DNA 117
XII-1 SLF of N-acetyl-glycine 122
XII-2 Dipolar spectra of N-acetyl-glycine 124
XII-3 SLF of DNA 127
XII-4 Dipolar spectra of DNA 129
B-1 DNA fiber frame 143
B-2 Phosphate molecular frame 145
B-3 Double helix geometry 147
B-4 ^{31}P NMR of Poly A-(Poly-U)$_2$ 150
C-1 VHF inductor model 153
C-2 L-match circuitry 155
C-3 Tuning and matching example 158
C-4 L-match synthetic equations 160
C-5 Double tuning virtual grounds 163
D-1 Spectrometer block diagram 166
D-2 Transmitter switch 172
E-1 ORTEP plot of $MePO_3H_3$ 179

LIST OF ABBREVIATIONS

A	adenine
abs	absolute
ADRF	adiabatic demagnetization in the rotating frame
AQT	aquisition time
AU	duplex polymer Poly-A-Poly-U
AU_2	triplex polymer Poly-A-$(Poly-U)_2$
BDEP	barium diethyl phosphate
BP	base pair
C	Cytidine
CP	cross polarization
CS	chemical shift
CSA	chemical shift anistropy
db	decibels
Dc	calculated density
Dm	measured density
ds	double stranded
$D_{\|\|}$	rotational diffusion coefficient parallel to a unique axis
$D_{\perp}$	rotational diffusion coefficient perpendicular to a unique axis
EDTA	ethylene diamine tetraacetic acid
FID	free induction decay
G	guanine

Hz	Hertz
KA	kilo ampere
KHz	kilo Hertz
KV	kilo volt
KW	kilo watt
MASS	Magic angle sample spinning
MHz	mega Hertz
MREV-8	Mansfield, Rhim, Elleman & Vaughn 8-pulse cycle
nM	nano meter
NMR	Nuclear Magnetic Resonance
OD	optical density
ORTEP	Oak Ridge thermal ellipsoid plot
PFU	plaque forming units
PPM	parts per million
Q	quality factor
RF	radio frequency
RMS	root mean square
RPM	revolutions per minute
SF	scaling factor
SL	spin lock
SLF	separated local field
S/N	signal to noise
T	Thymine, Tesla
TRIS	tri hydroxy amino methane
VHF	very high frequency

WAHUHA Waugh, Huber, Haeberlen 4-pulse cycle

XP cross polarization

INTRODUCTION

The structural and dynamic properties of intact functional biological systems are of greater interest than those of the constituent isolated subunits. However, substantially more is known about the latter. Much of this discrepancy in knowledge is due to the difficulty of applying diffraction and spectroscopic techniques to very large and complex systems, especially those that cannot be crystallized. The work presented here is the result of the application of the principles of Solid State NMR, which are well suited to probing large complexes, to study the structure and dynamics of DNA in large native macromolecular structures. The DNA studied here is in a variety of biochemically interesting forms including an anhydrous solid, a duplex polymer, the hydrated B-form and encapsulated in both prokaryotic and eukaryotic chromatin.

The variety of structures studied enables comparisons to be made of the various structures and the dynamics of each. In each of these systems only partial information has previously been available; for example, the structure of B-DNA is considered to be well established (Watson & Crick, 1953), however, the dynamics of this

form are virtually unknown. It is clear that both structural and dynamic information are necessary to fully characterize a system since one cannot be adequately understood without the other. NMR spectroscopy has been previously applied to the study of nucleic acids (Patel, 1979a; Hogan & Jarketzky, 1979), and valuable structural and dynamic information has been obtained, however, most of these experiments have been performed on low-molecular weight DNA fragments and the small subunits of chromatin (Otter & Lilley, 1977; Kallenbach *et al.*, 1978). In these cases, there has always been the question of how to relate these results to the macromolecular structures which is seldom a straightforward exercise and subject to many pitfalls. The situation is reminicent of the NMR study of macromolecular lipid structures and model lipid vesicles. There are modes of motion present in the sonicated vesicles which do not exist in the intact liposome structures. There is need of a method for studying structure and dynamics in large intact macromolecules directly.

NMR spectroscopy of very large molecules or aggregates is difficult because of the possibility for overlap or interference among the resonances from the large number of nuclei with similar properties and also because of the restrictions on rotational diffusion that accompany large size and the presence of tertiary and quartenary structure. The absence of rapid molecular motion means that the resonances are severely broadened by static nuclear spin interactions, such as dipolar couplings, chemical shift anistropy

(CSA) or very efficient nuclear spin relaxations. The combination of many similar resonance signals and broad lines severely limits the application of the technique. Not surprisingly, the biological systems that are aggregates of small similar subunits are potentially feasible for study since the total number of different resonances is reduced partially circumventing the overlap problem. The latter problem dealing with the absence of rapid molecular reorientation and the presence of many complicating spin interactions can be overcome using the techniques of Solid State NMR (Mehring, 1976). Briefly, it is the experimenter's job to average the interactions that nature has left untouched. This is performed by the use of a diverse group of methods which all consist of modulations of the total nuclear spin Hamiltonian using either spin or spatial rotations. The choice of which method is left to the experimenter and here is where the versatility of the general method arises; by selectively averaging all but one term in the total spin Hamiltonian (Haeberlen & Waugh, 1968), that term can then be studied in such a clear and unobstructed manner that any spectroscopist would be envious.

DNA is first studied as an anhydrous solid in order to determine its static NMR properties. This is necessary to provide a basis for the understanding of motional averaging present in some of the other forms. Double stranded DNA (dsDNA) in solution is then studied with an eye towards understanding the dynamics of the polymer free in solution. High molecular weight dsDNA presents a very difficult mag-

netic resonance problem; even though it is a co-polymer of only four types of monomers, it is large in size and the motional properties in solution are inconvenient, in fact, the first investigation of dsDNA by NMR noted that for helical nucleic acids "linewidths are too great to permit detection of nuclear resonances under high resolution conditions" (McDonald *et al.*, 1964). A few more recent attempts at observing spectra from dsDNA have been published (Smith *et al.*, 1975; Hanlon *et al.*, 1976 and Rill *et al.*, 1981) but it is clear that an integration of both solid state and solution NMR techniques is essential for the study of DNA because of its intermediate motional properties.

B-form DNA has been studied extensively by fiber diffraction methods for many years and most of what we now know about its structure comes from this work (see for example, Arnott, 1970). It has always been assumed in these studies that the polymer is rigid, in fact, any motion present with a correlation time shorter than a day would be effective in affecting the diffraction results. Partial occupancies or averaged structures would be observed. Since it is believed that this form is the biologically active form it would be useful to study its dynamics on a faster time scale. A recent NMR study by Shindo (1980) indicates the presence of motion in the DNA fibers and conformational heterogeniety in the DNA backbone. The results presented here are consistent with the experimental results of Shindo but by performing additional measurements we come to dif-

ferent conclusions.

The filamentous viruses fd and Pf1 are examples of prokaryotic DNA-protein complexes. Their extreme structural simplicity is particularly intriguing (fd consists of 88% a single type of protein and 10% a single covalently closed single strand of DNA) (Newman *et al.*, 1977; Beck *et al.*, 1978) since simple design principles would be expected for their construction; yet there are significant problems outstanding in the description of these particles especially with regard to how the DNA is packed in the coat protein shell. Previous work has had to rely almost entirely on physiochemical characterizations (Day & Wiseman, 1979; Day *et al.*, 1979). While others have used x-ray fiber diffraction to describe the coat protein structure, however, the protein signals have obscured the DNA (Marvin *et al.*, 1974). These two viruses provide for interesting comparisons because of their similarities. Each virus contains approximately the same amount of nucleic acid and the overall particle diameters are comparable, however, Pf1 is twice as long as fd and there is evidence that in both cases the DNA occupies the entire length of the viron (Makowski and Caspar, 1978). Comparative studies of their DNA offer some advantages for interpretation and understanding the possibilities for packing arrangements of DNA-protein complexes (Day and Wiseman, 1979 and Day *et al.*, 1979).

DNA complexed with histones in soluble chromatin (Finch and King, 1976) and with protamines in bull sperm heads (Coelingh *et al.*, 1968; 1972) are condensed forms of DNA in eukaryotes. These two

complexes represent several levels of compaction of the linear polymer into native biological suprastructures. Little is known about the conformation adopted by the DNA in chromatin. The stoichiometry of the major components has been established as having the overall dimensions (Kornberg, 1977). More interesting, however, are the dynamics of the DNA in this form since extremely little is known about how it functions in cells while condensed.

Since the details of each system studied here vary enormously including the type of information attainable and the exact solid state method that is used to aquire it, detailed descriptions will be left to the individual chapters.

II. SPECTROSCOPIC TECHNIQUES

II.1. Nuclear Magnetic Resonances of Solids

There is a great distinction in both the experimental practices and results between NMR of liquids and solids. It is the presence or absence of rapid atomic and molecular motions which distinguishes the realms of liquid and solid state NMR. The rapid reorientations and translations of molecules executing Brownian diffusion in the liquid (or for that matter gaseous) state have profound effects upon NMR spectra. For example, the chemical shift is commonly thought of as a scalar quantity and the image of an NMR spectrum consisting of broadened delta functions occurring at what is called the "chemical shift" is not unusual. Even the basis for the discrimination of various chemical sites is well known as the electronic "chemical shielding" of the nucleus from the static bulk magnetic field and is quite interesting to chemists since this reflects electronic structure. However, for all electronic orbitals except S the electronic distribution is anisotropic and the different chemical shifts should be observed for the molecules pointed in different directions. This is true except that the reorientation and translation which is occurring on a time scale that is so fast, with respect to the anisotropic chemical shift scale, that only the

isotropic time average is indeed observed (Mehring, 1976) (This concept of a time average of a time dependent system is quite pervasive in this field of spectroscopy and will be addressed in greater detail shortly). There are other spatially anisotropic interactions including the direct dipole-dipole and quadrapole which under the same conditions of fast averaging go to zero so that they exhibit no shifting of the resonance positions (Abragam, 1961). However, there can be (and are) effects from these terms by the way of relaxation processes (Farrar and Becker, 1971). Here is another way in which molecular motion shows itself in in this spectroscopy.

The coupling between the spin system and the lattice is effected by fluctuating magnetic fields (i.e., those arising from dipolar, quadrupolar or anisotropic shielding of the bulk static field, modulated by molecular motion). For relaxation to be effective there must be sufficient spectral density present at an appropriate frequency which is determined by the details of the relaxation interaction, Larmor frequency, gyromagnetic ratio, etc. (see Abragam, 1961). In general, however, as the reorientation rate goes down the spin-lattice relaxation rate will (after rising to a global maximum) also decrease with the relaxation time getting longer. It is also generally true that while these relaxation times become long, the values for proton relaxation tend to be shorter than those of other spin $S = \frac{1}{2}$ nuclei, an important factor discussed

later.

The situation in solids, however, is not hopeless. In fact, there is considerable impetus to do the spectroscopy because there is more information to be had in the solid state. For example, the anisotropy of the chemical shift interaction can be represented by a symmetric second rank tensor (Mehring, 1976) which consists of six unique components. A measurement of these values gives six times as much data to test theoretical predictions, such as valence orbital theories. Dipolar tensors (represented similarly) can give detailed knowledge of atomic positions in solids, even that of protons which are difficult to determine by other methods (Waugh, 1976). This type of information can be used to great advantage in understanding details of hydrogen bonding.

How then can these experiments be performed? First of all, the signals must be observable and as shown in Section II.2, a method, politely called cross-polarization, exists (Pines *et al.*, 1973). It relies on the large amount of magnetization stored in the abundant proton spin bath which can be transferred to another nucleus under observation, and thus, enhance the sensitivity. The transfer is governed by a relaxation process also, and its rate is minimized by experimentally adjusting the relevant spin spectral density function to achieve close coupling of the two spin systems and efficient cross-relaxation (Hartmann and Hahn, 1962).

Once the signals are observed they must be interpreted within

the framework of the spectroscopy. Averaging of interactions is a very important facet of NMR. Interactions are averaged by (spatial and spin) rotations of the internal Hamiltonian (Haeberlen, 1976; Mehring, 1976). If these rotations are fast enough then a time average is observed and can be calculated by taking a time average of the time dependent Hamiltonian. This was first performed by van Vleck (1949) where he made the high field secular approximation of the homonuclear dipolar interaction. This methodology has reached its pinnacle in the work of Haeberlen and Waugh (1968) where they developed the mathematical methods for analyzing complex rotations and obtaining an average plus a series of correction terms of increasing order.

It should be noted most emphatically that solid state NMR does not only use as its samples frozen liquids (a comment overheard at lunch) but intact high molecular weight structures that are unobservable otherwise. And it is not the goal to simply mimic liquid spectroscopy but to derive information about the solid state and phenomena that exist only there.

The remainder of this Chapter will be devoted to a review of the magnetic resonance methods used in this thesis.

II.2. Cross Polarization

Sensitivity enhancement by cross polarization is perhaps the most significant advancement in ^{13}C Solid State NMR (Pines *et al.*, 1973). Due to the paucity of atomic motions in real solids the ^{13}C T_1's can be excruciatingly long making the cross polarization, a necessity to see any signal at all rather than a technique of signal enhancement.

The methods of cross polarization can take on a variety of forms. Sequentially one must: (1) polarize the I spins (protons), (2) hold them in some ordered state, (3) transfer order to the S spins and (4) observe the S magnetization. In organic and biological solids the most common method for I polarization is a $\pi/2$ pulse. Optical or quadrapolar dynamic polarization have not been widely utilized in these systems. There are however, several methods for generating and maintaining I spin order then transferring the order to the S spins. These are shown schematically in Figure II-1. An ordered dipolar state can be developed by means of adiabatic demagnetization in the rotating frame (ADRF) (Slichter and Holton, 1961) or by a two pulse polarization-transfer sequence developed by Jeener and Broekaert (1967). The former has the advantage of being the most efficient at generating dipolar order from Zeeman order but requires a special piece of hardware while the latter which can be performed

Figure II-1. Cross polarization schemes.

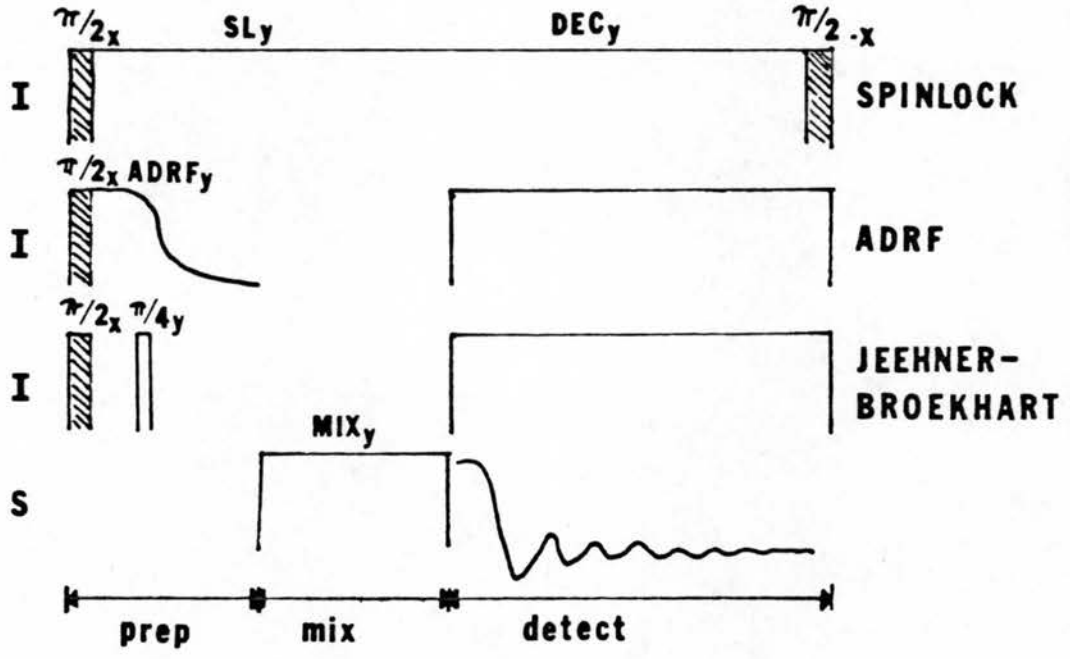

using a typical pulse programmer but is only 50% efficient. Both of these experiments, however, can not be used in the MASS regime since spinning modulates the dipolar Hamiltonian and destroys the order. It is possible to maintain an ordered state by spin locking the I magnetization in the rotating frame. If the "size" of the spin locking field is larger than the spinning frequency then no loss of order is seen due to the spinning. Spin locking fields of 50 KHz are commonly used.

Sensitivity to the Hartmann-Hahn matching condition is sometimes strongly modified by spinning (Stejskel *et al.*, 1977). Adamantane proves to be very sensitive to the match conditions and serves as a good test sample for it. Most other carbon samples are considerably less stringent in this respect as are the ^{31}P solids that have been studied here. The same is roughly true of ^{15}N solids except possibly in the case of the free amines of nucleic acids.

The rate of cross polarization (T_{IS}) also varies in these solids. The time of contact between I and S systems for proton enhancement is called the mix time and values ranging from 0.1 to 20 msec are commonly used.

II.3. Proton Decoupling

In principle a great deal of structural information is available from the proton dipolar interaction, however, in practice there is too much of a good thing. As shown by Waugh (1976), six coupled protons can yield just under 1000 different splittings. It is a much better idea to obliterate the interaction initially then admit it under well defined conditions (Chapter XII).

Proton decoupling is effected by irradiating the spin system with large amounts of radio frequency radiation (RF) at the proton Larmor frequency (Sarles and Cotts, 1958). This irradiation renders the heteronuclear dipolar Hamiltonian (H_{IS}) time dependent and if the time dependence is fast enough only the time average remains, in this case it is zero so there is no observed effect of proton dipolar fields. It may be naively thought that it is only necessary to have time modulation faster than the relevant H_{IS} for a given site, however, the communication of I spins with each other via the homonuclear Hamiltonian (H_{II}) also modulates the system causing a loss of coherence. In order for the decoupling to be effective the larger H_{II} must be averaged (Stejskal *et al.*, 1977). We find that for ^{13}C as much as 40 Gauss must be used to narrow lines completely.

II.4. Pulse Sequences

A variety of pulse sequences are now available for acquiring spectra of solid samples. Some are shown schematically in Figure II-2. These have been broken into three categories which describe their usage.

II.4.1 Short Time Behavior

Due to a fundamental theorem of Fourier Transformation, the information in a broad frequency domain spectrum lies in the short time domain (Bracewell, 1965). However, this information is often obscured in the transient ringdown of the receiver/probe combination following the transmitter pulse. With our present generation of receivers good date can be taken ≃ 30 μsec after a transmitter pulse. The experiments for acquiring broad spectra were developed using one or more of the following strategies: (1) generate an echo so that there is enough time for the ringdown to die away before the data is taken (Powles and Strange, 1963; Meibrom and Gill, 1958), (2) saturate the spins so that the decay is solely due to the ringdown and can be subtracted from the real signal and noise artifacts, and (3) alter the phase of the nuclear signal without changing the character of the ringdown so that alternately adding

Figure II-2. Pulse Sequences.

SHORT TIME BEHAVIOR

PAPEN

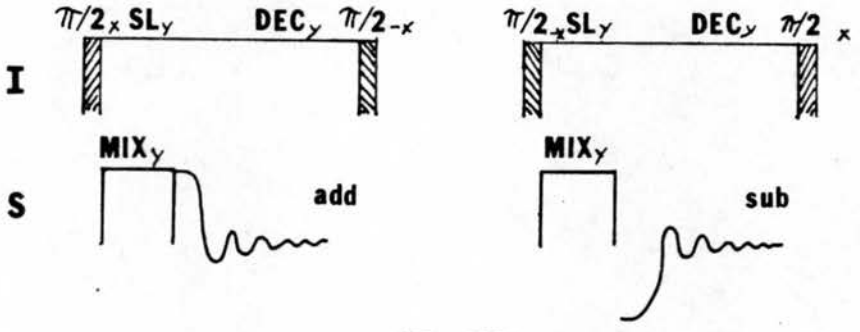

PAECHO

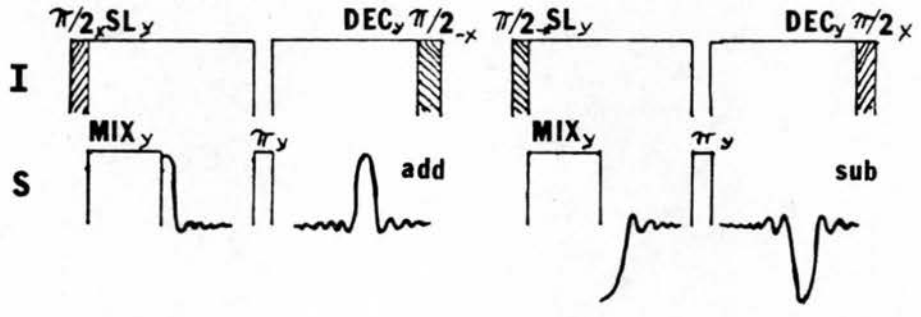

QUECHO

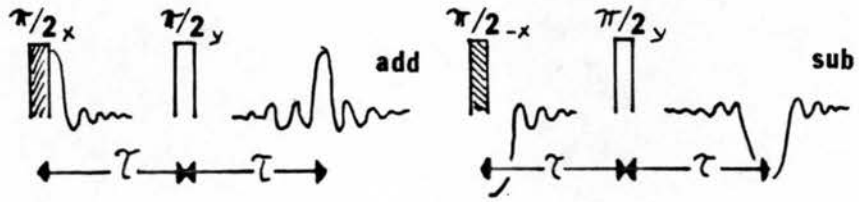

SATO

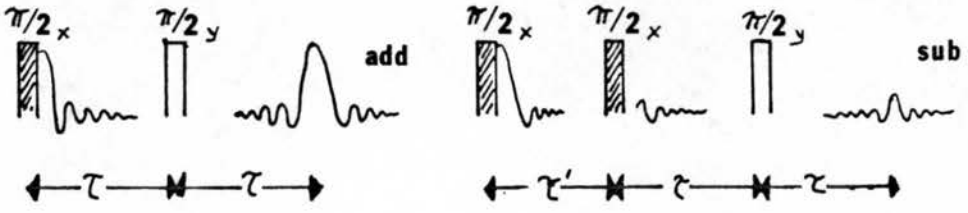

SELECTIVE AVERAGING

SELPEN

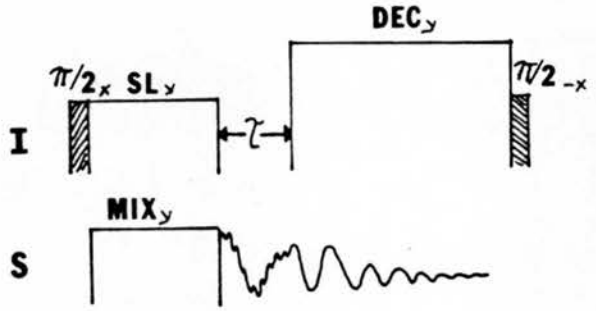

PECHO

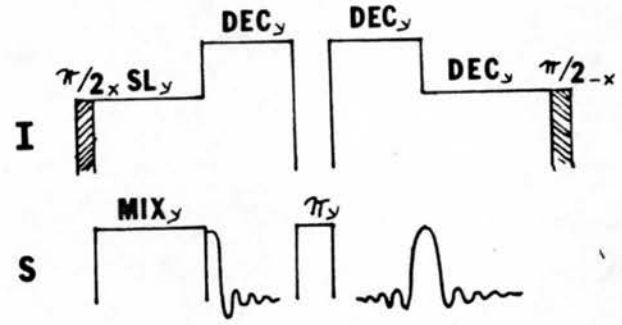

WAUGH-OSTROFF

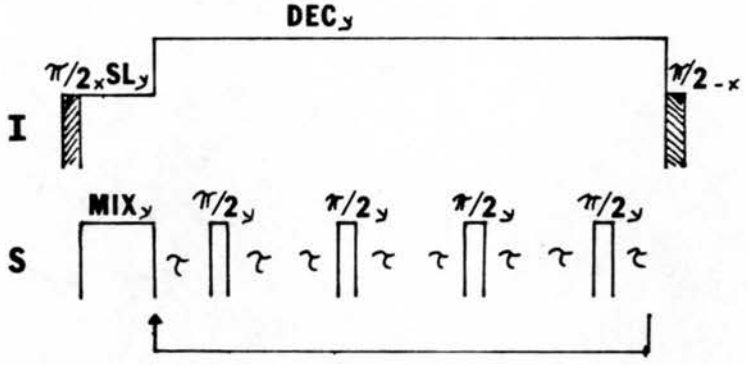

WAUGH-HUBER

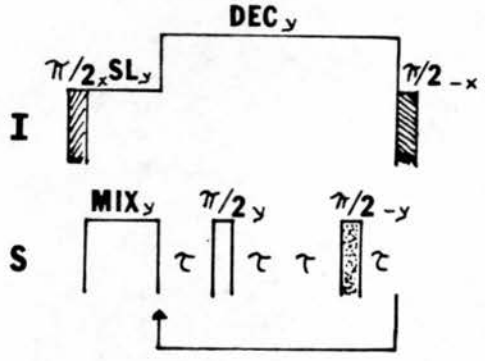

WAHUHA

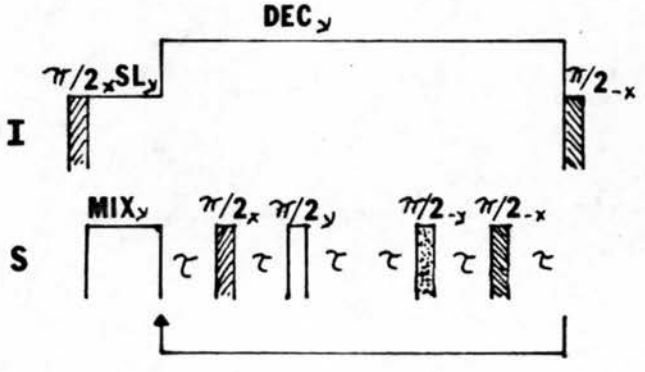

CONCERTINA

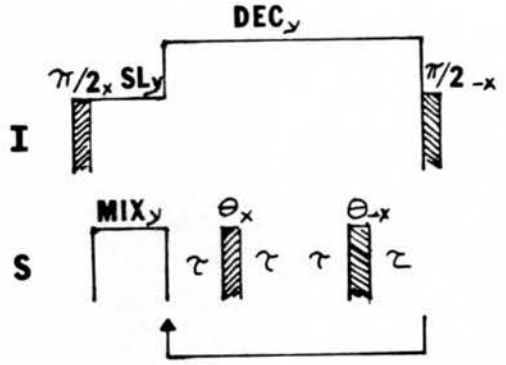

CORRECTED

CONCERTINA

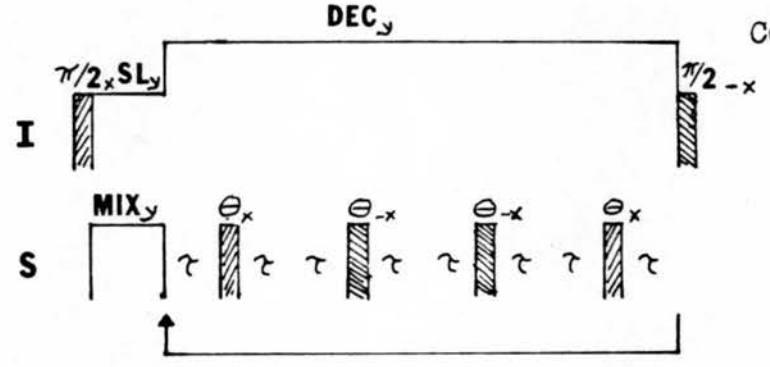

SEPARATED LOCAL FIELD SPECTROSCOPY

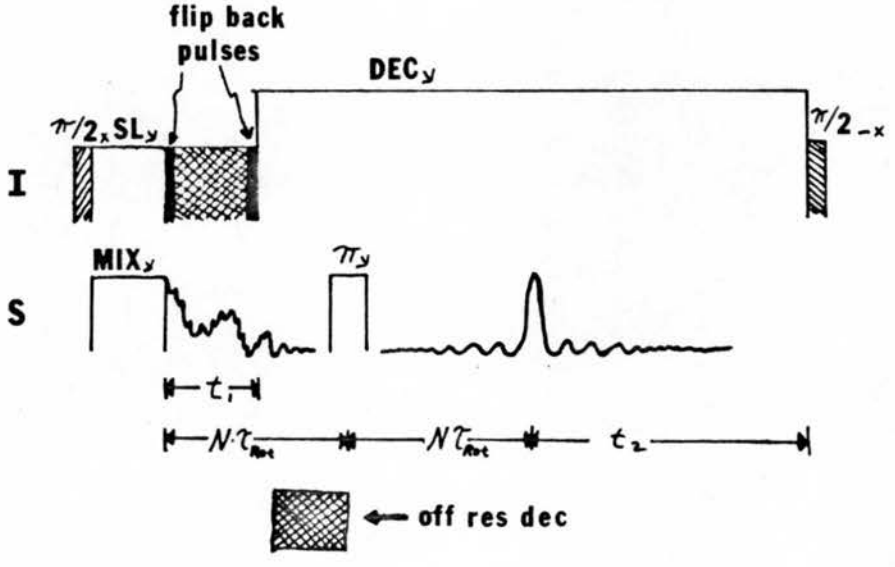

in these experiments refocuses the quadrapolar hamiltonian at twice the interpulse spacing which is usually 50 μsec. In practice, the data is acquired before the top of the echo and then subsequently left shifted in memory to the echo maximum. In some cases the supression of the background is not complete and more extreme measures are necessary. In SATO, the first echo consists of both signal and ringdown. The second echo sequence is preceded by another $\pi/2_x$ pulse and a τ' interval. The effect of this combination is to destroy the equilibrium magnetization by T_2 dephasing so that when the next pulse pair occurs it stimulates ringing but not signal. The choice of τ' is critical since it must be in the range of $T_2 << \tau' << T_1$. It is also important that the recycle delay is several T_1's long, even more so than in a simple experiment since reduction of the signal reduces the discrimination between signal and ringdown. This experiment has the disadvantage of taking twice the time for the same number of FIDS as QUECHO.

II.4.2. Selection of Non-Protonated Resonances

The experiment SELPEN was developed to aid in the assignment of spinning ^{13}C spectra (Opella and Frey, 1980). The basis of the experiment lies in the preferential destruction of carbon magnetization through coupling with directly bonded protons via the heteronuclear dipolar interaction and subsequent diffusion through the proton spin

and subtracting the data will result in cancellation of the undesireable element (Stejskal and Schaefer, 1975). The first experiment PAPEN (for Phase Alternated PENis) uses the third of these strategies. The I magnetization is alternately directly along the Y and -Y axes in the double rotating frame; this causes the polarized S spins also to be directed along the Y and -Y axes. Since the same RF is applied to the S spin system the immediate prehistory of the received is the same causing the ringdown to be identical for each free induction decay (FID) but the signal is alternately in phase and 180° out of phase. Adding and subtracting each other FID causes the signals to co-add but the ringdown to average to zero over a cycle of two. This procedure lowers the receiver deadtime to ≈ 10 usec. PAECHO is the same experiment with the addition of a Carr-Purcell-Meiboom-Gill echo (Meiboom and Gill, 1958) added and has great value in obtaining accurate powder pattern lineshapes for spin = ½ solids. It gives zero time resolution. The only restriction is that T_2 is not too short or an appreciable amount of intensity will be lost during the refocusing interval. A τ value of 10 to 100 usec is commonly used.

The experiments QUECHO and SATO (for QUadrapolar ECHO and SATuration echO) (Gall *et al.*, 1981) are used for acquisition of data from ^2H systems at 38 MHz. Since ^2H has a non-zero quadrapolar moment its spectra are very broad and zero time resolution is absolutely necessary for accurate line shape information. The $\pi/2_y$ pulse

reservoir (Waugh, 1976). This is accomplished by a slight modification of the normal cross polarization. A brief delay is inserted between the mix interval and the beginning of the acquisition, usually 40-60 usec long where the decoupler is turned off.

Molecular motion can reduce the strength of dipolar coupling; thus a rapidly rotating group could appear as if its protons were farther away as in methyl groups. In fact, it was the unusual behavior of phenylalanine towards this method that gave the first insights into its ring dynamics.

II.4.3. Selective Averaging

This category consists of pulse sequences designed to isolate a single spin interaction and facilitate its study. Experimentally, the desired interaction is made dominant by averaging all others with the appropriate manipulation. For example, PECHO isolates the ^{31}P-^{31}P dipolar interaction in rigid solids by decoupling the ^{31}P-^{1}H dipolar interaction with proton decoupling (II.2.) and a π_y refocusing pulse to cancel out the chemical shift effects. The experiment is repeated with different values of τ and the initial magnetization (at 2τ) or the integral of the frequency domain spectrum is seen to decay and reflects the strength of the ^{31}P-^{31}P couplings. This behavior is gaussian since the log of observed intensity falls off as (2τ) (Van Vleck, 1948). In these rigid solids the ^{31}P-^{31}P couplings

reflect structure.

The next several experiments have been used to probe the spin dynamics governing ^{31}P NMR in spinning solids (Chapter IX-X). In each case the ^{31}P magnetization is developed using the cross polarization technique and then manipulated to average certain of the remaining interactions. The Waugh-Ostroff (Ostroff and Waugh, 1966) method averages H_{SS} and $H_{\Delta S}$ leaving only $T_{1\rho}$ processes to account for the transverse decay. Waugh-Hubert (Waugh and Hubert, 1967), WAHUHA (Waugh *et al.*, 1968) and MREV-8 (Rhim *et al.*, 1973) all average H_{SS} to zero but only scale $H_{\Delta S}$ by varying amounts. The next two sequences Concertina and Corrected Concertina are interesting because they allow the experimenter to scale $H_{\Delta S}$ by amount desired simply by varying the length of the pulse θ. H_{SS} is uneffected by either of these experiments. The former was first described by Ellett and Waugh (1969) for use with liquids, we have developed and analyzed the latter which retains the useful features of chemical shift scaling but extends the experimentally accessable scaling range and corrects for certain spectral artifacts (see Chapter IX).

A most important feature of all of these pulsed/spinning experiments is the necessity for synchronizing the RF cycle to the spinner rotational period. This is necessary to prevent destructive interference among the spin isochromats from the compound modulation effects of the simultaneous rotation of both spin and spatial terms. The interpulse spacing is chosen to be a multiple of the the rotor

period to allow the effect of each rotation to be completed before the application of another pulse.

Lastly, the separated local field spectroscopy (SLF) (Waugh, 1976; Rybaczewski *et al.*, 1977; Hester *et al.*, 1975a, b and 1976) experiment is one of a class of two-dimensional methods that separates two different interactions into two orthogonal coordinates (For review see Freeman and Morris, 1978). This experiment retains isotropic chemical shift in one dimension and heteronuclear dipolar splitting in the other. In the T_1 interval the I irradiation is removed (or otherwise modified) and the S spins are allowed to precess under the influence of H_{IS} and $H_{\Delta S}$ then the full I irradiation (decoupling) is applied. After a short additional period, the total equal to an integral number of rotor periods a refocusing pulse is applied to the S spins and an echo is formed the same number of rotor periods later. The use of an echo prevents the generation of frequency dependent phase shifts in the chemical shift dimension (Munowitz *et al.*, 1981). The application of homonuclear decoupling to the I spins during the T_1 interval causes a dramatic improvement in the resolution in the dipolar dimension. This can either be a WAHUHA sequence (Waugh *et al.*, 1968), Lee-Goldberg (1968) type of off-resonance irradiation or any of a number of other manipulations which supress spin diffusion among the I spins (Chapter XII).

III. ^{31}P NMR OF SOLID DNA

To illustrate several of the aspects of solid state NMR the ^{31}P NMR properties of solid DNA will now be presented. The DNA used here is an example of a rigid solid meaning that there are no atomic motions of sufficient amplitude or rate which would be effective at reducing the static ^{31}P chemical shift anisotropy and/or the static ^{1}H-^{31}P dipolar interactions.

The static dipolar and CSA interactions of DNA are illustrated with ^{31}P NMR spectra of solid fibrous DNA in Figure III-1a-c. These spectra were obtained with cross polarization of the phosphorus nuclei from the protons for increased sensitivity. Figure III-1a is a broad, nearly featureless resonance that represents the natural ^{31}P line shape of solid DNA; the approximately 10 KHz linewidth is the sum of all ^{31}P-^{31}P and ^{31}P-^{1}H dipolar splittings and the ^{31}P chemical shift anisotropy. The application of strong radiofrequency irradiation at the proton resonance frequency decouples the ^{31}P-^{1}H dipolar interaction, giving the characteristic asymmetric chemical shift powder pattern of a phosphodiester, as seen in Figure III-1b.

In fact, 5.5 KHz of gaussian linebroadening is removed with proton decoupling reflecting the magnitude of the ^{1}H-^{31}P dipolar interactions. According to the definition originally developed by Van Vleck (1948) the second Moment (M_2) is related to the full width

Figure III-1. ^{31}P NMR of solid Calf Thymus DNA at 61 MHz.

A) Cross polarized.

B) Cross polarized and proton decoupled.

C) Cross polarized, proton decoupled and Magic Angle Spinning.

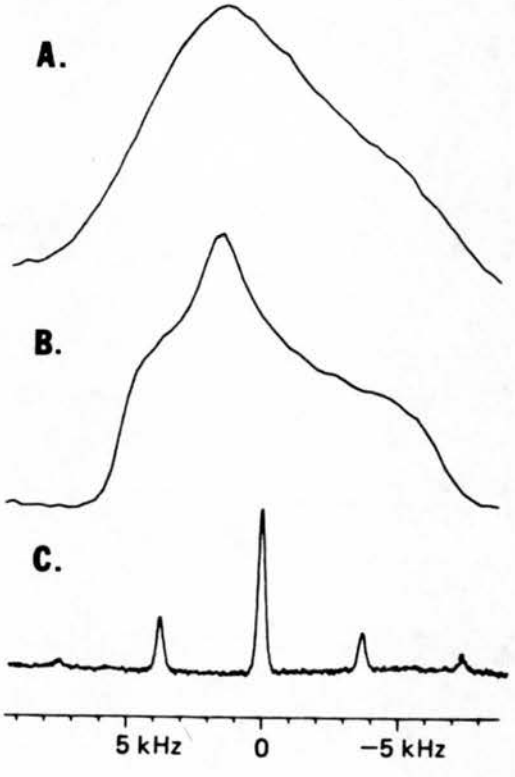

at half maximum ($\Delta\nu_{\frac{1}{2}}$) of a gaussian by the following relation:

$$\Delta\nu_{\frac{1}{2}} = 2\ 2\ell n2 \cdot M_2 \qquad \text{(III-1)}$$

The hetero-nuclear second moment (M_{2IS}) is 5.46 x 10^6 Hz^2 for rigid DNA. The magnitude of which reflects the interaction with the nearby 5' sugar protons. We shall see later how this parameter can be used to obtain structural and dynamic information. It can be seen that by selectively averaging an interaction it can be measured.

The chemical shift powder pattern is slightly rounded or broadened compared to the theoretical lineshape with abrupt discontinuities. This is due to ^{31}P-^{31}P dipolar couplings (Chapter VIII) which represents 400 Hz of gaussian line broadening (or M_{2SS} = 2.85 x 10^4 Hz^2) which is small because of the large distances between phosphate groups. In fact, analysis of X-ray fiber diffraction data shows that the nearest neighbors of any phosphate are located on the next molecule rendering the ^{31}P-^{31}P dipolar couplings inter-molecular. The principal values of the DNA phosphate chemical shielding tensor can be measured from the discontinuities of the powder spectrum of Figure III-1b as σ_{11} = 85 ppm, σ_{22} = 25 ppm, and σ_{33} = -109 ppm relative to external phosphoric acid; these values are within experimental error of those reported by Terao *et al.* (1977) and Shindo *et al.* (1980b).

Rapid rotation of a powder sample at the magic angle ($\theta = 55^o$) with respect to the applied magnetic field averages the chemical shift

anisotropy to its isotropic value ($\sigma_{iso} = 1/3(\sigma_{11} + \sigma_{22} + \sigma_{33})$) and reduces the ^{31}P-^{31}P dipolar coupling (Andrew *et al.*, 1958). The effect of this procedure on the proton-decoupled ^{31}P NMR spectrum of solid DNA is shown in Figure III-1c. A relatively sharp, single-line spectrum results with the intense center band at the isotropic chemical shift position flanked by spinning sidebands separated by the rotation frequency of 3.5 KHz. The linewidth of the central line is about 5 ppm, significantly larger than expected although it is similar to that observed for dinucleotides and other small polycrystalline molecules. Only about 0.5 ppm of the breadth would be expected to be from chemical shift dispersion among the various nucleotide neighbors (Patel, 1979a,b). A variety of NMR experiments have ruled out inadequate ^{1}H decoupling or T_2 of the phosphate group as sources of the linewidth of Figure III-1c.

IV. DNA DYNAMICS IN SOLUTION

IV.1. Introduction

While the main structural features of DNA are generally regarded as established from diffraction studies of fibers (Watson and Crick, 1953; Arnott, 1970) as well as oligonucleotide crystals (Kallenbach and Berman, 1977), much less is known about the dynamical properties of DNA. The structure of DNA as it is significantly affected by its environment of proteins, drugs, ions, etc., is not well-characterized; in these situations, more than structural details are of interest since the motions of DNA are an important influence on conformational flexibility (Crick and Klug, 1975; Sobell *et al.*, 1976). In general, the dynamics of native double-stranded DNA have not been described, although processes with rates varying over at least 10 orders of magnitude have been detected experimentally (Wahl *et al.*, 1970; Teitelbaum and Englander, 1975). Theoretical studies also suggest that a wide range of motions are present in DNA (Barkley and Zimm, 1979).

NMR spectroscopy can, in principle, provide a detailed description of the microscopic dynamics of all atoms in a molecule. However, NMR studies of DNA are problematical because of the very broad linewidths of nucleotide resonances that are a consequence of

the motions of the polymer being too slow to effectively average out static nuclear spin line-broadening mechanisms (McDonald *et al.*, 1964). Most previous NMR studies have been performed on low molecular weight or single-stranded materials because these samples have narrow resonances that can be characterized by using conventional high-resolution spectrometers (Yamane, 1971). ^{31}P NMR of nucleic acids has been successfully employed to monitor the conformation of phosphodiester groups (Gorenstein *et al.*, 1976) and their environment in oligonucleotides (Patel, 1979a; Davanloo *et al.*, 1979), polynucleotides (Akasaka, 1974; Akasaka *et al.*, 1975, 1977; Patel and Canuel, 1976), and drug-nucleic acid complexes (Patel, 1979b). Some motional information has come from ^{31}P relaxation studies of oligonucleotides and single-stranded polynucleotides (Davanloo *et al.*, 1979; Akasaka, 1974; Akasaka *et al.*, 1975).

Recently, a number of NMR studies of small fragments of double-helical DNA have been reported, generally with an analysis of DNA dynamics. The ^{31}P NMR experiments of Mariam and Wilson (1979) relied on the phosphate chemical shifts to describe the helix to coil transition. Three groups have analyzed the ^{31}P relaxation properties of double-helical DNA fragments. Both Hogan and Jardetzky (1979) and Bolton and James (1979a, 1980a,b) combine the phosphorus relaxation data with ^{1}H or ^{13}C data to derive a picture of a double helix having rapid internal motions, especially in the phosphodiester backbone. Shindo (1980) interprets his ^{31}P NMR results as showing some flexi-

bility in 140 base-pair pieces of duplex DNA. The ^{1}H NMR results of Early and Dearns (1979) and the ^{13}C NMR spectra of Rill *et al.* (1980) of similar DNA fragments are consistent with the presence of rapid segmental motions. Parallel ^{31}P NMR studies of the nucleosome core particles containing 140 base-pair segments of DNA (Cotter and Lilley, 1977; Kallenbach *et al.*, 1978; Klevan *et al.*, 1979; Shindo *et al.*, 1980) and the ^{1}H NMR study of Feigon and Kearns (1979) indicate that apparently the DNA motions are affected only slightly, if at all, by the presence of chromosomal proteins.

While there have been two reports of ^{31}P NMR spectra of high molecular weight native DNA (Hanlon *et al.*, 1976; Yamada *et al.*, 1978), a combination of high-resolution solid state and solution NMR techniques is needed to obtain reliable and interpretable data. The NMR studies described here are aimed at the problem of DNA dynamics. The spectroscopic appraoch used for duplex DNA is also suitable for characterization of DNA in supramolecular structures, such as viruses (Cross *et al.*, 1979; DiVerdi and Opella, 1981) or chromatin (Chapter VI).

IV.2. Sample Preparation

All experiments were performed on high molecular weight calf thymus DNA. The solution samples were made with DNA from Sigma Co. (Type I). The fibrous material was dissolved in a buffer of 12.5 mM Tris·HCl, 50 mM NaCl, and 1 mM EDTA at pH 7.4. The samples were dialyzed exhaustively against this same buffer. The final concentration of DNA was 20 mg mL^{-1}. Samples used in the NMR experiments were handled as gently as possible with no sonication or nuclease treatments. The DNA was found to be approximately 90 kilobases in length by 1% agarose-gel electrophoresis. The solid DNA used for Figure IV-1a-c was Sigma Type I fibrous material from the bottle.

The calf thymus DNA samples used for the solution experiments of field-strength dependence, decoupling, and temperature dependence were found to be very homogeneous material by gel electrophoresis. Some samples of DNA gave high-field NMR spectra significantly different from that of Figure IV-1d in that a very narrow resonance shifted slightly downfield from the center was superimposed on the broad resonance. It is not clear if the sharp resonance comes from single-stranded regions of DNA or from relatively low molecular weight impurities, although the sharp resonance could not be removed by dialysis. The sharp resonance can be generated by heating the DNA above the thermal transition temperature or mechanically transferring

material. This narrow resonance may have been observed by others.

These experiments were repeated using a 5KB linear plasmid kindly supplied by H. Nick (University of Pennsylvania) with identical results.

IV.3. Results

IV.3.1. Analysis of ^{31}P NMR Line Width

The conclusions about DNA dynamics from this NMR study are based on the analysis of the phosphorus resonance line width from native high molecular weight DNA; this is a straightforward exercise in spin physics. Theoretical and experimental aspects of solid state and solution NMR are required for the study of high molecular weight double-helical DNA because the polymer has dynamical characteristics between these two states. The use of ^{31}P NMR obviates any resolution or assignment problems since the phosphorus unclei are uniformly located in the phosphodiester backbone of DNA.

The first step of the line width analysis is to identify the nuclear spin interactions responsible for the substantially broader ^{31}P resonance of DNA in solution compared to that of a small molecule, such as a dinucleotide in solution. The measured parameter of the full width at half-maximum height, $\Delta\nu_{\frac{1}{2}}$, of the ^{31}P resonance as a

function of applied magnetic field strength, proton decoupling, magic angle sample spinning, and temperature can then be related to molecular properties of DNA.

The width of nuclear resonance signals arises from interactions of the nuclear spin with the applied magnetic field and nearby spins. ^{31}P has a nuclear spin of ½, therefore, dipole-dipole couplings and chemical shift anisotropy are the interactions which are most likely to affect the line width. Dipole-dipole interactions arise from the mutual magnetic coupling through space of two or more nuclei with nonzero spin. In a rigid lattice, the dipolar interactions split the energy levels, resulting in broadening due to the sum of splittings from the various distances, angles, and neighbors that are involved. The phosphorus atoms of DNA are relatively distant from other phosphate groups and protons because of the phosphodiester linkage; therefore, the broadening due to ^{31}P-^{31}P and ^{31}P-^{1}H interactions are less than those typically seen in ^{13}C or ^{1}H NMR solids. Chemical shift anisotropy (CSA) arises from the nonspherical distribution of electrons in the phosphate group screening the applied magnetic field to different extents, depending on the orientation of the group in the magnetic field. Static CSA results in a characteristic chemical shift powder pattern for the line shape of a polycrystalline sample (Mehring, 1976). Phosphodiester groups have large asymmetric chemical shift anisotropy that is emphasized by the relatively large phosphorus gyromagnetic ratio.

The line broadening from static interactions can be reduced in magnitude by motion. Rapid isotropic motion as in a liquid removes the influence of static nuclear interactions, and, to a first approximation, an infinitely sharp line results. In order to completely remove static line broadening, the effective motions must be fast compared to the strength of the interaction. Line broadening can also occur when the static broadening mechanisms are averaged by motion through nuclear spin relaxation which manifests itself in several relaxation parameters including T_2, the spin-spin or transverse relaxation time. The observed line width at half-height is described by $\Delta\nu_{\frac{1}{2}} = 1/(\pi T_2)$ when the line width is determined by relaxation. Motion has the dual function of removing static line-broadening effects and inducing fluctuations of local magnetic fields that result in relaxation broadening.

Dipolar couplings and chemical shift anisotropy can induce nuclear relaxation. Both of these interactions involve asymmetric local fields at the nuclear site, and molecular motion causes these fields to become time dependent. The relaxation parameters can be calculated by taking into account the physical basis of the interaction and the relevant spectral density functions, J_m, which describe the effectiveness of rotational reorientation rates, τ_i, for inducing relaxation. The expression for calculation of line sidth due to chemical shift anisotropy relaxation is given by equation IV-1 (Abragam, 1961; Hull and Sykes, 1975; Shindo, 1980)

$$\Delta\nu_{\frac{1}{2}} = \frac{1}{\pi T_2} = \frac{1}{40\pi}\gamma^2 B_0^{\,2}\delta z^2 \sum_{i=0}^{2} C_i\{3J_1(\omega_0) + 4J_0(0)\} \qquad \text{(IV-1)}$$

where γ is the gyromagnetic ratio, B_0 is the strength of the applied magnetic field, δ_z is the z component of the traceless chemical shift tensor, and the C_i are geometric parameters which relate the principal axes systems of the diffusion and chemical shielding tensors.

The static interactions of rigid DNA have been presented in the previous chapter.

High molecular weight DNA in solution gives the ^{31}P NMR spectra shown in Figure IV-1a-c under various experimental conditions. Figure IV-1b is the solution spectrum in a 3.5-T field with a line width of about 800 Hz at 30°C. The reduction of line width due to all nuclear spin interactions from Figure III-1a (10KHz) to Figure IV-1b (0.8 KHz) is a relection of the motional averaging that occurs in solution compared to the rigid solid. A comparison of Figure III-1b to Figure IV-1c also reflects motional averaging, but, because proton decoupling is utilized, only a single interaction, chemical shift, is influencing the spectra.

The moderate line width of the ^{31}P resonance of DNA in solution implies that no single interaction is extremely effective in inducing nuclear spin relaxation and the analysis of the line width might be complex. The solution spectra of Figure IV-1a-c illustrate some of the experiments performed to sort out the contributions to the line

IV-1. ^{31}P NMR of Calf Thymus DNA in Solution ($30^{o}C$).

A) 145 MHz.

B) 61 MHz.

C) 61 MHz, proton decoupled.

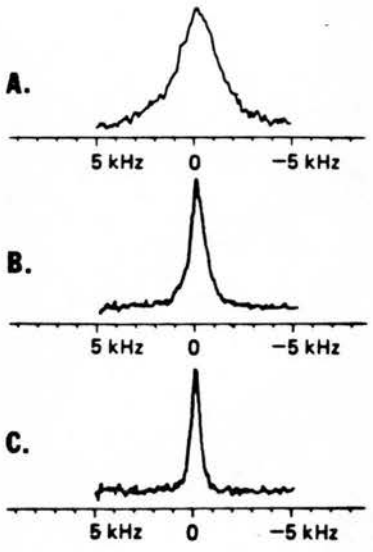

width. The ^{31}P resonance line width measured at 145 MHz (Figure IV-1a) is much larger than that measured at 61 MHz (Figure IV-1b); therefore, the line-broadening mechanism has a strong field strength dependence. The application of proton irradiation at levels suitable for decoupling ^{31}P-^{1}H dipolar interactions in solids narrows the ^{31}P line by about 400 Hz; therefore, there is some static ^{31}P-^{1}H dipolar coupling that is not removed by motion. Magic angle sample spinning has little effect on the proton-decoupled ^{31}P spectrum of DNA in solution at 61 MHz.

The effect of field strength on the line width of the DNA phosphorus resonance is shown in Figure IV-2. The line width is a linear function of the magnetic field strength squared, B_0^2. This type of dependence is completely diagnostic for CSA relaxation as a line-broadening mechanism, as can be seen from equation (IV-1). Other likely contributions to the phosphorus line width have quite different dependencies on field strength, since residual static chemical shift anisotropy or dispersion of chemical shifts have a linear dependence on B_0, dipolar relaxation does not have a strong B_0 dependence, and static dipolar couplings do not depend on B_0. If the entire line width is due to CSA relaxation, then the plot of line width vs. B_0^2 should pass through the origin of 0 Hz width at $B_0 = 0$. Instead, the intercept for no applied field is about 400 Hz; this 400 Hz of line width has to be from some spin interaction other than CSA relaxation.

Figure IV-2. Magnetic field dependence of line width at half-height for phosphorus resonance from a solution of DNA. The dashed line represents widths measured directly. The solid line was plotted after subtraction of 400 Hz of static dipolar width.

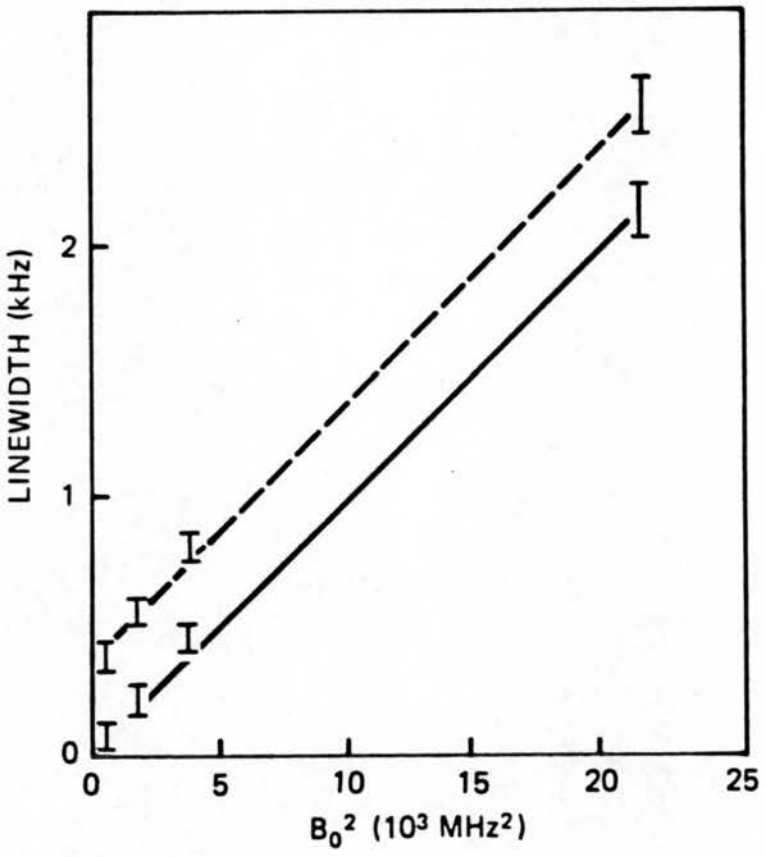

Proton decoupling significantly narrows the phosphorus resonance of DNA in solution, as can be seen in the comparison of Figure IV-1b-c. The line width at 61 MHz and 30°C goes from about 800 Hz to about 400 Hz. Proton decoupling removes the line broadening due to ^{31}P-^{1}H dipole-dipole couplings; therefore, the 400 Hz difference in line width corresponds to the strength of the dipolar interactions that are not averaged by motion. The strength of static dipolar couplings are independent of applied magnetic field; thus, the phosphorus line width of DNA in solution has a 400 Hz component from ^{31}P-^{1}H dipolar couplings at all field strengths, including zero field.

There are two spin interactions that dominate the ^{31}P resonance line width of DNA in solution, CSA relaxation and residual ^{31}P-^{1}H static dipolar couplings. The combination of magnetic field strength dependence and decoupling experiments separates these two effects. There are probably additional interactions that make small contributions to the phosphate line width that are not apparent in this analysis because of errors in measurement of line width and temperature as well as their influence being simply overwhelmed by the two large effects; the most likely candidates are dispersion of the isotropic chemical shift among the various phosphates (0.5 ppm) and heteronuclear dipolar relaxation.

The 400 Hz dipolar contribution is present in the line widths at all vaules of B_0 because of the field independence of static dipolar splittings. When the dipolar part is subtracted from the observed line

width, the solid line plot of Figure IV-2 is generated. This line has the squared-field dependence and passes through the origin at $B_0 = 0$. This line represents the CSA relaxation behavior of the phosphorus of DNA and can be used to determine the rotational correlation time of the phosphate group.

IV.3.2. Effective Rotational Correlation Time of Phosphate Motion

Rates of rotational diffusion can be determined from relaxation parameters, such as line width, when the relaxation mechanism is known. The evaluation of chemical shift anisotropy relaxation depends on knowing the appropriate chemical shielding tensor.

In principle, a thorough relaxation analysis including longitudinal and transverse relaxation processes that utilizes the (as yet undetermined) complete chemical shielding tensor from an oligonucleotide could characterize the directions and rates of phosphate motion of DNA in great detail. The more limited data set of the established principal values, σ_{ii}, of the chemical shielding tensor of DNA combined with the CSA relaxation contribution to the resonance line width can give a rotational diffusion constant for the phosphate group that is explicitly restricted to isotropic reorientation. The line width at half-height, $\Delta\nu_{\frac{1}{2}}$, can be directly calculated for a given correlation time, τ_c, by equation (IV-2).

$$\Delta\nu_{1/2} = \frac{1}{40\pi}\,\omega_0{}^2\delta_z{}^2(1 + \eta/3)\,\frac{3\tau_c}{1 + \omega_0{}^2\tau_c} + 4\tau_c \qquad \text{(IV-2)}$$

This was derived from equation (IV-1) for the case of isotropic reorientation where $J(\omega_0) = 2\tau_c/(1 + \omega_0{}^2\tau_c{}^2)$, $\Sigma C_i = 1 + \eta/3$, $\eta = (\delta_x - \delta_y)/\delta_z$, and $\delta_j = \sigma_{ii} - \sigma_{iso}$ (Abragam, 1961). At 30°C the observed line width for B_0 = 8.5 T is 2.15 KHz, of which 400 Hz is dipolar, so the relevant line width for equation (IV-1) is 1.75 KHz, which corresponds to an isotropic rotational correlation time of about 2×10^{-6} s.

IV.3.3 Activation Energy of Phosphate Motion

There is a substantial temperature dependence of the ^{31}P resonance line width of DNA as shown in Figure IV-3. The change in this parameter over a wide range of temperatures is by itself strong evidence for motion of the DNA structure at temperatures well below the thermal melting transition. The data of Figure IV-3 are for a relatively high magnetic field, so the line width is predominantly determined by the efficiency of the CSA relaxation which is directly related to the rate of phosphate reorientation. A relatively small but abrupt change in line width is seen at the melting temperature of the DNA, which emphasizes the important role of fluctuations in the helical structure relative to denaturation. Rearrangement of

Figure IV-3. Plot of ^{31}P line width versus temperature. It was obtained at 145 MHz.

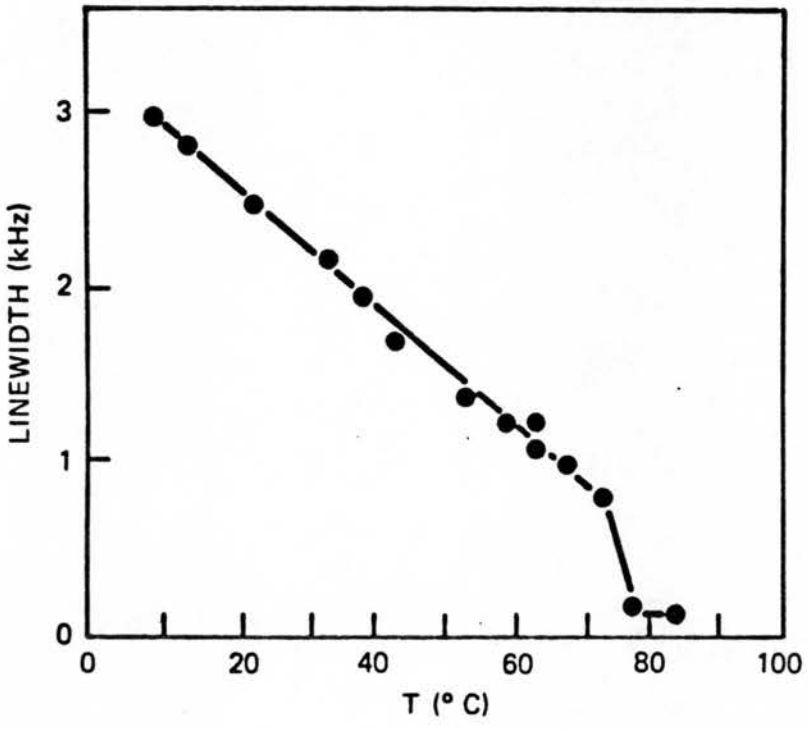

Equation (IV-2) shows that the linewidth is proportional to the correlation time except in the region where $\tau_c \approx 1/\omega_0 \approx 10^{-9}$ s. The correlation time determined at all temperatures is sufficiently far from 10^{-9} s to justify using a linear relationship between the line width and correlation time. An Arrhenius plot (not shown) of the data in Figure IV-3 exhibits a moderate curvature. This is most likely due to the simple correction used for the residual ^{31}P-^{1}H static dipolar couplings. To make this determination rigorously, the relative dipolar and CSA contributions have to be determined for the entire temperature range. There are technical difficulties in doing variable temperature work on aqueous samples when applying large decoupling fields because of dielectric heating that would make this part of the experiment unreliable with the present equipment. It is probable that at higher temperatures where phosphate motion is faster the ^{31}P-^{1}H dipolar couplings will be reduced from the 400 Hz contribution measured at 30°C, and the correspondingly smaller amount should be subtracted from the experimental line width of Figure IV-3. Although these values are not known at the present time, the activation energy for backbone motion of DNA can be determined with equation IV-3) within relatively narrow limits.

The activation energy, E_A, calculated by using equation (IV-3) and the data of Figure IV-3 is between 5 and 8 kcal/mol.

$$\tau_c = \tau_0 \exp(E_A/kT) \qquad \text{(IV-3)}$$

IV.4. Discussion

The phosphodiester linkage of DNA in solution has substantial mobility. The backbone motions of duplex DNA are the reason for the drastic reduction of the phosphate resonance line width of DNA in solution compared to the solid state. This is true when all nuclear spin interactions are taken into account as well as for just the chemical shift interaction (Figure IV-1). The primary question we want to address in the interpretation of the motional averaging of the ^{31}P resonance properties is whether the results can be explained by the relatively long-range flexibility of the polymer as expressed in the hydrodynamic persistence length or if the existence of large amplitude fast local motions is required.

The experimental results show that the motions of DNA influence the ^{31}P resonance line width through three different effects on three different time scales. The static ^{31}P chemical shift anisotropy and ^{31}P-^{1}H dipolar interactions are significantly reduced by the motions of DNA in solution. Efficient ^{31}P nuclear spin relaxation is induced by the chemical shift anisotropy due to the motion of the phosphates.

Rotational motions in solids or gels are generally restricted in amplitude, angular dispersion, or rate compared to those in liquids.

However, these motions are sufficient to reduce or average static nuclear spin interactions. A typical example is that of methyl carbon chemical shielding tensors of single crystals which are axially symmetric due to rapid rotation of the methyl group about its C_3 axis (Mehring, 1976). Substantial reductions of dipolar couplings and chemical shift anisotropy are found in liquid crystals and membranes (Urbina and Waugh, 1974). The motions of the DNA phosphates are such that the static ^{31}P-^{1}H dipolar couplings are reduced in magnitude to a fraction of their static value but are not completely eliminated. This finding is somewhat unusual but not unprecedented. This situation is found for the well-studied plastic crystal adamantane where reorientation of the molecules in the solid state is rapid enough to average out ^{13}C chemical shift anisotropy and intramolecular dipolar couplings but not intermmolecular dipolar couplings (Pines *et al.*, 1973). The extended aliphatic tail of cholesterol in model membranes behaves similarly, since the C_{26} resonance narrows with proton decoupling to a very sharp line (Opella *et al.*, 1976). Averaging of all of the CSA but not the full magnitude of the dipolar interactions has been seen for some of the amino acid side-chain carbon resonances in collagen (Jelinski and Torchia, 1980).

The motions of the DNA backbone completely average the 10^4-Hz static CSA but only partially average the 5×10^3 Hz static heteronuclear dipolar couplings of the phosphates. This discrepancy in

frequency scales is not severe and can be explained in several ways. First of all, the chemical shift powder pattern is a "tentlike" shape with abrupt discontinuities at the frequency limits of σ_{11} and σ_{33}, while the dipolar ^{31}P-^{1}H broadening has the form of a Gaussian function with some intensity significantly beyond the nominal 5×10^3 Hz at half-height of the static interaction. Therefore, much more rapid motions are required to completely remove the dipolar coupling than an equivalent chemical shift anisotropy. Exactly the same argument is used in describing the formation of spinning sidebands separate from the center band at rotation rates on the order of or less than the magnitude of the chemical shift anisotropy (Waugh *et al.*, 1978), and this is illustrated in Figure III-1c where rotation at 3.5×10^3 Hz is sufficient to narrow the 10 KHz chemical shift powder pattern to a recognizable isotropic chemical shift with small sidebands. A second reason may be that the effective motion is not isotropic and the chemical shielding tensor or dipolar coupling tensors respond differently to the rotations. Additional possibilities include the CSA reflecting only phosphate side motions, while the ^{31}P-^{1}H dipolar couplings must take into account the changes in any distances between protons and phosphorus atoms as well as angular dispersions.

The phosphate motion of DNA is characterized by the rotational correlation time of 2×10^{-6} s at 30°C derived from the chemical shift anisotropy relaxation contribution to the line width. This rotational correlation time can only be considered an order of magnitude estimate

because of the relatively large errors in measuring broad line widths and the explicit assumption used in equation (IV-2) that the motion effective in inducing relaxation is isotropic. However, all of the ^{31}P NMR results on DNA in solution are consistent with the presence of effectively isotropic phosphate motion. If rotations of the phosphate groups in one or a few directions are rapid while other motions were slow, then an axially symmetric ^{31}P chemical shift powder pattern reduced in magnitude would be observed. This is the case for the phosphodiester head groups of lipids in membranes (Griffin, 1976). There is no evidence in the line shapes of Figure IV-1, the frequency dependence of line width in Figure IV-2, or the magic angle spinning results on DNA in solution that the ^{31}P resonance has any residual powder pattern from CSA. This means motions in all directions are fast compared to 10^4 Hz. The effective rotational diffusion constant of the phosphate groups is readily derived from the calculated isotropic rotational correlation time as $\mathcal{D}_{rot} = {}^1/_{6\tau_c} = 8 \times 10^4\ s^{-1}$ at 30°C. This value is larger than the static CSA (10^4 Hz) and ^{31}P-^1H dipolar couplings (5×10^3 Hz) but not so much larger that it is unreasonable for a relatively small part of the Gaussian dipolar broadening to be unaveraged.

High molecular weight native DNA is a flexible polymer rather than a rigid rod. Hydrodynamic results show that DNA has a persistence length of about 180 base pairs that corresponds to the distance between independently oriented parts of the polymer (Bloomfield *et al.*, 1974).

This independence of phosphate groups is both spatial and angular and is a consequence of bending motions in the backbone of the polymer. Bending motions occur in all directions, giving rise to apparently isotropic motion at a given position in the chain. A correlation time for this long-range bending has been calculated to be around 10^{-7}-10^{-5} s (Bloomfield *et al.*, 1974; Barkley and Zimm, 1979; Bolton and James, 1980a,b). This general description of DNA as a flexible polymer is an excellent accord with the ^{31}P NMR results, in particular, the finding of an effectively isotropic rotational correlation times of 2×10^{-6} s at 30°C. The slow fluctuations in structure detected by hydrogen-exchange experiments or formaldehyde reactions with bases are invisible on the time scales of the ^{31}P NMR experiments (Teitelbaum and Englander, 1975; McGhee and von Hippel, 1975).

There are several sources of evidence for the existence of rapid local motions in DNA with correlation times near 10^{-9} s, which are quite distinct from those with correlation times near 10^{-6} s associated with bending as well as the very slow breathing modes of the double helix. Fluorescence studies of ethidium bromide intercalated into DNA bases indicate that fast fluctuations of the bases are occurring (Wahl *et al.*, 1970; Genest and Wahl, 1978). Robinson *et al.* (1980) have intercalated acridines with attached stable free radicals into DNA and obtained electron spin resonance spectra consistent with rapid internal motions of DNA. Both of these experiments suffer from the limitations associated with the use of probe molecules

which can have independent motions or perturb the system being monitored.

Recent high-resolution NMR studies on duplex DNA do not have to contend with probe molecules; however, they do have to use relatively low molecular weight DNA to obtain narrow lines with conventional high-resolution spectrometers. These studies strongly suggest the presence of large amplitude rapid motions in the backbone of DNA. ^{31}P NMR studies of 140 base-pair fragments of DNA obtained by nuclease digestion by Hogan and Jardetzky (1979) are interpreted in terms of internal phosphate motions with rates near 10^{-9} s while those of Shindo (1980) are interpreted as indicating some flexibility of the DNA rod through bending or twisting motions. The ^{31}P and ^{13}C NMR experiments of Bolton and James (1979, 1980a,b) on somewhat larger sized fragments of DNA formed by sonication indicate that both a long correlation time process (10^{-6} s) and short correlation time processes (10^{-9} s) are occurring in duplex DNA. ^{1}H NMR studies of Early and Kearns (1979) and the ^{13}C NMR spectra of Rill *et al.* (1980) also suggest that fragments of DNA have some rapid internal motions. This group of NMR experiments indicates that the phosphodiester linkage of DNA has motions with correlation times around 10^{-9} s.

There is about 3 orders of magnitude difference in rates of phosphate motion between our ^{31}P NMR results in high molecular weight double-helical DNA and those of the work cited above on fragments of double-helical DNA since we measure an effective rotational correla-

tion time of 10^{-6} s. The qualitative conclusions about DNA dynamics are very different since with phosphate motion on the microsecond time scale there is no need to invoke the presence of large amplitude local phosphate motions.

There are several possibilities for this discrepancy in rates of phosphate motion in DNA. First of all, the DNA samples are substantially different in length with our experiments performed on material with 9×10^4 base pairs compared to 140 base pairs for most of the other studies. Fragments of DNA may have internal modes of motion not present in high molecular weight DNA. It is not unreasonable that rotational motions are significantly damped for a group in the middle of a long polymer compared to those of a short rod, especially since a phosphate group in the middle of a 140 base-pair fragment of DNA is much less than a persistence length from either end. A second possibility concerns the fragile nature of the DNA double helix since even in the best quality high molecular weight samples of DNA rapid backbone motions can be easily induced experimentally by handling the sample. The fragments of DNA found to have rapid motions were generated by harsh nuclease or sonication procedures which may have irreversibly altered the DNA. In addition to these reasons associated with the DNA samples being of different sizes, the NMR experiments and interpretation are quite different. The rapid overall and internal motions of DNA fragments result in narrow resonances that were studied with spectrometers and relaxation

theory suitable for liquids, while the high molecular weight DNA line widths are broad from motional averaging with both solid-like and liquid-like character which required both the solid state and solution NMR experiments. Further work on well-defined high molecular weight DNA samples, such as plasmids, using solid state NMR and relaxation measurements at multiple field strengths can more completely describe DNA dynamics for the native double helix.

V. DNA IN A PROKARYOTIC VIRUS

V.1. THE FD VIRUS

fd is a filamentous virus that infects *Escherichia coli* (Marvin and Hohm, 1969). The virus is a protein-DNA complex with no associated membrane components. The particle weight is 16.4×10^6 daltons, 88% of which is from 2700 copies of the 5000-dalton major coat protein (Newman *et al.*, 1977), 10% is from the 6400 nucleotides of the circle of single-stranded DNA (Beck *et al.*, 1978), and 2% is from about 5 copies of a minor coat protein located at one end of the filament (Day and Wiseman, 1978). In solution, fd is a 900 by 9 nm rod with somewhat smaller diameter in the absence of water (Newman *et al.*, 1977; Marvin *et al.*, 1974). fd is similar to other single-stranded DNA bacteriophages, such as M13, Pf1, and Xf, in life cycle as well as structure (Marvin and Hohn, 1969).

There is a substantial amount of experimental evidence that filamentous bacteriophages have their DNA extended lengthwise within a tubular chamber made from the major coat-protein subunits (Marvin and Wachtel, 1975). Simple design principles are expected for biological supramolecular structures like viruses, yet there are significant problems outstanding in the description of filamentous viruses especially with regard to how the DNA is packed inside the coat-pro-

tein shell. X-ray diffraction data combined with molecular model building have shown that the coat-protein subunits are arranged in an overlapping helical array (Marvin *et al.*, 1974). While the details of the coat-protein helix are under active investigation (Marvin, 1978; Makowski and Caspar, 1978), there is little doubt that the protein shell of these viruses is highly symmetrical.

The difficulties with understanding the architecture of fd as a nucleoprotein complex start at the most basic level since a circle of DNA is packed in a cylinder with a length to diameter ratio of around 300:1. The X-ray diffraction results that have been interpreted to give the model for the coat-protein arrangement do not have intensity recognizable as from the DNA; therefore, there is no diffraction data on how the DNA is arranged in the virus interior or how the nucleotides interact with the amino acids of the coat-protein (Marvin *et al.*, 1974). There is no evidence of base pairing of the phage DNA (Beck *et al.*, 1978). A particularly glaring piece of data about fd is the nonintegral ratio (2.3:1) of nucleotides to coat-protein (Newman *et al.*, 1977) which is difficult to reconcile with most plausible models of symmetrical DNA-protein interactions and differs from the integral ratios found for other filamentous viruses (Day and Wiseman, 1978). There are few spectroscopic means of separating the nucleotide and aromatic amino acid chromophores, although laser Raman spectroscopy does indicate that the DNA is not in the A form (Thomas and Murphy, 1975). Day and co-workers (Day and Wiseman,

1978; Day *et al.*, 1979) have had to rely almost exclusively on physicochemical sharacterization of the virus particles to propose models for the packing of DNA in the filamentous viruses. Photochemical cross-linking experiments indicate that a small part of fd DNA exists in a hairpin structure, and this may fix the location of the DNA relative to one end of the particle (Shen *et al.*, 1979; however, this approach gives no indication of overall packing arrangements of the DNA.

There are several possible explanations for the apparent lack of symmetry between the nucleotides and coat-protein subunits of fd and the absence of diffraction intensity from DNA in oriented fibers of fd. These include the DNA having significant motional freedom within the confines of the coat-protein shell or the DNA being disordered relative to the coat-proteins without specific DNA-protein interactions. It is also possible that specific and rigid nucleotide-amino acid interactions exist but are complex, and the diffraction from the relatively large mass of highly ordered coat-proteins simply overwhelms that from the DNA with lower symmetry.

NMR spectroscopy of the filamentous viruses and their coat-proteins and DNA can contribute to a description of their structure and dynamics (Cross *et al* ., 1979; Cross and Opella, 1980a,b; Opella *et al.*, 1980b). By studying the individual protein and DNA subunits and the intact viruses, it should be possible to describe the conformational changes that occur upon assembly of the nucleoprotein struc-

ture. The only phosphorus atoms in fd are in the phosphodiester linkages of the DNA backbone; therefore, ^{31}P NMR will select for resonances only from the DNA without interference from the more abundant coat-proteins.

^{31}P NMR is a valuable technique for the study of nucleic acids. The chemical shift reflects electronic shielding and geometry of the phosphodiester groups (Gorenstein, 1975; Gorenstein and Kar, 1975), and additional structural information is available from ^{31}P-^{31}P and ^{31}P-^{1}H dipolar couplings. The rotational motion of the phosphates is reflected in the averaging of the chemical shift and dipolar interactions found in solid samples as well as nuclear spin relaxation induced by these interactions (Shindo, 1980).

Since fd is a highly organized high molecular weight particle with correspondingly slow reorientation rates in solution, solid state NMR techniques are appropriate for its study.

V.2. Sample Preparation

fd is grown on *E. coli* K3300 F^+ in a buffered super rich media of beef tryptone and yeast extract (Difco Laboratories, Detroit, Michigan). A colony of *E. coli* is grown for 14 hours in 50 ml of rich media, transferred to the preculture which is 500 ml of rich media, grown for another 8 hours, and then used to innoculate a 10 l growth.

The cells are grown under oxygenation to an optical density of 2 to 4 at 550 nm before infection with fd at a multiplicity of 10. Antifoam B is used to control excessive foaming in the culture. After 4 more hours of growth the yield of virus plateaus at 1-2 x 10^{13} plaque forming units (PFU) per milliliter.

The cells are removed from the growth medium by centrifugation. The virus is precipitated from the supernatant with polyethylene glycol (Sigma-6000; Sigma Chemical Corp., St. Louis, Missouri), resuspended in distilled water, and banded on cesium chloride (Em Laboratories, Inc., Elmsford, New York; reagent grade) block gradients. Typically, a yield of 2 g of purified virus from 1 10-1 growth is obtained as measured by PFU and optical density at 268 nm using an extinction coefficient of 3.84 mg^{-1} cm^2. The virus is stored at 4^oC in 0.02% NaN_3 water after extensive dialysis.

Single-stranded fd DNA was isolated from fd after the virus structure was disrupted with sodium dodecyl sulfate or phenol extraction. The DNA was separated from the coat proteins by chromatography on Sephacryl S-200 superfine in 10 mM sodium dodecyl sulfate, 40 mM borate, and 8% glycerol, pH 9.0, buffer.

V.3. Results and Discussion

The anisotropic character of nuclear spin interactions is manifested in the NMR spectra of rigid solids. Structural information is available without complications from motional averaging of the measured parameters. The ^{31}P spectra of solid fd in Figure V-1 were obtained with high-power proton decoupling; therefore, the spectrum of Figure V-1a contains the static chemical shift powder pattern of the fd DNA phosphates broadened slightly by about 200 Hz of ^{31}P-^{31}P dipolar couplings (Opella and DiVerdi, 1981; and Chapter VIII). The ^{31}P spectrum of solid fd in Figure V-1a is a typical asymmetric chemical shift powder pattern of a phosphodiester (Herzfield *et al.*, 1978). The principal values of the ^{31}P chemical shielding tensor can be measured directly at the spectral discontinuities as σ_{11} = 85 ppm, σ_{22} = 22 ppm, and σ_{33} = -109 ppm relative to external 85% phosphoric acid. The spectra of Figure V-1a are from a lyophilized powder of fd; however, the spectrum of Figure V-1a is indistinguishable from that obtained from a frozed solution of fd.

The spectrum of Figure V-1b was obtained from a sample of fd powder spun rapidly (4.5 KHz) at the magic angle (55°) with respect to the applied magnetic field. Proton irradiation was used to decouple the ^{31}P-^{1}H interaction so the magic angle spinning averages out only the anisotropic chemical shift and the ^{31}P-^{31}P dipolar

Figure V-1. ^{31}P NMR Spectra of Solid fd.

A) Stationary powder (10000 scans).

B) Magic angle spinning of powder at 4.5 KHz (1000 scans).

Both spectra were obtained at 61 MHz with cross polarization for 1-ms mix time, 1-s recycle delay, and 2.3-mT proton decoupling during the 20-ms data acquisition period.

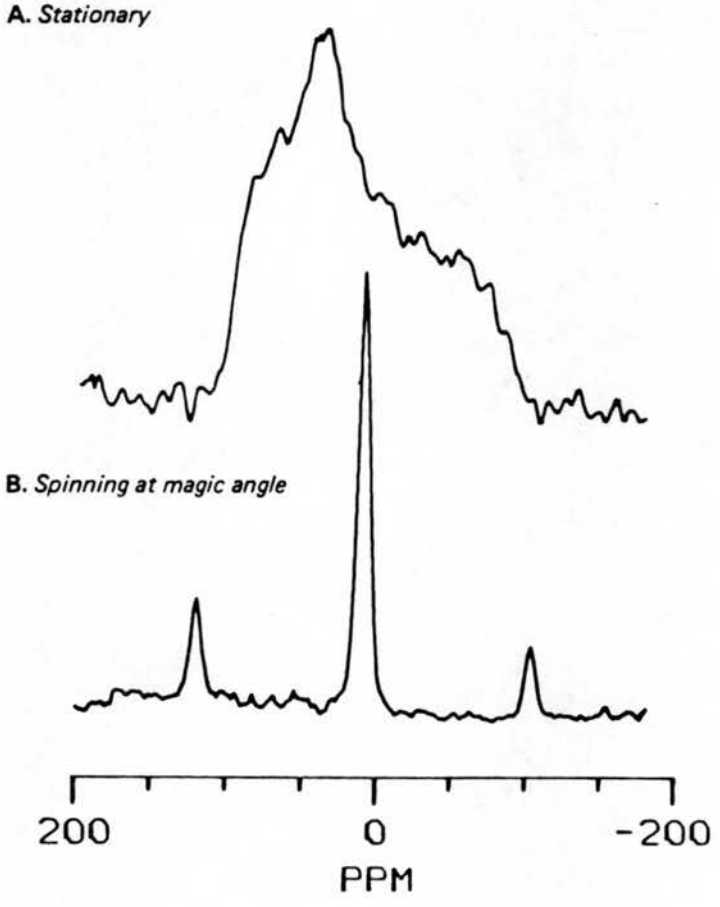

couplings to give the isotropic chemical shift spectrum of Figure V-1b. Except for the presence of spinning sidebands symmetrically located about the center at the spinning frequency, this spectrum corresponds to that which would result from a conventional high-resolution experiment on a very low molecular weight sample tumbling rapidly in solution.

Since the spectra of Figure V-1 are derived from powder averages of chemical shift properties, the angles of the molecular frame with respect to the principal axis system are not available and interpretation must rely on the magnitudes of the principal values. The magic angle spinning spectrum in Figure V-1b has a single center band, demonstrating the presence of a single type of phosphate group with an isotropic chemical shift of -0.9 ppm. This chemical shift is the same as that observed for many types of DNA in solution (Gorenstein *et al.*, 1976). A single type of phosphate contributes to the chemical shift powder pattern of Figure V-1a; therefore, the principal values of this tensor are identical within experimental error with those observed for DNA in the absence of proteins.

These chemical shift measurements on solid fd show that the phosphates are characterized by a single chemical shielding tensor with principal elements and isotropic chemical shift indistinguishable from the constituent nucleotides. The ^{31}P chemical shift of fd DNA is not affected by packaging in the virion. There is no evidence of distortion of the backbone or altered chemical structures in the viral

DNA. However, the sensitivity of ^{31}P chemical shift to phosphate conformation is not fully established. In addition, the line width of the magic angle spinning resonance of Figure V-1b is about 5 ppm. This is unfortunate since that breadth is capable of masking the presence of more subtle changes or dispersion of isotropic chemical shifts.

The presence of molecular motion has an important influence on NMR spectra. The time scale of motion that is monitored spectroscopically is a function of the nuclear spin interaction that dominates the resonance properties. With the static chemical shift parameters determined for solid fd, the influence of hydration on the ^{31}P resonance can be interpreted in terms of DNA dynamics. The ^{31}P chemical shift interaction at 61 MHz resonance frequency has a "size" of about 10^4 Hz with $\Delta\sigma = \sigma_{33} - \sigma_{11} = 194$ ppm. Motions that occur more often than about 10^4 s^{-1} will strongly influence the line shape of the chemical shift powder pattern (Mehring, 1976), with isotropic motion significantly faster than 10^4 s^{-1} averaging the powder pattern to a single line. Motions slower than about 10^{10} s^{-1} will cause efficient nuclear spin relaxation due to the fluctuating fields from the asymmetric electronic shielding.

The ^{31}P NMR spectrum of solid fd in Figure V-1a displays the full chemical shielding anisotropy of the phosphodiester group. There, no molecular motions of significant amplitude faster than about 10^4 s^{-1} are present in the phosphodiester linkages of lyophi-

Figure V-2. ^{31}P NMR Spectra of fd and fd DNA.

A) Stationary powder of fd (0% R.H., 10000 scans).

B) Stationary powder of fd (92% R.H., 10000 scans).

C) Solution of fd (50 mg/ml, 50000 scans).

D) Isolated fd DNA in solution (2000 scans).

Spectra A, B, and C were obtained with cross polarization and proton decoupling as described for Figure V-1. Spectrum resulted from pulsed free induction decays at 145 MHz by using weak (10W) proton decoupling.

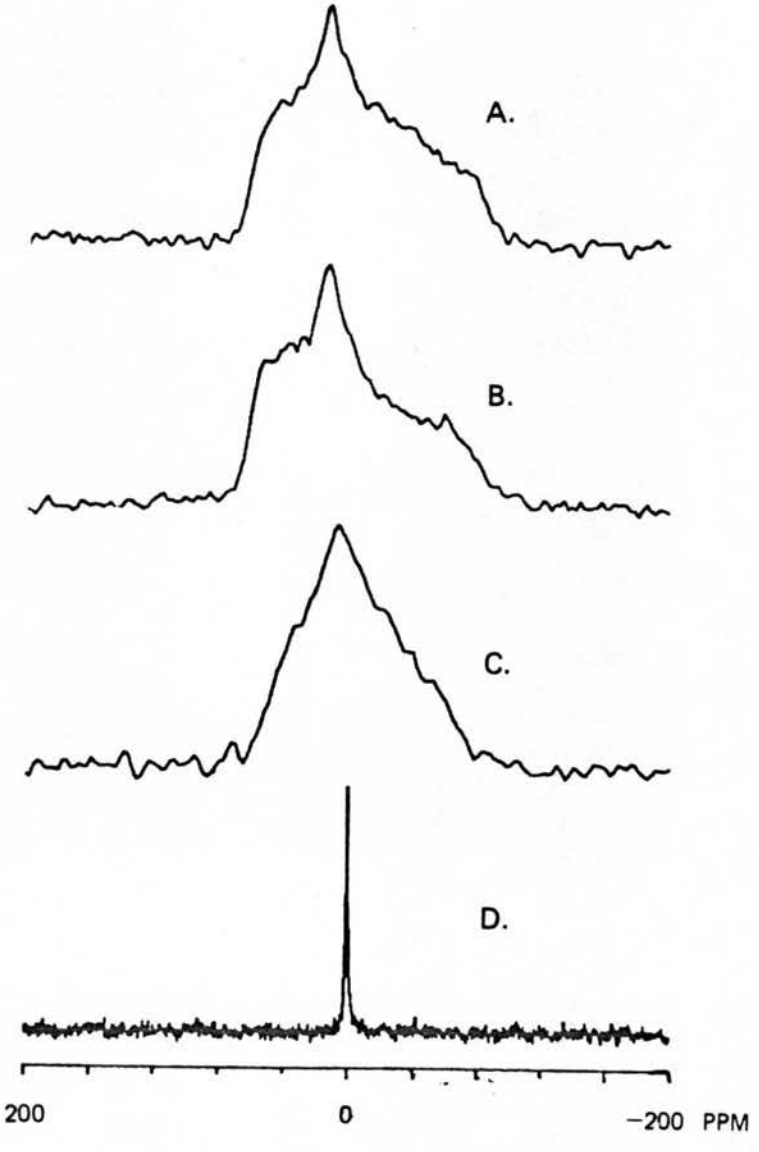

lized or frozen solutions of fd. Figure V-2 compares the proton-decoupled ^{31}P NMR spectra of fd in several situations. The chemical shift properties seen in these spectra reflect motions of DNA resulting from fd being in an aqueous environment. Figure V-2b is an asymmetric powder pattern with slightly reduced magnitudes of the principal elements of the chemical shielding tensor (σ_{11} = 78 ppm, σ_{22} = 16 ppm, σ_{33} = -96 ppm) compared to those of Figure V-2a which is from completely dehydrated sample. fd equilibrated in an atmosphere of 92% relative humidity corresponds to the hydration of the fibers used in the X-ray diffraction experiments (Marvin *et al.*, 1974). The finding of the substantial $\Delta\sigma$ of 174 ppm for the ^{31}P resonance of fd rules out molecular motion as an explanation for the lack of diffraction intensity attributable to DNA in the X-ray fiber diffraction patterns of fd fibers. The DNA is not "rattling around" inside the hollow tube of coat-proteins and does not have rapid local motions.

Figure V-2c contains the proton-decoupled ^{31}P spectrum of fd in solution while Figure V-2d has the solution spectrum of isolated single-stranded fd DNA. The chemical shift phosphorus dominates the line shape in all the spectra of Figure V-2 because of the use of proton decoupling. Single-stranded fd DNA in solution gives a ^{31}P NMR spectrum which consists of a narrow resonance near 0 ppm. The phosphodiester backbone of this DNA is undergoing very rapid rotational reorientation since the static chemical shift aniso-

Figure V-3. ^{31}P NMR Spectra of fd in Solution (200 mg/ml).

A) Stationary sample (5000 scans).

B) Magic angle sample spinning at 1.5 KHz (1000 scans).

Both spectra were obtained with cross polarization and proton decoupling as described in Figure V-1.

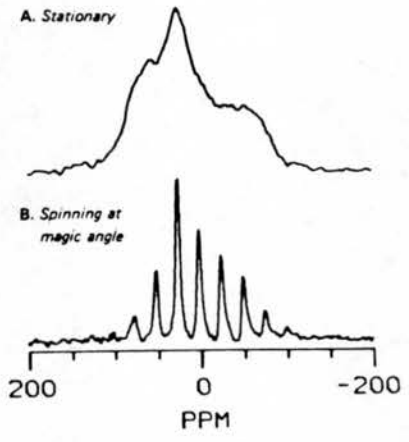

tropy is fully averaged out and the line is not broadened by very efficient relaxation processes that occur with relatively slow rates. While we have not studied the NMR properties of the isolated fd DNA in detail, the line width is similar to that found for other single-stranded polynucleotides (Akasaka *et al.*, 1977) which were found to have rotational correlation times of about 10^{-9} s for phosphate motion. The ^{31}P NMR spectrum of fd in solution is shown in Figure V-2c. The fd resonance is broad with slight asymmetry and is clearly not Lorentzian in shape. The width near the base is nearly 200 ppm while the measured width at half-height is around 110 ppm (6.5 KHz at 61 MHz). The line shape of the ^{31}P resonance of fd in solution is not altered by proton decoupling or magnetic field strength; however, samples with higher concentration of virus or at lower temperatures give spectra that appear more asymmetric with partially defined discontinuities.

The ^{31}P line width of fd in solution is due to static chemical shift anisotropy that is not averaged by motion. This is shown with several NMR experiments. The line width is insensitive to high-power proton decoupling; therefore, ^{31}P-^{1}H dipolar couplings do not significantly broaden the line. Figure V-3 and V-4 compares the ^{31}P spectra of the same sample of fd in solution for stationary and magic angle spinning experiments. When fd in solution is spun at the magic angle at a moderate rotation rate. The broad ^{31}P resonance breaks up into discrete sidebands, demonstrating that the broadening is due to

Figure V-4. ^{31}P NMR Spectra of the fd Virus in Solution (50 mg/ml).

A) Stationary spectrum (100000 scans).

B) Magic Angle sample spinning at 2.0 KHz (20000 scans).

Other conditions as in Figure V-3.

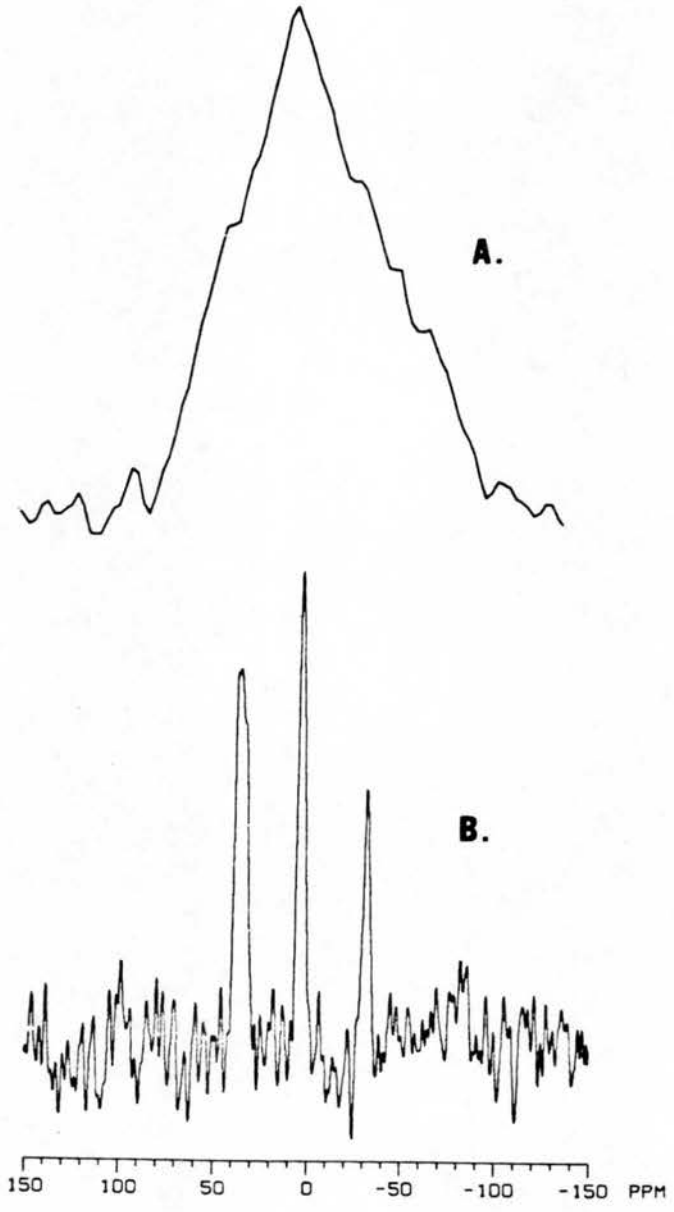

the inhomogeneous chemical shift interaction. The plot of line width of the phosphorus resonance of fd vs applied magnetic field strength in Figure V-5 shows that the line width increases linearly with field strength. This is as expected for a dispersion of isotropic chemical shifts or a chemical shift powder pattern but not chemical shift anisotropy relaxation. While there is substantial error in measuring broad line widths with poor signal to noise ratios that result from not being able to develop the ^{31}P magnetization from cross polarization at all field strengths, the line width clearly does not depend on the square of the field strength. The zero-field intercept is about 0.5 KHz, which is probably from unaveraged ^{31}P-^{1}H dipolar couplings and is sufficiently small as to not be apparent in the spectra compared to the several kilohertz broadening due to chemical shift. This conclusion is reinforced by the more asymmetric line shapes seen for samples with high virus concentration (Figure V-3a).

Corraborating evidence for this interpretation is obtained by a T_2 measurement of the ^{31}P resonance of the fd solution. The method used was that of Carr and Purcell (1954) and the data are shown in Figure V-6. The value of T_2 obtained by a least squares fit is 0.75 msec and corresponds to a Lorenzian line width of 425 Hz. This proves the inhomogeneous nature of the resonance since a T_2 of $\simeq$ 50 usec would be necessary to account for breadth of the observed spectrum.

fd in solution is well approximated as a 900 by 9 nm cylinder

Figure V-5. Line Width of ^{31}P Resonance of fd in Solution (50 mg/ml) as a Function of Field Strength. The spectra for this plot were obtained without proton decoupling.

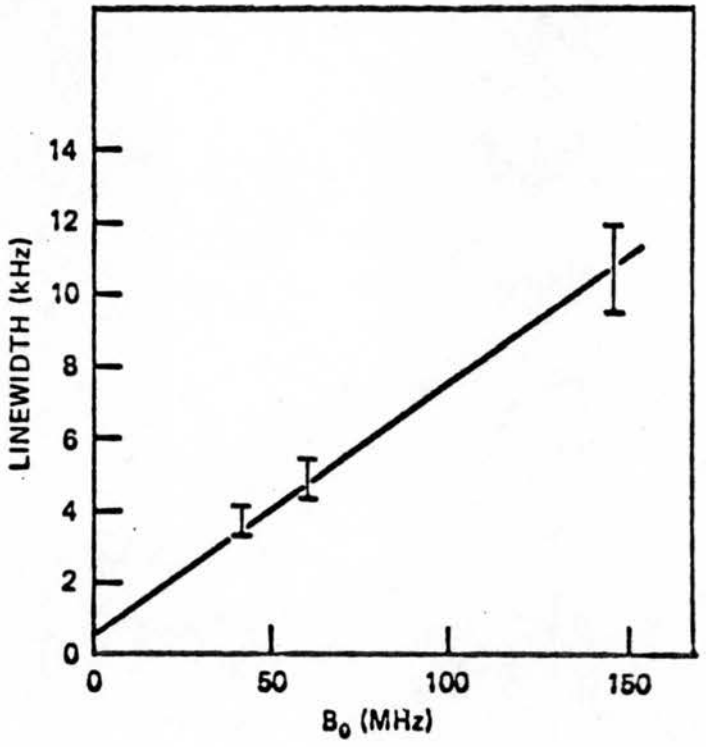

(Newman *et al.*, 1977). The diffusion coefficients for rotation parallel ($D||$) and perpendicular ($D\perp$) to the long axis of fd can be calculated for such a cylinder (Edsall, 1953). $D|| = 20\ s^{-1}$ is calculated for fd in solution, and a value of $D|| = 21\ s^{-1}$ has been measured by Newman *et al.* (1977). This reorientation rate is too slow to affect the NMR spectra. However, $D\perp = 10^4\ s^{-1}$ by these calculations. This is the time scale of the ^{31}P chemical shift anisotropy The rounding of the chemical shift powder pattern seen for fd in solution is consistent with such a rotational diffusion constant (Mehring, 1976; Speiss, 1978; Campbell *et al.*, 1979).

The spectra of Figure V-2c, d demonstrate the drastic influence of virus assembly on the dynamics of the single-stranded fd DNA. Since the data on solid fd show no evidence of structural change in the phosphodiester backbone induced by the coat-protein shell, the spectral changes in Figure V-2 can be only due to motional effects. While single-stranded fd DNA in solution has substantial motions in the nanosecond time range, the DNA in the virion has a limited amount of motion faster than $\sim 10^{-4}$ s, which indicates the DNA is immobilized by being packaged inside the virus particle.

Figure V-6. T_2 Measurement of ^{31}P Resonance of fd Solution (50 mg/ml). ^{31}P resonance is at 61 MHz. The straight line corresponds to a value of 0.75 msec.

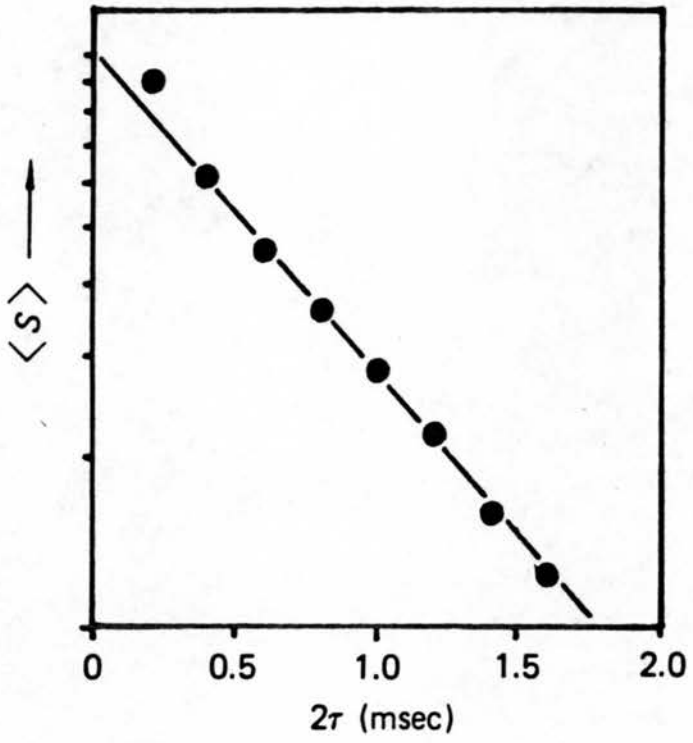

VI. DNA IN EUKARYOTIC CHROMATIN

VI.1. INTRODUCTION

The DNA within eucaryotic cell nuclei is enormously condensed compared to the polymer free in solution; it has been estimated that the extent of linear compaction is greater than 10^3-fold (Sadat and Manuelidies, 1978). Several levels of coiling structure contribute to the condensation of DNA in nuclear chromatin, only the first of which has been characterized in detail. The binding of histones to DNA in the fundamental mononucleosomes subunit reduces the length of DNA by about a factor of five (Kornberg, 1977; McGhee and Felsenfeld, 1980). The nucleosome unit contains a core particle resembling a flattened cylinder with about 145 base pairs of DNA wrapped around a protein center, and a variable length of linker DNA complexed with the histone H_1. Repeated (core + linker) units have been visualized as the well known "beads on a string" structures in electron micrographs (Finch and King, 1976). The next level of folding involves formation of helical fibrils from several nucleosomes connected by the linker DNA segments and histone H_1 (Suau *et al.*, 1975; Toma and Koller, 1977). Further coiling of these fibrils ultimately gives rise to the extremely compact nuclear material (Sedut and Manuelidies, 1978; Benyajati and Woreel, 1976).

Few details of the organization of DNA and proteins in bull sperm chromatin are known. A single major protein component, protamine, packages the DNA int the extremely small sperm heads; this protein has only 47 amino acids, of which 24 are arginine and 6 cysteine (Coelingh *et al.*, 1969; 1972). Apparently the cysteines form intermolecular cross-links among the protamines (Marushige and Marushige, 1974).

The two nucleoprotein systems studied here thus represent extremes of the higher folding levels of eucaryotic DNA. The soluble chromatin prepared from chicken erythrocyte nuclei by mild nuclease digestion consists of about ten nucleosomes linked together; in the low ionic strength conditions used here, these fibrils have an apparent diameter of 10 nm (Suau *et al.*, 1975). Only the first level of folding beyond that of the nucleosome core particle is present in the soluble chromatin. In contrast, at least two orders of magnitude more in linear compaction of the DNA is present in demembranated heads of bull sperm.

Previous NMR studies of DNA protein complexes have been concerned with mononucleosome core (Cotler and Lilley, 1977; Kallenbach *et al.*, 1978; Shindo *et al.*, 1980). Larger and potentially more interesting complexes have not been studies because their slow reorientation rates do not average out the dipolar and chemical shielding interactions that are responsible for the overwhelming line width of resonances in solids. In solid state NMR, radiofrequency irradiations

and mechanical sample spinning substitute for molecular motions as line narrowing mechanisms. The usefulness of this approach for the study of biological supramolecular structures has been demonstrated for viruses (Chapter V) and high molecular weight duplex DNA (Chapter IV).

VI.2. Sample Preparation

Chicken erythrocyte chromatin in solution was prepared by lysing red blood cells with Nonidet NP-40 detergent (Sigma). The resulting nuclei were briefly digested with microccocal nuclease (Worthington) according to Lutter (1978). After stopping the reaction with the addition of EDTA the material was dialyzed into 10 mM tris buffer with 1 mM pH 7 and pelleted by spinning at 40,000 rpm for 18 hours in a Ti50 rotor. The final NMR sample had an OD of 650 at 260 nm in a volume of approximately 0.3 ml.

The DNA of the chromatin sample was analyzed by electrophoresis on a 0.5% agarose + 2.5% polyacylerylmide gel as described in reference (Kallenbach *et al.*, 1978) after being released from the chromatin by treatment with proteinase-K and sodium dodecyl sulfate. This method shows that this DNA in the soluble chromatin is approximately 23000 daltons. Therefore, there are about 12 nucleosome units per particle. Polyacrylmide gel electrophoresis of the chromatic proteins showed that histones H_1, H_{2a}, H_{2b}, H_3, and H_4 were present.

A suspension of bull sperm was demembranated by treatment with Nonidet detergent. The sperm tails were removed by sonication and the final samples were concentrated by low speed centrifugation.

The duplex DNA samples were high molecular weight material from cell thymus. The sample preparation is described in Chapter IV.

VI.3. Results and Discussion

The lineshapes of the ^{31}P NMR spectra of Figure VI-1 are determined by chemical shift anisotropy, since high power proton decoupling was used to remove the influence of ^{31}P-^{1}H dipolar interactions. Figure VI-1a is the spectrum of solid fibrous DNA. The discontinuities of the powder pattern reflect the rigid lattice values of the phosphodiester chemical shielding tensor; this corresponds to a total breadth $\Delta\sigma$ = 194 ppm. In a magnetic field of 3.5T this is 11.8 KHz which determines the timescale for detection of motional averaging; motions slower than this will not affect the spectrum, while those faster will reduce the observed width and alter the lineshape. DNA in solution has backbone motions with rotational correlation times near 10^{-6} sec (Chapter IV); Figure VI-1d shows that these relatively fast motions completely average the chemical shift anisotropy. Soluble chromatin and bull sperm heads in solution give the ^{31}P NMR spectra shown in Figures IV-1b and c. The asymmetric powder pattern for soluble chromatin $\Delta\sigma$ = 132 ppm and is a striking result, since

Figure VI-1. ^{31}P NMR Spectra of DNA and Nucleoprotein Complexes.

A) Solid fibrous calf thymus DNA (Sigma).

B) Chicken erythrocyte chromatin in solution.

C) Bull sperm heads in solution.

D) High molecular weight calf thymus DNA (Miles) in solution.

Spectra A, B, and C resulted from cross-polarization with 1 msec mix time and 1 sec recycle delay. Data was acquired for 10 msec with 2.3 mT ^{1}H decoupling field. Spectrum D was from $\pi/2$ pulses rather than cross polarization.

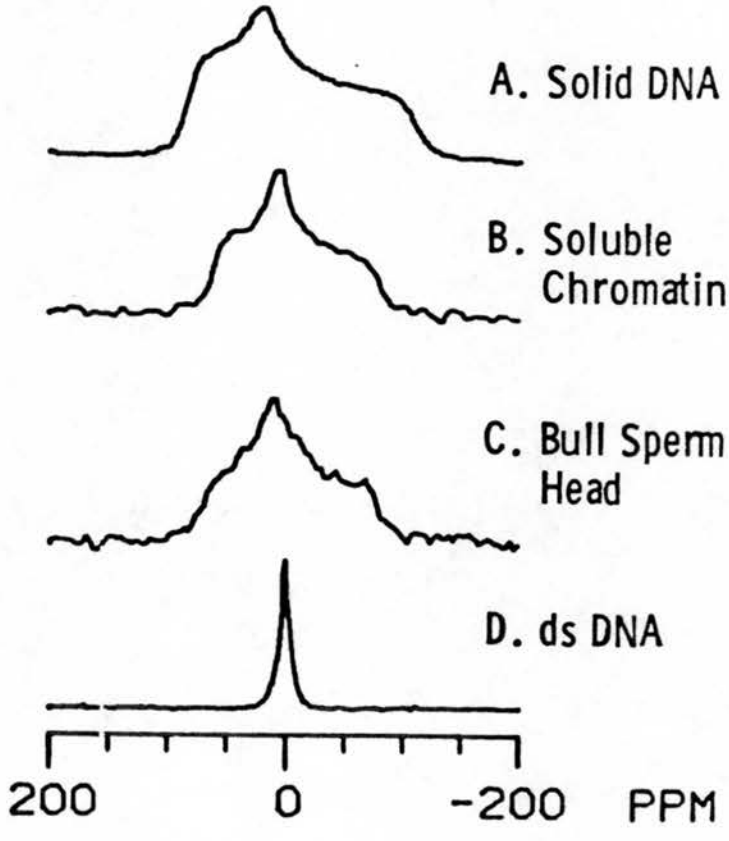

it means that bending motions of DNA that are rapid compared to 11.8 KHz are damped out be the protein-DNA interactions. The observed $\Delta\sigma$ for the DNA-protein complexes in solution is reduced by about 30% from the static value of Figure VI-1a. It is difficult to fully characterize the source of the reduction except to say that it must be from motions of the particle or local structural fluctuations of limited amplitude that are fast compared to the 11.8 KHz timescale. If such motions were of large amplitude, such as rotation about a single axis, then the shape of the spectrum would be that characteristic of an axially symmetric powder pattern (see Appendix B). The spectra in Figures Vi-1a-c were obtained by cross-polarization of the ^{31}P spins from the ^{1}H spins; this procedure relies on a solid state effect, namely the existence of static ^{31}P-^{1}H dipolar couplings as a transfer mechanism. This means that the techniques selects for solid-like spins. When soluble chromatin samples are subjected to nonselective $\pi/2$ radiofrequency pulses instead of cross-polarization, the ^{31}P NMR spectra exhibit a narrow resonance near the isotropic shift position (0 ppm) superimposed on the powder pattern. We believe this liquid-like spectral component represents a minor fraction of degraded DNA becuase it varies in relative intensity from sample to sample and increases in size as samples get older. Since chromatin samples with and without histone H_1 give similar ^{31}P NMR spectra, we do not think the narrow resonances represent mobile linker regions of DNA although

Figure VI-2. A) Soluble chromatin in solution. Same as Figure VI-1b. B) Chromatin sample in an Andrew type rotor spinning at 2.5 KHz at the magic angle (θ = 54.7) with respect to the applied magnetic field with a 25 msec acquisition time.

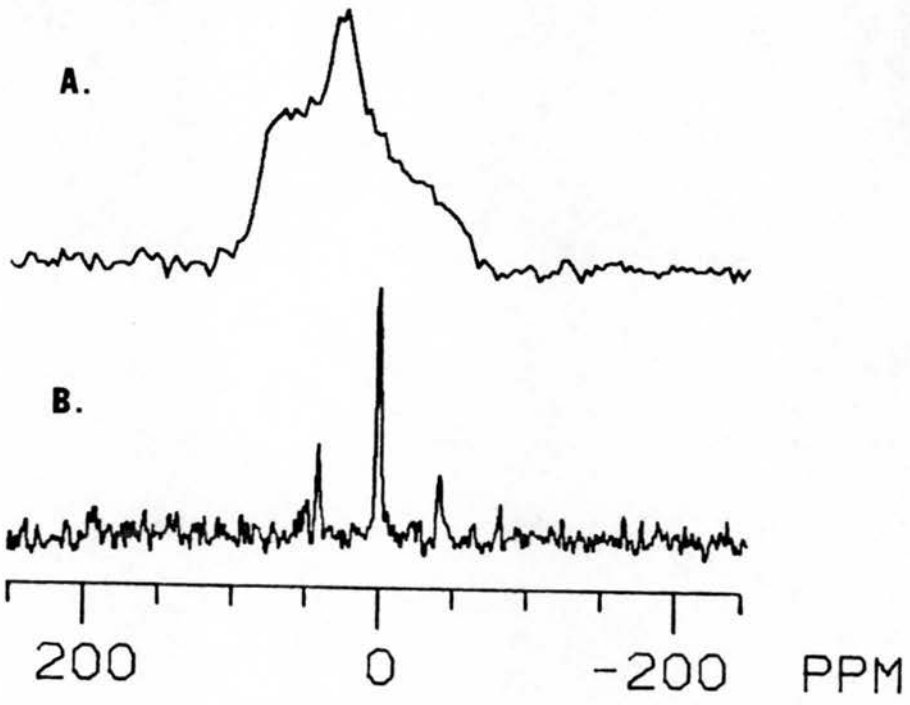

the present experiments do not rigorously rule this out.

Magic angle sample spinning averages chemical shift anisotropy to its isotropic value. The results from this procedure are shown in Figure VI-2 for chromatin in solution; there is a single narrow centerband at the chemical shift position observed for DNA alone or isolated mononucleosome core particles in solution. This implies that there is a single type of environment with no evidence of chemical modification or severe geometrical distortion of the phosphodiester linkages. However, it must be remembered that the sensitivity of ^{31}P chemical shifts to structural changes in not fully established (Gorenstein *et al.*, 1976). The presence of spinning side-bands separated from the centerband by the 2.5 KHz spinning frequency and the drastic narrowing of the center-band demonstrate further that the lineshape of the stationary samples is due to chemical shift anisotropy.

Solid state NMR techniques clearly make it possible to study high molecular weight DNA and DNA-protein complexes. The picture that is emerging is that while structural perturbations of DNA by protein interactions are subtle or not detectable by ^{31}P chemical shift measurements the associated dynamical effects are profound. DNA alone has a flexible backbone (Chapter IV). However, in soluble chromatin, bull sperm heads, and filamentous viruses the packaging of DNA by quite different

proteins at various levels of folding and compaction results in substantial immobilization of the DNA. Greater detail can be gained by using other nuclei, spin interactions, and magnetic field strengths to vary the timescale sensitive to motion.

VII. DYNAMICS OF B-FORM DNA IN THE SOLID STATE

VII.1. INTRODUCTION

Structural information must always be interpreted in terms of a timescale usually dictated by the experimental measurement itself. X-ray diffraction has been applied quite successfully to the elucidation of DNA structure (Watson and Crick, 1953). The structural parameters obtained are time averages over the time of the experiment which can be as long as days. Any motions present are smeared out in space and only an average structure is observed.

NMR is capable of yielding structural and dynamical information on many timescales. The anisotropic lineshapes observed in an NMR spectrum of a solid serves to define a timescale upon which motional averaging can be observed. Interaction strengths and hence timescales, can range from a few Hz (chemical exchange), through several KHz (chemical shift anisotropy) to hundreds of MHz (T_1). This is at least 7 orders of magnitude.

B-DNA in the form of a hydrated solid has been studied by both x-ray and NMR techniques. The x-ray experiments performed on one-dimensional oriented fibers have yielded a wealth of structural information (Arnott, 1970). NMR has been used to observe bound water molecules (both H_2O and D_2O) and bound ions indlucing Na^+ and Li^+

(Migchelsen *et al.*, 1968; Edzes *et al.*, 1972). In these cases splittings of the NMR signals followed a $3\cos^2\theta-1$ dependence indicative of an axially symmetric system. From the magnitude of the splitting it can be seen that there is substantial motion present which averages the predominant interaction. This is not to say that the DNA polymer itself possesses this motion but the probe molecule does. The recent ^{31}P NMR study of Shindo *et al.* (1980) is in general agreement with the structural parameters from the diffraction work, but indicates the presence of motion in the DNA fibers and conformational heterogeneity in the DNA backbone. The results presented here are consistent with the experimental data of Shindo *et al.* (1980) but by performing experiments that monitor the dynamics of both the bases and the phosphodiester backbone over a large temperature range we reach different conclusions about the motions of solid B-form DNA. The structural parameters of DNA are not addressed with these experiments.

In the present work, ^{2}H and ^{31}P NMR are used to obtain dynamic information from an unoriented sample of B-form DNA as a hydrated solid. Phosphorus NMR shows the phosphodiester backbone while specific labeling of the C-8 position of purines with deuterium allows direct observation of the bases.

VII.2. Sample Preparation

DNA was deuterated in the C-8 positions of the purines by modification of standard procedures (Doppler-Bernardi and Felsenfeld, 1969). Briefly, DNA (Sigma, Type I) was dissolved in 2.5 M NaCl in 99% D_2O (Bio-Rad) at a concentration of 1-4 mg/ml. The flask was sealed in a flame and incubated at 83°C for 8 hours. After cooling to 4°C the flask was opened and sample dialyzed for several days against 0.75 M NaCl, 10 mM tris·HCl, pH 7 to remove D_2O. The DNA was precipitated by addition of 2 volumes 95% ETOH at 4°C and briefly cooling to -20°C. The fibrous solid was then washed 2x with 70% ETOH and 2x with abs ETOH for 15 minutes each then dried *in vacuo* at room temperature. This sodium DNA was then exposed to 92% R.H. (saturated NaH-tartarate) and equilibration followed by weight gain.

All NMR experiments were performed on the same sample. Temperature control was effected by passing N_2 gas at the desired temperature past the sample. Sample temperatures are accurate to ± 2°C.

VII.3. Results and Discussion

Figure VII-1 shows the effect of temperature in the ^{31}P NMR spectrum of B-DNA. At -20°C motion is frozen out and a lineshape depicting a rigid chemical shielding tensor is obtained. The structural aspects of this lineshape have been discussed previously (Chapter III). As the temperature is raised motion is imparted to the polymer which is reflected in the spectrum by narrowing of the broad resonance. The effect of motional averaging is very sensitive to the rates and types of motion relative to the nuclear spin interaction which dominates the spectrum. For any motion to be effective in modifying the observed resonance it must be at least as fast or faster than the dominant interaction. The ^{31}P static chemical shift anisotropy of 200 ppm is dominant in this case. At 60.9 MHz for ^{31}P this results in an interaction strength of 1.2×10^4 sec^{-1}. Thus for any motion to effect the observed ^{31}P spectrum it must possess significant amplitudes with rates equal to or greater than 10^4 sec^{-1}.

As can be seen in Figure VII-1, as the temperature is raised the static chemical shift powder pattern observed at -20°C collapses. There must be appreciable motion present in B-form DNA with a correlation time less than 10^{-4} sec. The 20°C spectrum is very similar to that reported by Shindo *et al.* (1980).

The averaged lineshape can be used to obtain information about

Figure VII-1. ^{31}P NMR (60.9 MHz) of B-form DNA. Chemical shifts were measured from external 85% H_3PO_4. 10^3 transients were recorded at each temperature using a cross polarization time of 1 ms, acquisition time of 50 ms (with high power proton decoupling) and a recycle delay of 1 s. Both proton and phosphorus $\pi/2$ pulses were 5 μs.

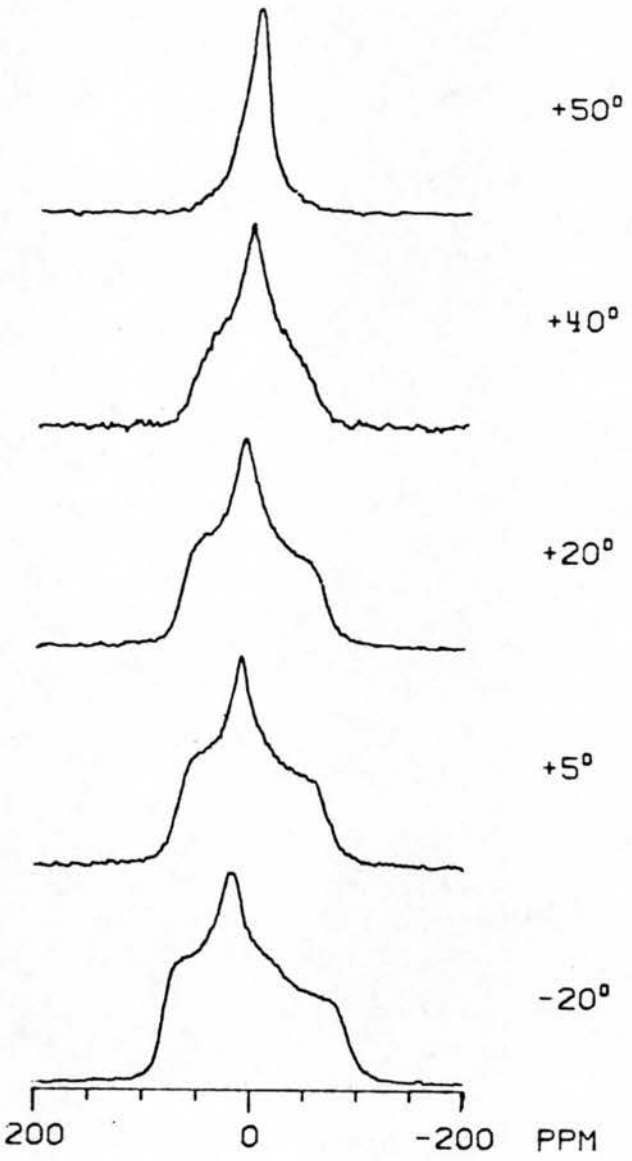

the type of motion present in the molecule. For example, if the motion was confined to fast rotation about a single axis then the averaged spectrum would be a characteristically axially symmetric powder pattern. This is obviously not the case here. The lineshapes of ^2H NMR spectra of solids are determined by the nuclear quadrupole interaction of C-D bonds. Deuterium has spin $I = 1$ and a static quadrupole coupling constant of e^2qQ/h = 177 KHz with near axial symmetry for an aromatic C-D bond (Barnes and Bloom, 1972; Gall *et al.*, 1981). A theoretical static ^2H NMR powder pattern is compared to the experimental spectra for the purine C-8 labelled DNA at 20°C and 50°C in Figure VII-2. These solid state ^2H NMR spectra are nearly indistinguishable within the limits of experimental signal to noise especially with respect to the splitting of the major discontinuities which is 128 KHz in all of these cases. By contrast, the ^{31}P chemical shift powder patterns from the same sample at the same temperature show significant reductions in breadth compared to the static theoretical chemical shift anisotropy.

These data show that the backbone of B-form DNA in the solid state has motions of substantial amplitude that occur more rapidly than 10^4 Hz at 50°C as well as at lower temperatures. There are no motions influencing the bases that are on the order of or faster than 10^6 Hz, even at 50°C. These results are incompatible with a model of reorientation about the long axis of DNA as proposed by Shindo *et al.* (1980) (see Appendix B). First of all, rotation about any axis

Figure VII-2. ^{31}P (60.9 MHz) and ^{2}H (37.8 MHz) NMR Spectra of B-form DNA. ^{31}P NMR spectra are reproduced from Figure VII-1 for comparison. The theoretical ^{31}P powder pattern was calculated for the experimentally determined principle elements of the chemical shielding tensor for DNA with σ_{11} = 85 ppm, σ_{22} = 25 ppm, and σ_{33} = -109 ppm. The ^{2}H NMR spectra were 10^4 quadrupolar spin echoes (QUECHO, see Chapter II) at each temperature using 2 μs $\pi/2$ pulses, 50 μs inter-pulse delay, 1 ms acquisition time and 0·1 s recycle delay. The theoretical ^{2}H powder pattern was calculated for the experimentally determined static quadrupole coupling constant e^2qQ/h = 177 KHz and asymmetry parameter η = 0.046.

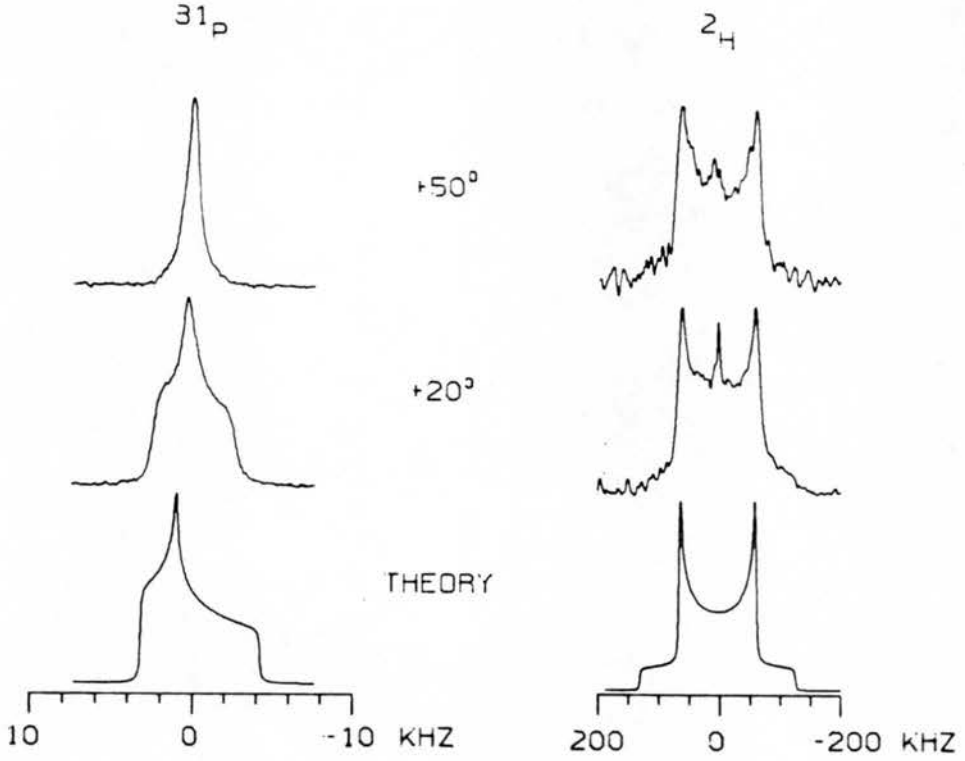

defined in a molecular frame would average the ^{31}P chemical shift lineshapes to axially symmetric powder patterns. Instead, at the higher temperatures the lineshape becomes completely averaged to its isotropic value, indicative of motions in all directions faster than the relevant NMR timescale. Second, rotations much faster than 10^4 Hz would reduce the ^2H quadrupole powder splitting of 128 KHz observed in the powder patterns from the C-8 deuterium labels. This does not occur, since the 50°C ^2H NMR spectrum is essentially identical to the 20°C spectrum. It is unlikely that the somewhat smaller timescale for phosphorus chemical shielding compared to the deuterium quadrupole interaction affects the conclusions because of the large extent of motional averaging of the phosphorus lineshape at 50°C.

The data presented here are too limited to provide a detailed description of the motions of solid B-form DNA. Even though the influence of specific models of rotational or jump motions on powder patterns can be calculated, the effectively isotropic averaging of the ^{31}P chemical shift pattern and the complete lack of averaging of the ^2H quadrupole pattern make such modelling difficult. However, the qualitative conclusions of independent reorientations of the phosphodiester groups on a timescale faster than 10^4 Hz and the rigidity of the bases are valid. Backbone motions in DNA clearly could have a significant influence on the interpretation of diffraction data, and it may be of interest to examine such data for a sample of B-form DNA at an elevated temperature where these NMR results would predict rigid

bases and significant motions of the phosphodiester groups.

VIII. STRUCTURAL PARAMETERS FROM ^{31}P-^{31}P DIPOLAR COUPLINGS

VIII.1. INTRODUCTION

Perhaps the greatest potential of solid state NMR lies in its ability to yield structural information with atomic resolution. In no case is this more true than with the dipolar interaction. There are many cases in the literature where this interaction has been used to determine spatial coordinates (Pake, 1948; Waugh *et al.*, 1953; Andrew and Berhson, 1950; and Deeley and Richards, 1954). The reason for this success is the simple dependence of the interaction of internuclear distances and angles without relying on assumptions based on molecular theories. As can be seen in the dipolar Hamiltonian Equation (VIII-1) the spatial dependence is neatly contained in the b_{jk}'s:

$$H_{II} = \sum_{j>k} \sum b_{jk}(3\vec{I}_{zj}\vec{I}_{zk} - \vec{I}_j \cdot \vec{I}_k) \qquad \text{(VIII-1)}$$

$$\text{where } b_{jk} = \frac{\hbar\gamma_i^2}{r_{jk}^3} \cdot P_2(\cos\theta_{jk})$$

Macroscopically oriented samples are required to obtain angular information, however, radial parameters are still accessible in polycrystalline materials.

The ^{31}P dipolar interaction can be used to obtain structural information from biological samples. Phosphorus atoms constitute a

chemically rare species, simplifying assignment, and they usually occur at biologically interesting sites.

In order to observe the ^{31}P-^{31}P dipolar couplings they must be made to be the dominant interaction in the total spin Hamiltonian. The interactions which usually dominate ^{31}P NMR are: (a) ^{31}P chemical shift anisotropy (10^4-10^5 Hz), (b) ^{1}H-^{31}P dipole (1 - 5 x 10^3 Hz), (c) ^{31}P-^{31}P dipole (10^2-10^3 Hz) and (d) ^{31}P t_2 ($\leq 10^2$ Hz). Each interaction is followed by the "magnitude" of its internal Hamiltonian.

The ^{31}P-^{31}P dipole interaction in rigid solids is most conveniently expressed as a second moment (VIII-2) as shown by Van Vleck (1948). In polycrystalline solids averaging over all angles yields a reduced form (VIII-3) containing only distances. Dipolar broadening takes the form of convolution of frequency domain with a gaussian function which is also expressible as a second moment. This brings

$$M_2 = {}^3/_4(\hbar\gamma^2_I)^2 I(I+1)\frac{1}{N}\sum_{j>k}^{N}\sum \frac{(P_2(\cos\theta_{jk}))^2}{r^6_{jk}} \qquad \text{(VIII-2)}$$

$$M_2 = {}^3/_4 \cdot {}^4/_5(\hbar\gamma^2_I)^2 I(I+1)\frac{1}{N}\sum_{j>k}^{N}\sum r^{-6}_{jk} \qquad \text{(VIII-3)}$$

to mind a method for determining ^{31}P-^{31}P dipolar couplings i.e., fitting the observed powder pattern to a theoretical one convoluted with a gaussian. However, it is impractical since it is desired to measure an interaction of approximately 10^2-10^3 Hz in the presence of

one at least one hundred times greater.

A schematic representation of the pulse sequence used is shown in Equation (VIII-4). During the preparation interval a transverse magnetization is developed by cross polarization. In the

$$XP_y - \tau - \pi_y - \tau - AQT \qquad \text{(VIII-4)}$$

evolution period the spin Hamiltonian is manipulated so that the ^{31}P-^{31}P dipolar couplings dominate. High power proton decoupling averages ^{1}H-^{31}P couplings and ^{31}P T_2 effects are small and can be neglected. A π_y pulse refocuses the magnetization and cancels out chemical shift effects. At the end of the evolution period the remaining transverse magnetization is sampled in the usual way. This constitutes the detection period. During the evolution period the decoupling level is raised to insure the complete decoupling of protons, while during the detection period it is lowered to minimize sample and probe heating. Also, the decoupling is turned off during the π_y refocusing pulse to prevent any transient cross polarization effects.

There is a strong analogy between this present experiment and the Carr-Purcell T_2 experiment (Carr and Purcell, 1954). In both cases the transverse magnetization developed is allowed to evolve under the appropriate interaction for a variable time and the remaining magnetization is then sampled. In the C-P liquid experiment it is the experimenter's choice whether to measure peak heights or integrals since for Lorenzian lines, commonly seen in liquids, these

two parameters are directly related an both give the desired information i.e., the remaining magnetization at the end of the evolution period. In the present experiment we choose to measure the integral of the frequency domain. Since, as mentioned before, the effect of dipolar broadening in the frequency domain is convolution by a gaussian, the time domain signal is expected to drop off as a gaussian also. This is shown in Equation (VIII-5). For analysis, the logarithm of the observed intensity obtained with various times is plotted

$$\langle I(\tau)\rangle = \langle I(0)\rangle \exp(-2\pi^2 M_2 \tau^2) \qquad \text{(VIII-5)}$$

versus the square of the corresponding time. For a gaussian function this will result in a straight line. The linearity of this plot also is an indication of the validity of neglecting the T_2 processes. First order exponentials would yield a downward curving line on this type of plot.

VIII.2. Sample Preparation

Sodium pyrophosphate decahydrate (Fisher) and anhydrous calcium pyrophosphate (Sigma) were used without further purification. fd virus grown on *E. coli* was prepared as described in Chapter V. pF1 grown on *S. aureas* was prepared similarly. Samples for NMR were lyophilized powders stored in a dessicator under vacuum at room temperature for

24 hours then sealed in sample tubes.

VIII.3. Results and Discussion

Figure VIII-1 shows a plot at the sodium pyrophosphate ^{31}P intensity as a function of evolution time using the described experiment. The result is a straight line the slope of which yields the second moment. The value obtained is 2.05×10^5 Hz^2. The crystal structure for this molecule has been determined by s-ray diffraction methods (McDonald and Cruickshank, 1967). The phosphorus atoms of a single pyrophosphate are shown to be 2.93 Å apart, moreover the nearest neighbors are pyrophosphates no less than 10 Å away (McDonald and Cruickshank, 1967). This fulfills the requirement of an isolated pair and simplifies the calculation greatly (Pake, 1948). The only structural parameter is then the distance between the phosphates in a single pyrophosphate molecule (r_{12}). Using Equation (VIII-3) a value of 3.08 Å is obtained. The agreement is reasonable and shows that the dipolar decouplings reflect structure. The small difference between the two measurements may be due to some vibration of the phosphorus atoms which would reduce the measured (M_{2SS}) (Chapter II.3.2). However, similar experiments using $Ca_2P_2O_7$, modifying the preparation interval to a ^{31}P $\pi/2$ pulse and omitting the proton decoupling have given excellent results ($M_{2SS} = 2.75 \times 10^5$ Hz^2, $r_{NMR} = 2.93$ Å and $r_{x\text{-}ray} = 2.90$ Å (Calvo, 1968).

Figure VIII-1. Plot of the integral of observed intensity of the ^{31}P NMR resonance (60.9 MHz) versus time squared under the ^{31}P-^{31}P dipolar interaction for $Na_4P_2O_7 \cdot 10H\ O$. From the slope of the fitted line the second moment (M_{2ss}) can be determined.

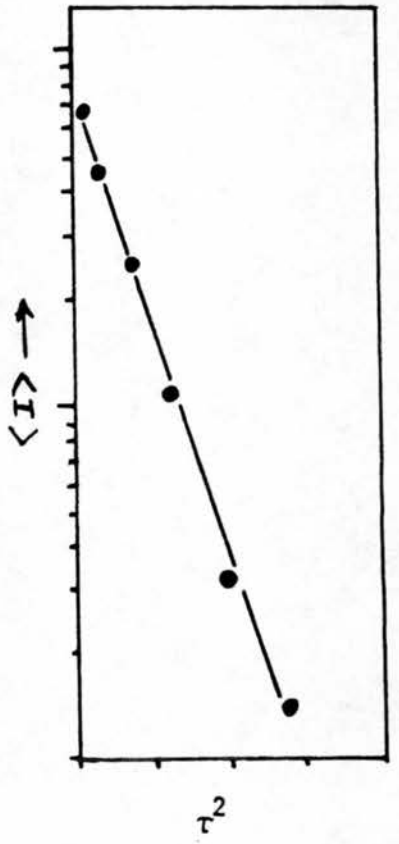

VIII.4. Application to Filamentous Viruses

The ^{31}P-^{31}P dipolar interaction is now applied to elucidate structural parameters of fd and Pf1 viruses.

The filamentous bacteriophages are long thin rods of DNA and protein. There are a number of related viruses in this category with somewhat different structures. fd from infected *Escherichia coli* and PF1 from infected *Pseudomonas aeruginosa* represent the extremes of overall length with fd being 0.9μ long and PF1 2μ long even though the number of nucleotides in their DNA's is similar (6400 versus 7400). Comparative studies of their DNA offer some advantages for interpretation and understanding the possibilities for packing arrangements of DNA-protein complexes (Day and Wiseman, 1978; Day *et al.*, 1979). The DNA in both viruses is a circle of single-stranded DNA. It is confined within a cylindrical core region of about 20 Å in diameter as deduced from X-ray diffraction data. Mechanical shearing experiments show that the DNA occupies the entire length of the virus particle so that there exist two antiparallel chains of DNA stretched between the ends of the filament interior. The DNA strands are assumed to be regular helices as shown in the diagram of Figure VII-3. However, basepairing does not occur in either fd of PF1, since the A-T and G-C ratios are not integers. The number of nucleotides for each virus is known as are their total lengths, thus, the axial rise per

Figure VIII-2. Plot of the integral of observed intensity of the ^{31}P NMR resonance (60.9 MHz) versus time squared under the ^{31}P-^{31}P dipolar interaction for the filamentous viruses fd and Pf1. Also shown are the data from Figure VIII-1 for comparison.

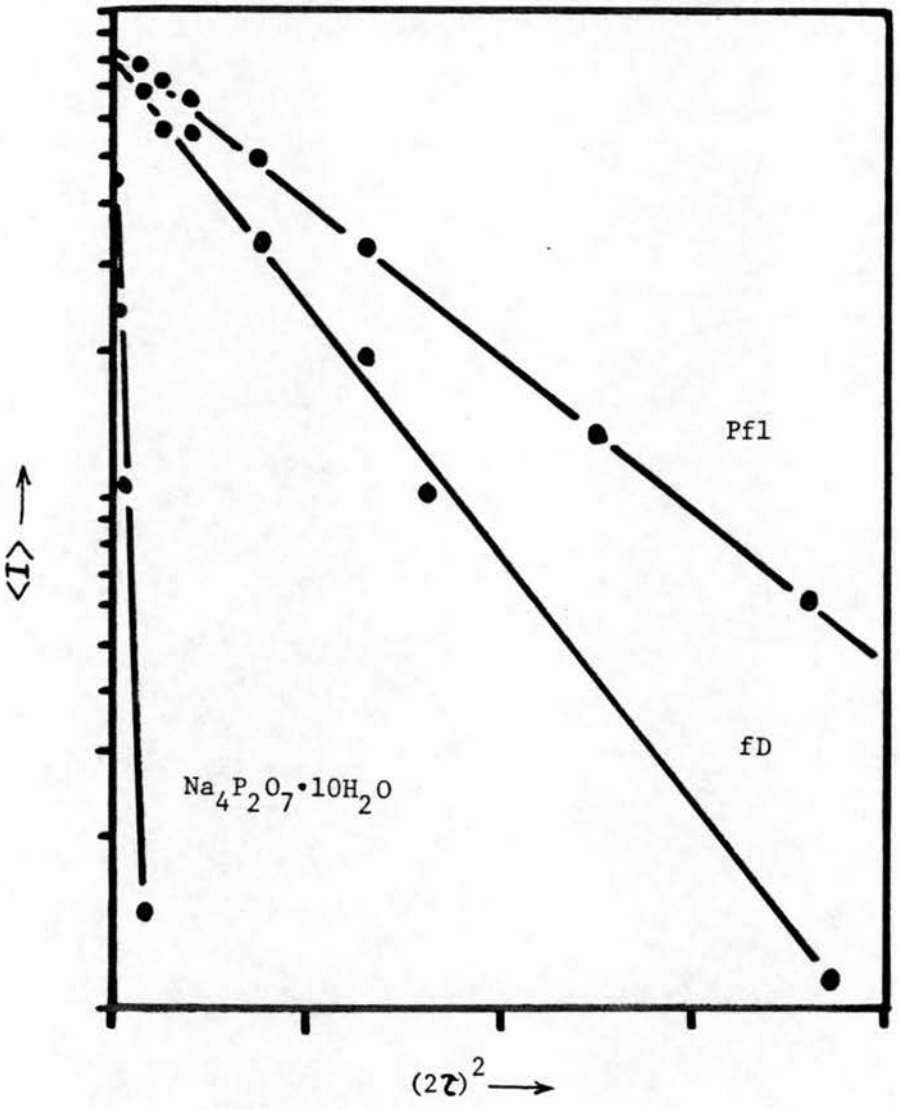

Figure VIII-3. Schematic diagram of the model used for the phosphodiester backbone of DNA packaged in filamentous phages. The right side depicts the general helix structure. Note that the base pairing is not implied by the inter-strand lines. The left side shows the 4 parameters used to define the helix.

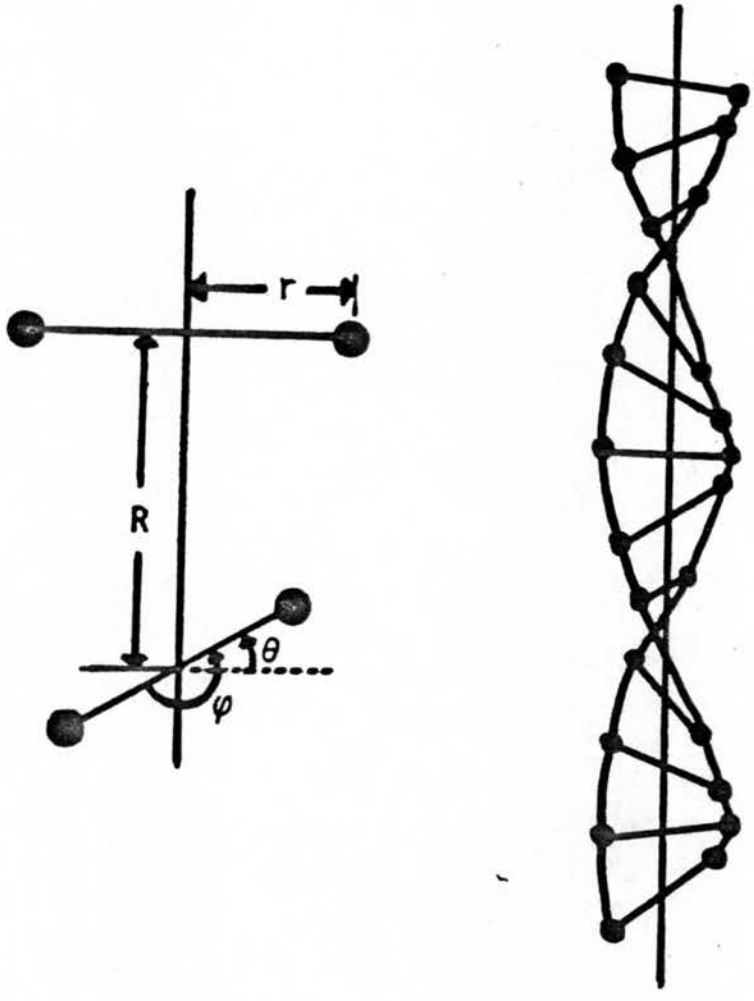

base (projected on the long axis of the virion) can be calculated by dividing the total length of the virus particle by 1/2 the number of bases. The axial rise per base is 2.8 Å and 5.4 Å for fd and Pf1, respectively.

The DNA helical parameters can be deduced by comparison with coat-protein helix parameters. For Pf1 there is a one to one stoichiometry between nucleotides and coat-protein subunits, and there are 5.4 protein subunits per turn of protein helix. If the bases interact alternately on the up and down chains of the DNA, there are 2.7 bases per turn of DNA helix for each chain giving a twist of the helix per base of 133° (Day *et al.*, 1979). The non-stoichiometric relationship of nucleotides to coat-proteins in fd makes the determination of this parameter less certain, but it appears to be between 60° and 72° per base.

It is assumed that intermolecular repulsions will cause the DNA strands to be maxially distant, i.e., 180° apart looking down the twist axis. It is also assumed that the bases of antiparallel chains are not staggered (Day *et al.*, 1979). This leaves the radial distance of each strand undefined. The second moment of the phosphate resonance was calculated for the five nearest neighbors of any phosphate as a function of the radius of the DNA helix in the virus. For Pf1, the observed second moment corresponds to a radial distance of 4.9 Å, while for fd a range based on the range of helix twist of the bases is 5.4-4.8 Å. These data are listed in Table VIII-1. It appears, at

least to the present level of resolution in the experiment, that the phosphates of fd and Pf1 are located at the same radial distance, midway out of the central cylindrical core. The predominant difference in the packaging of fd and Pf1 DNA appears to be related to the lengthwise stretch in the cylinder rather than radial displacement.

TABLE VIII-1

		Pfl	fd
M_2	Hz^2	4.4×10^3	7.3×10^3
R	$\overset{o}{A}$	5.4	2.8
r	$\overset{o}{A}$	4.9	5.4-4.8
θ^o		133	60-72
$\emptyset^o$		180	180

IX. CHEMICAL SHIFT SCALING IN NMR OF ROTATING SOLIDS

All types of spectroscopy have in common several goals including increased sensitivity and resolution, and isolation of certain interactions. The latter is an important part of high resolution NMR of solids commonly called Selective Averaging. Its popularity is in part due to the wide variety of techniques available to the experimenter for controlling which terms of the nuclear spin Hamiltonian are dominant in a particular spectral display. This particular aspect has been a principle factor in the development of modern NMR since it enables NMR to yield a great deal of information about the chemical physics of many systems, producing on one hand, structural information at the atomic level and the other dynamical information sensitive to motions over a range of at least 8 orders of magnitude.

In this chapter a technique is presented which is capable of scaling the Chemical Shielding terms of the spin Hamiltonian in liquids and solids. This is a direct extension of the previous work by Ellet and Waugh (1969) on liquids. It is intended to extend the experimentally accessable scaling range of the previous method and to extend its use to solids.

The theoretical basis of the method relies on Coherent Averaging techniques (Haeberlen and Waugh, 1968) whereby a spin system irradiated

Figure IX-1. Chemical shift scaling factor (SF) as a function of nutation angle (θ). Line represents calculated function of equation (3). Experimental values from the 4 pulse experiment are circles (o) while those from the 2 pulse experiment are crosses (x). Data from Figure (2) along with additional points from the same liquid sample are plotted.

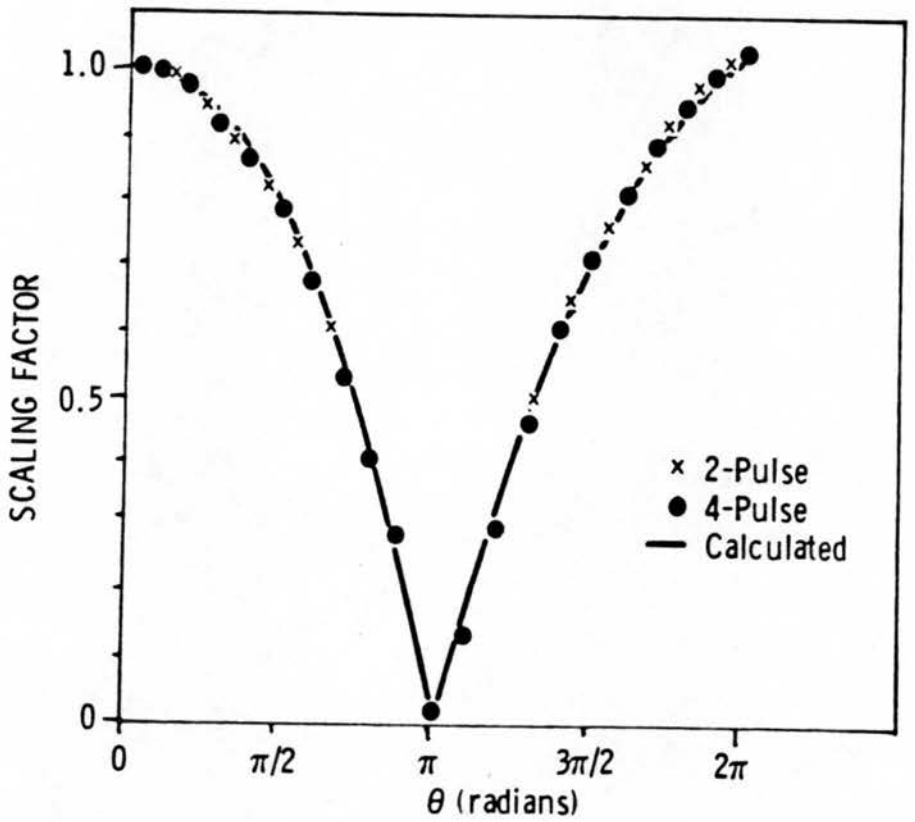

by a train of intense radio frequency pulses can, under the appropriate circumstances behave over long times as though under the influence of a time-dependent Average Hamiltonian. The relevant pulse sequence is shown in Equation (IX-1).

$$X P_y \; \tau_s \left[\theta_{-x} \tau_s \theta_x \tau_s \theta_x \tau_s \theta_{-x} \tau_s\right]_N \qquad \text{(IX-1)}$$

Transverse S magnetization is developed by cross polarization from the I (proton) spin bath although a $\pi/2_x$ pulse would function as well. Next, a train of pulses, each θ in length, is applied to the S spins with high power decoupling of the protons.

The zero order Hamiltonian (Appendix A) calculated using the coherent averaging methods is:

$$\bar{H}_{\Delta}^{(o)} = -\Delta\nu \; \frac{4}{\tau_c} \{2\frac{\tau\omega}{\theta} \sin \theta/_2 + \tau_s \text{ Cos } \theta/_2\} \; x \cos \theta/_2 \vec{I}_z \qquad \text{(IX-2)}$$

This should be compared with Equation (11) of Ellett and Waugh (1969). The term in brackets results in scaling of the chemical shift in the same manner as does the original two pulse experiment (the difference in the factor or two comes from the difference in cycle time between the two experiments) in addition the magnetization in the 4 pulse experiment precesses about the z-axis ($\vec{B}_o || \vec{z}$). In contrast the precession axis for the two pulse experiment is $\vec{I}_z \cos \theta/_2 - \vec{I}_y \sin \theta/_2$. Within this lies on of the defects of the two pulse sequence. The signals from the two pulse experiment consist of both oscillations and DC signals. The oscillations are said to "ride on pedestals" as in a

Figure IX-2. ^{32}P NMR spectra of a liquid 85% H_3PO_4 sample. The carrier frequency was offset 100 Hz from the resonance frequency near 60.9 MHz. Spectra A., C., and E. were scaled with the two pulse cycle of reference (2). Spectra B., D., and F. were scaled with the four pulse cycle described by equation (1). Initial magnetization was developed with $\pi/2$ pulse of x phase, τ_s = 50 μsec, and π pulse length was 10 μsec.

A. and B. $\theta = 126^{\circ}$, SF = 0.56.

C. and D. $\theta = 90^{\circ}$, SF = 0.83.

E. and F. $\theta = 18^{\circ}$, SF = 1.00.

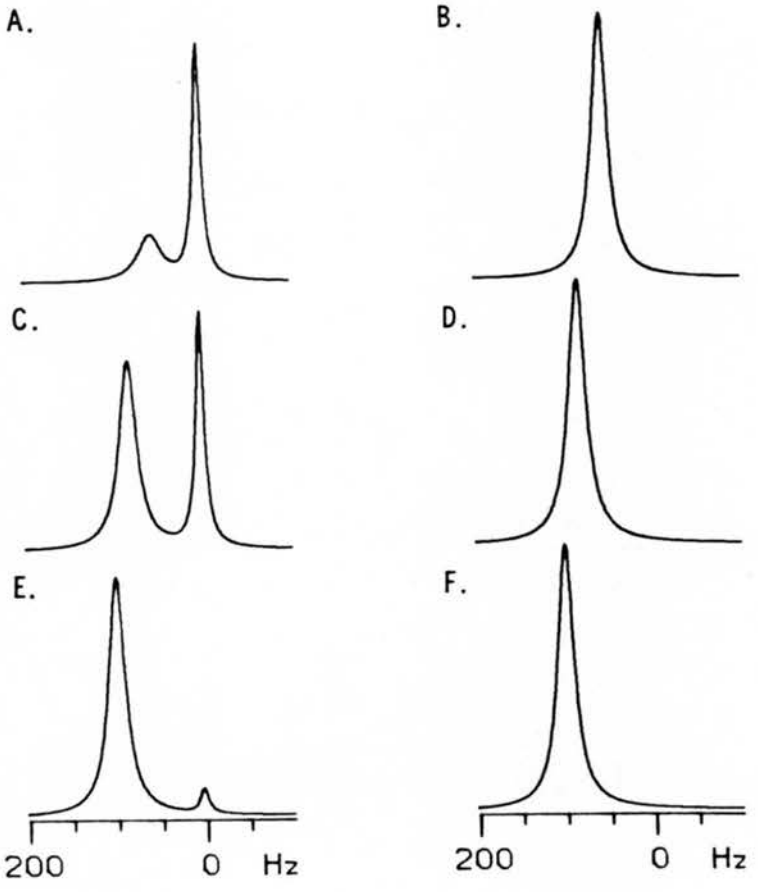

WAHUHA experiment. The DC signals derive from a nonzero component of the initial magnetization ($\vec{S}_o$) in parallel with $\vec{B}_{eff,t}$, the effective field in the toggling frame (Haeberlen, 1976; Haeberlen *et al.*, 1971). In the two pulse experiment the direction of the effective field is an explicit function of θ and the intensity of the DC signal will then vary as $\vec{B}_{eff,t} \cdot \vec{S}_o$, the effective field dotted with the initial magnetization. This results in an artifact at zero frequency which tends to obscure the region of interest. In the 4 pulse experiment, $\vec{B}_{eff,t}$ is fixed along the z axis and the dot product of it and the initial magnetization is zero for all θ.

Since the cycle times used are on the order of the rotational period it is necessary for the pulses to be synchronized with the rotation. The pulse widths are small in relation to the cycle time they are neglected and the interpulse spacing, τ_s, is made equal to τ_{rot}. This is necessary to prevent destructive interference among the spin isochromats from the compound modulation effects of rotation of both spatial and spin terms of the internal Hamiltonian. Typical values are $\tau_{rot} = \tau_s = 333$ μsec and ($\pi/2$ pulse length) = 5 μsec.

The zero order scaling factor calculated from (IX-2) is given by:

$$SF^{(o)} = 4\frac{\tau_w}{\tau_c} \sin {}^{\theta}/_{2} + (1 - \frac{\tau_w}{\tau_c}) \cos {}^{\theta}/_{2} \qquad \text{(IX-3)}$$

and is plotted in Figure IX-1 along with the experimental data from 85% H_3PO_4 (Fischer Reagent) using both pulse sequences. While both

cycles agree quite well with the theoretical predictions the two pulse cycle is useful out to a flip angle of $\approx 100^{o}$. Figure IX-2 shows representative spectra used in Figure IX-1. It can be seen that as the flip angle increases more intensity moves from the real offset signal to the zero frequency position.

The same experiment was performed on stationary and magic angle spinning solid methylphosphonic acid (ALFA Products, Danvers, Massachusetts). The stationary spectra show the chemical shift anisotropy of the phosphate ester being scaled and in the limit (SF = 0) a gaussian line remains with a full width at half maximum of 900 Hz. This is in excellent agreement with second moment measurements and calculations based on X-ray studies (Chapter X and Appendix E). The scaling data for the sample spinning at 3.0 KHz are shown in Figure IX-3. A chemical shift scaling range of 20x is easily accessible and flip angle dependent artifacts are also seen to seen to be minimized by the ability to "wrap around" greater than 360^{o} flip angle.

There are many possible applications for this experiment including the study of chemical exchange processes and separation of isotropic and anisotropic chemical shift in 2-dimensional spectroscopy. It will be used in the next chapter to study the spin physics governing the line width of ^{31}P NMR in rotating solids.

Figure IX-3. Chemical shift scaling factor (SF) as a function of nutation angle (θ). Experimental results from a rotating sample of methyl phosphonic acid.

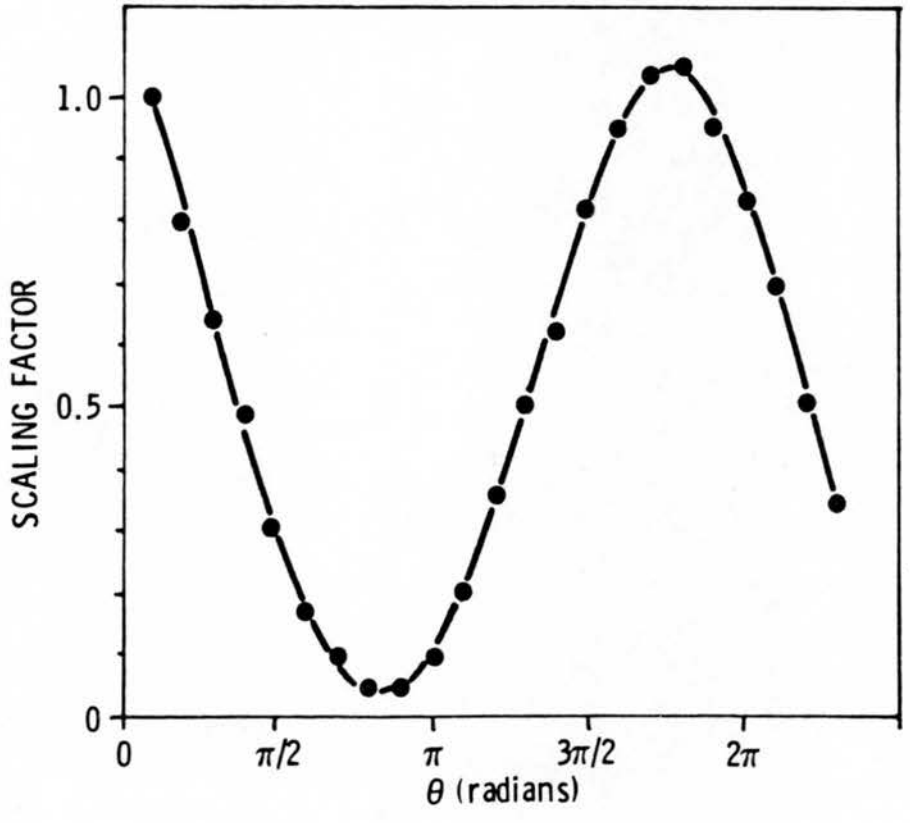

X. ANALYSIS OF THE ^{31}P LINEWIDTH IN ROTATING SOLIDS

One of the goals of solid state NMR is the observation if (isotropic) chemical shift information in solids. This must be performed on dilute spins in samples that contain one or more magnetically inequivalent sites and also contain abundant protons. In this case the result mimics the more conventional liquid spectroscopy with one delta function representing one site. However, these samples cannot be observed in conventional liquid spectrometers.

These are experimentally observed by a combination of solid state techniques. High power resonant proton decoupling removes the effects of the large static dipolar broadening between the abundant protons and the dilute spin of interest while magic angle spinning averages the chemical shift anisotropy to its isotropic value.

The intrinsic worth of this technique is directly related to the degree in which the linewidth can be narrowed and inversely to the final linewidth. This combination has been bery successful for ^{13}C NMR of solids where the linewidth can be as narrow as 1 Hz and is reduced from greater than 10^4 Hz. The situation for ^{31}P, however, is quite different. Residual linewidths are substantial, being on the order of 1-5 ppm (at 60.9 MHz) and this substantially degrades the resolution, reducing the ability of the method to discriminate sites

Figure X-1. Multiple pulse sequencies applied to solid methylphosphonic acid spinning at the magic angle. The spin rate was 3.0 KHz. The value of τ for each sequence was made equal to the rotor period as described in the text.

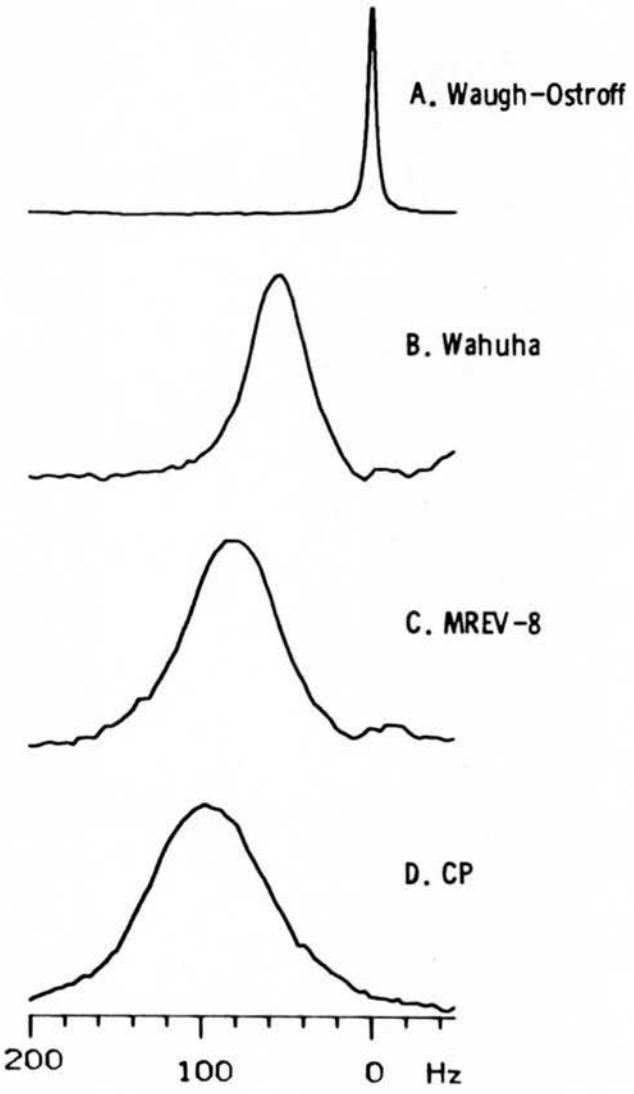

(Chapters 3-6).

There exists a class of experimental pulse sequences which have the remarkable ability to attenuate and even eliminate selected terms in the total spin Hamiltonian. This enables the contribution of each type of spin interaction to be determined in the experimental spectrum. These experiments have been used to analyze the linewidth of the ^{31}P resonance in magic angle spinning experiments with an eye towards improving the resolution if possible.

Figure X-1 shows the spectra obtained from a sample of methyl phosphonic acid powder using several multiple pulse sequences and also just cross polarization. These sequences were selected because they all average the homonuclear dipolar Hamiltonian to zero ($\bar{H}^{(o)}_{SS} = 0$) and scale the chemical shift by different amounts ($H^{(o)}_{\Delta S} = \alpha \cdot H_{\Delta S}$). The linewidth and the chemical shift scaling factor are plotted against each other in Figure X-2. This shows that when the effects of homonuclear dipoles are removed the residual linewidth is dominated by chemical shift-like terms (i.e., linear in $\vec{S}_z$). Chemical shift dispersion and bulk susceptibility anisotropy are possible candidates. From the Waugh-Ostroff sequence (SF = 0) the linewidth is dominated by $T_{1\rho}$ processes and a limiting linewidth of 5 Hz is obtained. The chemical shift concertina from Chapter IX was also used since this experiment leaves H_{SS} unaffected. Data was obtained with various scaling factors and plotted in Figure X-3. It can be seen that the dependence is more complex, however, in the limit of SF = 0, where

Figure X-2. Experimental scaling factor linewidth obtained from Figure X-1.

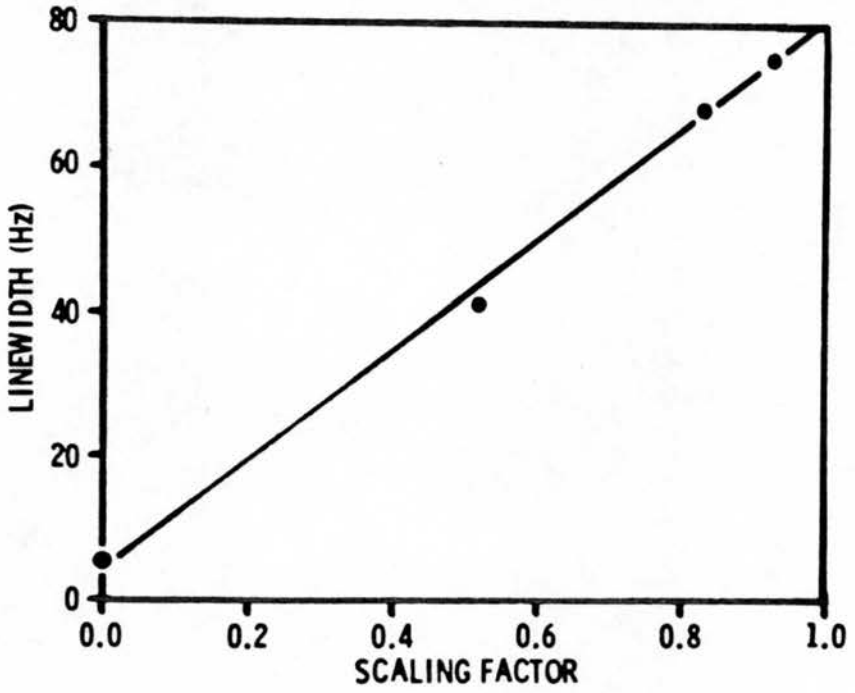

Figure X-3. Experimental scaling factor and linewidth obtained by scaling chemical shift-like terms using the chemical shift concertina described in Chapter IX.

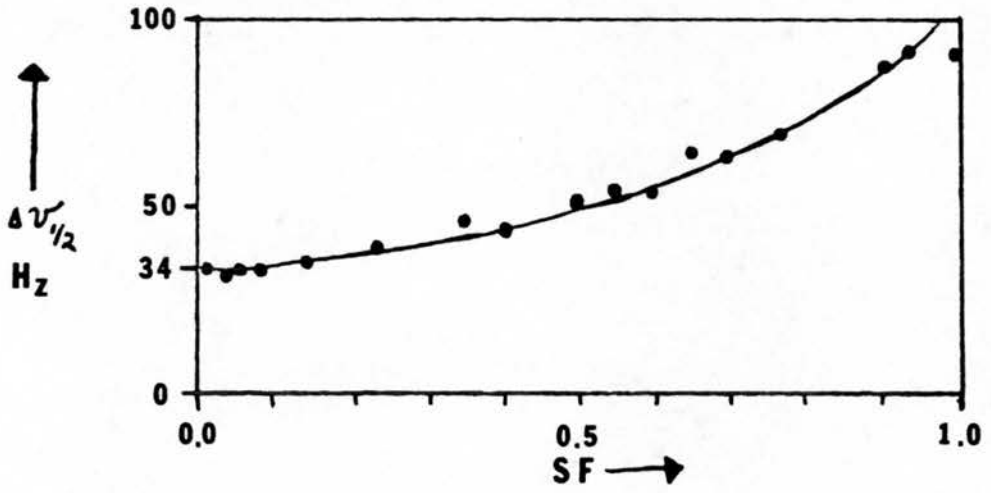

the effects of chemical shift are removed there is a residual linewidth of 34 Hz. This indicates that approximately 50 Hz is then due to the terms that are linear in spin.

It is clear that the residual $^{31}P-^{31}P$ dipoles contribute to the linewidth. Haeberlen and Waugh (1968) have shown using Average Hamiltonian theory, that the first order correction term depends on terms related to the static dipolar strength. Using the technique shown in Chapter VIII the $^{31}P-^{31}P$ dipolar strengths of $MePO_3H_2$, DNA, and fd virus are 1.48×10^5, 4.23×10^4, and 6.30×10^3 Hz^2, which directly measure dipolar strength. Since DNA and fd have smaller second moments they can be expected to have smaller contributions from this interaction. From this it can be inferred that the linewidth of $\approx$ 330 Hz (gaussian) seen in both DNA and fd are due to the chemical shift-like terms although at this time it is not possible to determine the exact nature of these. It would be possible to ascertain the extent that chemical shift dispersion influences these linewidths by the use of synthetic homo-polymers.

XI. ^{15}N NMR OF DNA

XI.1. INTRODUCTION

The nuclear properties of the stable isotopes of nitrogen present difficulties for high resolution NMR spectroscopy. ^{14}N although over 99% abundant has spin S = 1 with a large quadrapole coupling constant which results in broad lines in solution due to efficient nuclear quadrapolar relaxation. In solids, the lines in powder samples are very broad (although inhomogeneous) due to the large quadrapole moment. With single crystals splittings can be as large as several MHz (Stark *et al.*, 1978) making the spectroscopy difficult by feasible. Samples with the linewidth reduced by motional averaging are also possible (Siminovitch *et al.*, 1980).

The other stable isotope of nitrogen is ^{15}N with spin S = ½ but with a natural abundance of only 0.3% and a small negative gyromagnetic ratio. While labelled site studies are difficult due to long T_1's and negative Nuclear Overhauser effects (Levy and Licther, 1979) natural abundance work is presently all but out of the question on all interesting biological samples except formamide.

Spin S = ½ nuclei offer great opportunities for NMR spectroscopy of biological solids since observation of resonances from individual sites of biopolymers affords measurements that can give structural and

dynamic information with atomic resolution. Of the four spin S = ½ nuclei found in biopolymers (^{1}H, ^{13}C, ^{15}N, ^{31}P) only ^{15}N has not been exploited as a consequence of its unfavorable spin properties.

XI.2. ^{15}N LABELLING OF DNA

Meselson and Stahl (1958) first showed that when *E. coli* are grown on a medium with $^{15}NH_4CL$ as the sole nitrogen source, ^{15}N is incorporated into the newly synthesized biopolymers. By growing *E. coli* with the appropriate genetic compliment, whether wild type, or some arranged by mutation clonging, plasmid or viral infection, any gene or gene product of prokaryotic or eukaryotic origin can be uniformly labelled with ^{15}N. Growth on ^{15}N containing media has been used to provide several *in vivo* systems (Llinas *et al.*, 1975) and isolated biomolecules for solution NMR studies (Schaefer *et al.*, 1979).

E. coli infected with the filamentous bacteriophage fd were grown on minimal media supplemented with 1 gm/l $^{15}NH_4CL$ as the sole nitrogen source (Opella *et al.*, 1980b). After growing as usual the cells were spun down and the DNA was isolated using standard procedures (Smith, 1966). Briefly, cleared lysates were deproteinized using $CHCL_3$-amyl alcohol extractions followed by a phenol (Equilibrated with 1 M tris·HCl, pH 7) extraction. The high molecular weight DNA was

selectively precipitated leaving behind low molecular weight DNA and cellular RNA as shown by agarose gel electrophoresis. The gels also showed that a substantial fraction of the DNA is the same size as the replicative form of fd DNA. The DNA was then dissolved, dialyzed and precipitated with 0.75 M NaCl and 66% ETOH. The fibrous solid was washed in a Buchner funnel with 70% ETOH, abs. ETOH and briefly with acetone. It was dried at room temperature.

XI.3. Assignment of Resonances

Solid state NMR techniques (Chapter II) were used to differentiate between protonated and non-protonated nitrogen atoms. Protonated spins are selected for by early termination of the cross polarization mix interval after substantial magnetization has been transferred to the nitrogen atom with directly bonded protons but before it has reached the others. In this experiment a mix time approximately one-tenth as long as that necessary for maximum polarization was used (i.e., 0.2 versus 2.0 msec).

The SELPEN sequence (Chapter II) selects for non-protonated nitrogens by draining away magnetization from those atoms with directly bonded protons after all have been polarized; exactly the reverse of the previous situation.

With this simplification, the resonances were then fitted to theoretical spectra generated using chemical shift values of mono-

Figure XI-1. ^{15}N NMR (15.3 MHz) of ^{15}N perlabelled DNA spinning at the magic angle. The spin rate was 2.5 KHz. On the left are experimental spectra and theoretical spectra are to the right. Approximately 2000 transients were acquired for each spectrum. The protonated and all spectra were taken using cross polarization with 0.2 and 2.0 msec mix times, respectively. The non-protonated spectrum was taken using the SELPEN sequence with a 2.0 msec mix and 70 μsec delay times.

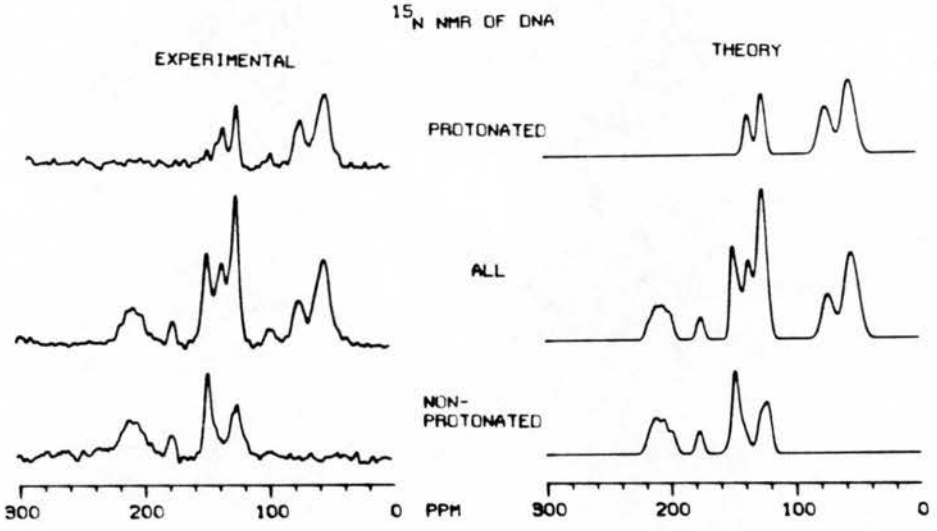

nucleotides in solution (Buchner *et al.*, 1978; Bachovitch and Roberts, 1978). The fit was improved manually by adjustment of each chemical shift value, linewidth and area under reasonable constraints. The resulting values obtained are shown in Table XI-1 and the spectra are shown in Figure XI-1. From the spectra it can be seen that the agreement is excellent with all resonances accounted for (the small peak at 100 ppm is due to a very small amount of protein amide resonances which are very strong). The table shows that most resonances are within 3 ppm of their solution values (one half of the line width) with only one resonance (C-3) being significantly moved.

TABLE XI-1 ^{15}N DNA CHEMICAL SHIFTS

Assignment	σ_{obs} ppm[a]	σ_{lit} ppm[a],[b]
G-NH_2	51.9	51.6
A-NH_2	56.8	58.0
C-NH_2	73.1	73.2
T1	123.8	125.4
G1	123.0	126.0
C1	129.4	132.0
T3	134.9	137.7
G3	142.1	145.1
A9	146.6	147.5
G9	146.8	147.1
C3	173.2	180.4
A3	196.6	196.7
A1	202.7	203.3
A7	207.5	210.4
G7	213.4	213.8

(a) Referenced to $^{15}NH_4NO_3$

(b) From Buchner *et al.*, 1978; Bachovitch and Roberts, 1978.

XII. ^{1}H-^{15}N SEPARATED LOCAL FIELD SPECTROSCOPY OF DNA

XII.1. THE METHOD

Separated Local Field Spectroscopy (SLF) is a method of determining hydrogen atom positions with very high accuracy by measuring the dipolar field (local field) generated by the proton.

The concept of a local field is not a new one (see for example; Slicther, 1978). It was first used by Pake (1948) to measure proton positions as described in Chapter VIII. The dipolar interaction has been used in many determinations of proton positions in solids (Opella and Waugh, 1977; Stoll *et al.*, 1976; Hester *et al.*, 1975a,b; Hester *et al.*, 1976; and Rybaczewski *et al.*, 1977). However, in each case an important condition was necessary; that the protons of interest form an isolated (separated) spin system with very few members. A pair provides a simple case and the addition of just one more member can be seen to increase the difficulty of calculation immensely (Gutlowsky *et al.*, 1949). The important point is that the spin system must be simple in order for the interpretation to be straight forward.

The heteronuclear dipolar interaction can also be used for this type of measurement. In this case, the relevant spin system would appear to be limited to the number of protons that can bond to a single atom. To achieve this simplicity in solids it is necessary

to decouple the protons from one another otherwise coupling of these protons will destroy the local field and complicate the calculation.

Waugh and his co-workers first performed this experiment on single crystals. I-I decoupling was not necessary since the dipolar linewidth due to proton spin diffusion was much smaller than the I-S dipolar splitting. Linder *et al.* (1980) took the next step to analyze the results from powders. In order to measure accurate lineshapes in both dimensions I-I decoupling was employed to reveal the fine structure. Although interesting, this experimental regime was disappointing due to the inability to discriminate detailed relative tensor orientations of the Hamiltonians involved and overlap of chemical sites.

Magic Angle Sample Spinning is useful for deserving powders since chemically shifted sites could be separated and their bond lengths (with bonded protons) could be measured. However, it was quickly determined that the heteronuclear dipolar interaction (under the conditions of the separated field) was inhomogeneous and the dipolar powder pattern broke up into sidebands. A sideband analysis similar to that used for chemical shift powder patterns would be appropriate (Hertzfeld and Berger, 1980). The details of a spinning dipolar pair have been worked out previously (Evans and Powles, 1967; Dreitlen and Kessemeir, 1961; and Andrew and Newing, 1958).

Figure XII-1 shows this experiment applied to ^{15}N-acetyl-glycine powder spinning at 1.7 KHz. The contour plot displays the entire 2-dimensional data matrix ($S(\omega_1, \omega_2)$) at once, while each of

Figure XII-1. 2-D Separated Local Field Spectrscopy of ^{15}N-acetyl-glycine spinning at 1.7 KHz. A total of 4096 transients were obtained to generate this spectrum. Also shown are slices in each of the isotropic chemical shift and dipolar dimensions.

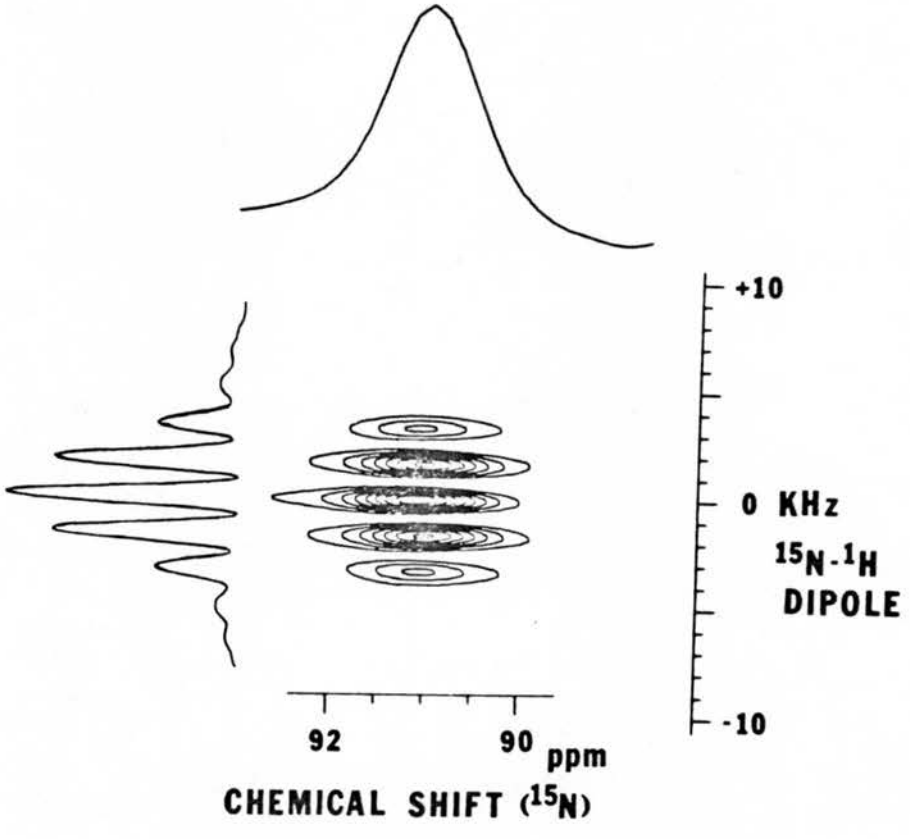

the orthogonal dimension slices give spectra that correspond to different terms of the total spin Hamiltonian. The slice taken at the center of the dipole dimension ($\Delta\upsilon_{IS} = 0$) gives the isotropic chemical shift spectrum. While the orthogonal slice at constant chemical shift (σ_S = 91 ppm) shows the ^1H-^{15}N dipolar powder pattern broken up into sidebands spaced at multiples of the spinner period. The analysis of this dimension reduces to a problem of fitting the intensity pattern of the sidebands (Hertzfeld and Berger, 1980).

Figure XII-2 shows just this type of analysis. Spectra obtained with and without spin locking of the protons at the magic angle are shown. This manipulation has two effects : 1) decoupling of the protons from one another ($\bar{H}_{II}^{(o)} = 0$) and 2) attenuating the heteronuclear dipolar interaction by $1/\sqrt{3}$ ($\bar{H}_{IS}^{(o)} = 1/\sqrt{3}\ H_{IS}$). The second effect changes the relative sideband intensities while the first effect results in the convolution of the dipolar spectrum with a several KHz wide Gaussian that is related to the rate of spin diffusion. The dipolar spectrum obtained by complex Fourier transformation of the chemical shift interferograms are shown in the bottom of the figure while those obtained by transforming the real part of the interferograms are in the middle. This is equivalent to taking only the even frequency terms of the dipolar spectrum. The theoretical spectra are shown in the top of the figure.

Figure XII-2. Sections of Figure XII-1 at constant σ. To the left are I-I decoupled spectra and to the right are I-I ceoupled. (A) Theoretical spectra for ν_{rot} = 1.7 KHz and r_{is} = 1.01 Å, (B) Dipolar spectra with only even dipolar terms present, and (C) Dipolar spectra with all terms present. All sections were taken at σ = 91 ppm. Full sweep width is 32 KHz. The experimental scaling factor is 0.49.

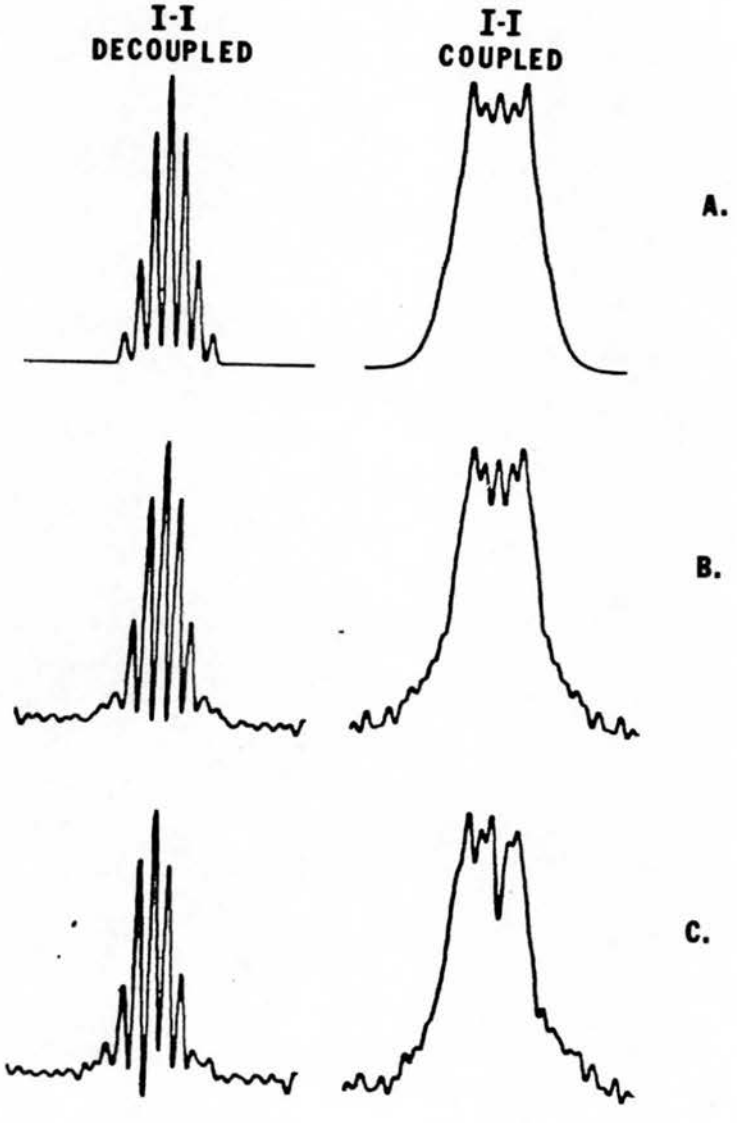

XII.2. Configuration of DNA

Since the sample used was dehydrated DNA, the configuration must be established. The DNA was stored at a relative humidity under 55% where Franklin and Gosling (1953) observed x-ray diffraction pictures showing no ordered structure. There is no diffraction data available to decide whether the base pairs are hydrogen bonded or not so other spectroscopic data must be used to settle this point.

It is a well known fact that the presence of water among DNA helicies is not a directly contributing influence on the formation of hydrogen bonds and that the helical form can exist in the absence of many H-bonds. This is demonstrated by the observation that H-bonding occurs between base pairs in non-aqueous solvents (Voet and Rich, 1970; Bovey, 1972). In fact, water molecules form stronger H-bonds with the bases. It has been suggested that the helical structure of DNA is stabilized by maximizing the number of relatively strong water-water contacts (Herskovits *et al.*, 1961) and it is most unlikely that the removal of water from the grooves of the helical structure itself weakens the base pairing H-bonds. In a spectroscopic study of oriented DNA samples Falk *et al.* (1963) have interpreted the lowering of the ultraviolet dichroic ratio as an indication of a loss of systematic base stacking and base pairing, although the basis for the latter interpretation is rather sparce. In fact, they interpret the

IR bands at 3206 and 3353 cm^{-1} in dry DNA as arising from H-bonds in the range of 2.92-3.02 Å, along with a negligible fraction of the total H-bonds being somewhat stronger and then conclude on this basis "...that the bulk of the hydrogen bonds which exist in the solid denatured state are of equal length and therefore, nearly equal strength to those formerly existing in the B configuration."

XII.3. Measurement of N-H Bond Lengths in DNA

Figure XII-3 presents the two dimensional results from ^{15}N labelled duplex DNA. The chemical shift axis is the same as that used in the assignments of the previous chapter. By correlating chemical shifts with the dipolar sideband spectra, the ^{15}N sites can be divided into those without nearby protons showing up as single lines; those with one and two protons showing fine structure.

Quantitative analysis involves evaluation of spinning sideband intensities of slices at constant chemical shift. These are shown in Figure XII-4 for three protonation states of the nitrogens. The non-protonated nitrogen shows no evidence of sideband structure, this would indicate that a proton is no closer than 2 Å. The singly protonated nitrogen assigned to guanine N-1 is the proton donor of a hydrogen bond. The experimentally measured N-H bond length is 1.11 ± 0.03 Å. This is slightly longer than expected on the basis of various

Figure XII-3. 2-D SLF spectrum of ^{15}N DNA spinning at 2.5 KHz. Note the effects of nearby protons in the dipolar dimension.

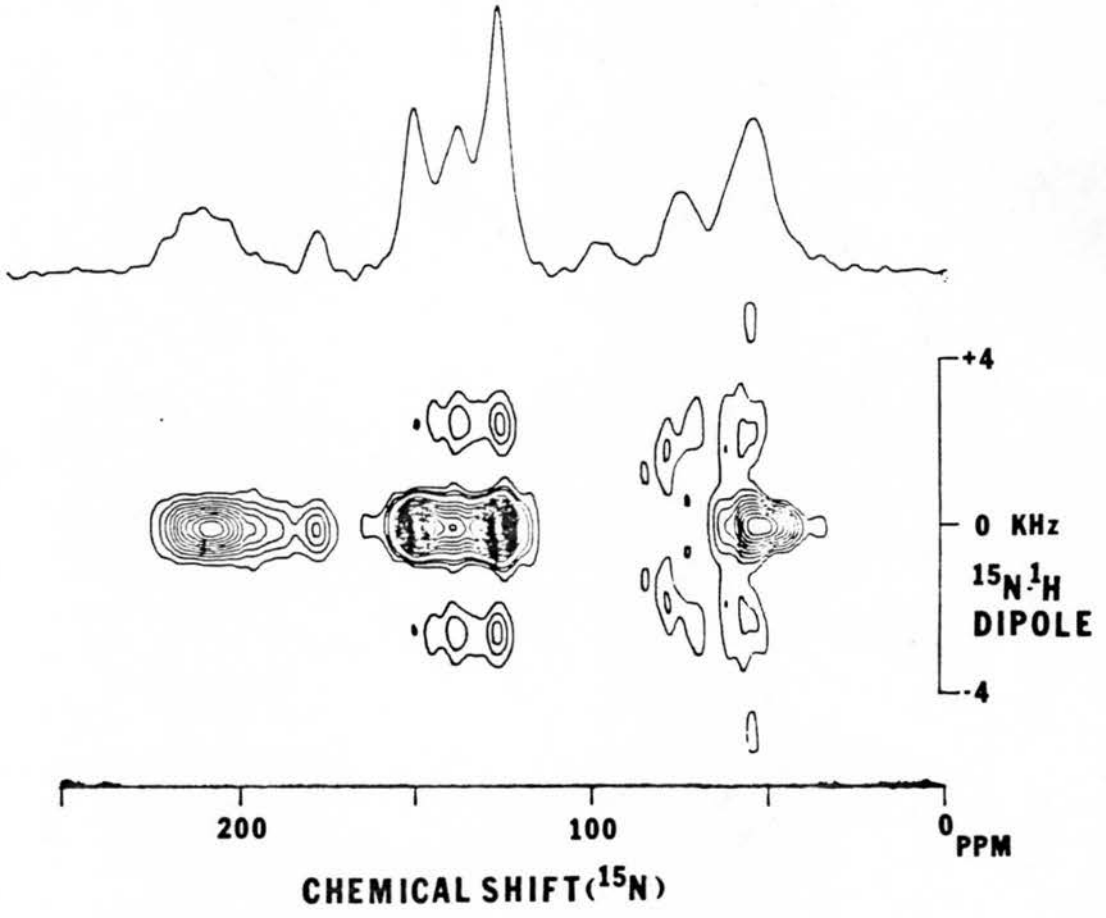

neutron diffraction studies of small H-bonded molecules (Vinogradov and Linnell, 1971) and a model base pair (Frey *et al.*, 1973). The source of this disagreement could be due to experimental errors in the measurement of the scaling factor or it could be due to the disorder in the anhydrous solid. Since there is no other data available on this latter point it is difficult to assess its merits. Alternately, there might be some averaging of the interaction by motion of the hydrogen atom which would cause the bond length to appear longer. In an interesting high precision neutron diffraction study of potassium hydrogen bisacetyl salicylate, Sequeira *et al.* (1967) found a large thermal motion in the hydrogen atom relative to the oxygen atoms along the H-bond (apparent amplitude-0.19 $\mathring{A}_{rms}$). Assuming harmonic motion,this corresponds to an apparent amplitude of 0.27 $\mathring{A}_{peak}$. Perpendicular to the bond the amplitudes were much smaller (0.03 and 0.08 $\mathring{A}_{rms}$). In the presence of motion such as this, the measurement of the average interaction yields the average cubed bond length ($\langle\overline{r^3}\rangle$) which is quite different from the average bond length cubed ($\langle\bar{r}\rangle^3$). If the equilibrium N-H bond length is 1.01 $\mathring{A}$ then an apparent deflection of 0.55 $\mathring{A}_{peak}$ would be necessary to account for an observed bondlength of 1.11 $\mathring{A}$. Even though this is much larger than the value observed by Sequeira *et al.* it is not unreasonable since their H-bonded system was unusually short.

The data for the NH_2 group are also shown here except that the experimental and calculated spectra do not agree at all. It is likely

Figure XII-4. Sections of Figure XII-3 at constant σ representing nitrogen atoms with (a) no, (b) one, and (c) two bonded protons (top). Theoretical spectra for non-protonated (a), singly protonated (r_{is} = 1.11 Å), (b) and doubly protonated (r_{is} = 1.13 Å, ISI = 109.7°) (c). Full sweep width is 16 KHz. The experimentally determined scaling factor was 0.49.

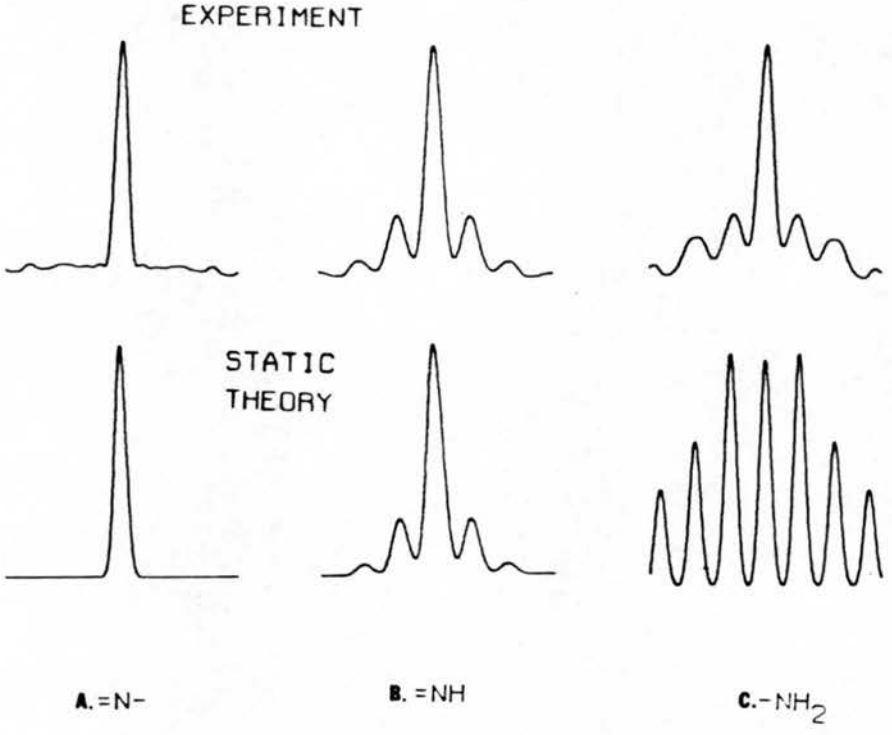

that the protons are undergoing a fast exchange via quantum mechanical tunneling since there is ample evidence for this type of phenomenon occurring in solids (see Ikeda *et al.*, 1979 and references contained therein). To analyze this a flip averaged tensor would have to be generated from the static dipolar tensor and then the usual sideband analysis performed. A preliminary analysis has been performed based on the work of Waugh *et al.* (1953) in the linear bifluoride ion, however, the results have been equivocal. More work is necessary using model substances such as ^{15}N urea.

XIII. CONCLUSION

These NMR experiments provide information on the properties of DNA. The purpose of the study is to compare DNA in the solid state, in solution and in DNA-protein complexes with regards to structure and dynamics. Solid state NMR techniques clearly make it possible to study high-molecular weight DNA and DNA-protein complexes.

The phosphodiester backbone of DNA itself in solution has substantial mobility. The single stranded polymer is capable of nanosecond motion (Akasaka *et al.*, 1977). While the pairing of two polymers reduces the mobility somewhat, the resulting dsDNA is still a flexible polymer. In addition, it is seen that the motion is isotropic, that is there is no preferred bending direction. The addition of still another strand to create triple helix as in Poly-A-$(Poly-U)_2$ (see Appendix B) converts the flexible polymer into a rigid rod.

Although not conclusive, our results suggest that the phosphodiester backbone of these polymers retains its flexibility and it is the association of several of these strands and the interstrand interactions that result in the immobilization.

DNA packaged in or associated with proteins is substantially immobilized. No perturbation of the phosphodiester backbone has been observed by ^{31}P NMR and in fact, the picture is emerging that while structural perturbations of DNA by protein interactions are subtle or

not detectable by ^{31}P chemical shift measurements the associated dynamical effects are profound.

DNA encapsulated by the fd coat-protein which constitutes the intact virion loses its flexibility and adopts the dynamics of the whole particle, that is, moderately slow rotation about the long axis of the filament as shown conclusively by a number of experiments. This has important implications for the x-ray fiber diffraction studies since it rules out internal motion of the DNA as a reason for the lack of observable signals from fd DNA by this technique.

Double stranded DNA complexed with eukaryotic histones and protamines is substantially immobilized. This case is slightly more complicated because there is some reduction of the static ^{31}P NMR chemical shift powder pattern. This reduction could be explained by either of two mechanisms. Firstly, the interaction of the phosphates with the complexing proteins may alter the electronic distribution about the phosphorous nucleus resulting in a smaller static anisotropy. This however, is considered unlikely since a change in the anisotropy itself would probably be felt at one or two of the principle elements of the chemical shielding tensor. This would result in a change of the isotropic chemical shift a parameter that was measured in the MASS experiment and found to be unchanged. The resolution is not limited in this case by the broad linewidth of the spinning sample since the reduction of 60 ppm would result in as much as 20 ppm worth of shift in the isotropic chemical shift.

Alternately, the presence of fast motion ($>>10^4$ s^{-1}) of limited amplitude would explain the results. This type of motion would be effective in reducing the anisotropy without changing the isotropic chemical shift. Since only a small range of angles would be averaged over, a small reduction of the static anisotropy would be expected. The remaining anisotropy would then appear to be static (at least at the time scale monitored in this experiment) and sidebands would be expected in the MASS experiment. It is clear that the experimental evidence favors the latter explanation. This would imply that the DNA is rattling around in some kind of protein cage which would allow it to move freely and quickly over limited excursions while restraining it from making large amplitude rotations. Except for this small amplitude fast motion these nucleoprotein complexes are completely immobilized on a 10^{-4} s timescale.

The possibility of extreme mobility in this state of extreme compaction has profound implications for the occurrence of biological processes. It is conceivable that this mobility is indicative of an accessibility of the nucleic acid to not only the solvent and small molecules but to larger ones. This could be effected by a loose linkage between the protein and DNA that could allow the nucleosomes to pass along the length of the polymer giving all regions of the DNA free access. It would be interesting to study the DNA dynamics as a function of the state of reconstitution of these types of complexes in an attempt to elucidate more details of this compaction.

B-form DNA in the solid state is the only form of DNA studied here that exhibits local motion. Averaging of the ^{31}P chemical shielding tensor is observed for temperatures over $5^{o}C$ while the ^{2}H quadrapolar tensor of C-8 deuterons on the purine bases remains unaffected at temperatures as high as $50^{o}C$. Since the timescales for these interactions are approximately equal the difference in the result must lie in the sites that are monitored. Hence, it can be concluded that the phosphate groups of this sample are mobile above $5^{o}C$ whereas the interior base pairs are immobile on a $10^{-4 \rightarrow -5}$ s timescale. This finding is most interesting for the interperation of x-ray fiber diffraction data of B-DNA. It is likely that the phosphate structures are smeared out in space (as the diffraction technique would see it) and that improved fit between the observed and calculated diffraction intensities would be obtained if the local mobility of the phosphates was included.

^{31}P isotropic chemical shifts have been disappointingly insensitive to DNA structure. The sensitivity of ^{31}P NMR chemical shifts is reasonable enough as shown by Gorenstein (1975), but it could be that the perturbations are just to small to be seen by this interaction. The large linewidth of the spinning ^{31}P resonance could be obscuring the detailed chemical shift information. In fact, this linewidth probably contains some structural information by virtue of the chemical shift dispersion as determined in Chapter X. It is likely that part of the linewidth represents a distribution of chemical

shifts representative of a distribution of environments of the sites from the micro-variations of nearby neighbors. It appears that the presence of small amounts of water has important effects in the solid state. Very recent work in this laboratory has shown that MASS linewidth of hydrated solids is narrower that that of lyophilized solids. This is quite dramatic in the case of ^{15}N MASS NMR of B-form DNA where lines have sharpened enough to almost allow single site resolution across the entire spectrum. This could be due to the freezing out of molecules in slightly different configurations each of which has slightly different isotropic chemical shifts. It would not be surprising to find a gaussian distribution here. The addition of a small amount of water could be sufficient to allow these molecules to reach their local energy minima essentially all of them being in the same configuration. An interesting test of this would be ^{31}P MASS of the B-form DNA in the solid state. A narrower resonance would then be expected possibly revealing detailed chemical shift information.

The various dipolar interactions have yielded a great deal of structural information. In the case of the filamentous viruses, evidence has been presented against the need to invoke an unusual DNA structure for the fd DNA. It is clear however, that this work is in its preliminary stages and many improvements are envisioned. For example, it is commonly presumed that the basic amino acids of the coat-protein lie in close proximity to the phosphates of the DNA

which would bring the quadrapolar ^{14}N nuclei near to the ^{31}P nuclei. The effect of this type of interaction has been neglected in this work. To determine the contribution that this makes the experiment would be repeated using per ^{15}N-labelled virus and/or with nitrogen decoupling.

The SLF experiment constitutes the first measurement of an N-H bond length in a high molecular weight DNA polymer. And while there may still be some question as to whether this is a hydrogen bonded system these experiments are being repeated using B-form DNA hydrated as in Chapter VII as this thesis is being written. Preliminary results are in complete agreement with the bond length presented here and also agree with the conclusion of Chapter VII that the base pairs are rigid on a 10^{-4} s timescale. It would be of great interest to repeat these experiments using DNA-complexes to attempt to localize any specific hydrogen bonding with the proteins and to look for more details of the nucleic acid dynamics.

APPENDIX A. CALCULATION OF ZERO ORDER AVERAGE HAMILTONIAN FOR CHAPTER IX

In this appendix the methods developed by Haeberlen and Waugh (1968) for calculation of Average Hamiltonians will be applied to the 4 pulse chemical shift averaging sequence presented in Chapter IX.

CORRECTED CONCERTINA

$$90_x\ \tau_s\ [\theta_{-x}\ \tau_s\ \theta_x\ \tau_s\ \theta_x\ \tau_s\ \theta_{-x}\ \tau_s]_N$$

$$
H_{rf}(t) = \begin{cases}
-\theta/\tau w\ \vec{I}_x & 0 < t < \tau w \\
0 & \tau w < t < \tau w + \tau s \\
+\theta/\tau w\ \vec{I}_x & \tau w + \tau s < t < 2\tau w + \tau s \\
0 & 2\tau w + \tau s < t < 2\tau w + 2\tau s \\
+\theta/\tau w\ \vec{I}_x & 2\tau w + 2\tau s < t < 3\tau w + 2\tau s \\
0 & 3\tau w + 2\tau s < t < 3\tau w + 3\tau s \\
-\theta/\tau w\ \vec{I}_x & 3\tau w + 3\tau s < t < 4\tau s + 3\tau s \\
0 & 4\tau w + 3\tau s < t < 4\tau w + 4\tau s
\end{cases}
$$

$$H_{int} = \Delta\omega \vec{I}_z$$

where: $\Delta\omega = \gamma(1 - \sigma)B_o$

The time development of the density matrix $(P(t))$ is given by:

$$P(t) = L(t)P(o)L^{+}(t)$$
$$\dot{L}(t) = -H(t)L(t)$$
$$L(o) = 1$$

The formal solution of which is:

$$L(t) - T_{exp}(-i\int_{o}^{t}H(t^{1})dt^{1})$$

Since $(H(t + \tau_c) = (t))$ (i.e., H is cylic modulo τ_c)

$$L(N\tau_c + t) = L(t)\ [L(\tau_c)]^{N} \quad N = 0, 1, 2,.....$$

We can factor into two parts

$$H(t) = H_1(t) + H_2(t) \text{ then:}$$
$$L(t) = L_1(t)\tilde{L}_2(t)$$

$$L_1(t) = T_{exp}(-i\int_{o}^{t}H_1(t^{1})dt^{1})$$
$$\tilde{L}_2(t) = T_{exp}(-i\int_{o}^{t}\tilde{H}_2(t^{1})dt^{1})$$
$$\tilde{H}_2(t) = L_1^{-1}(t)H_2(t)L_1(t)$$

The Hamiltonian for this experiment can be factored into:

$$H(t) = H_{rf}(t) + H_{int}(t)$$

where: $H_{rf}(t) <> H_1$

$H_{int}(t) <> H_2$

then: $L(t) = L_{rf}(t)\ L_{int}(t)$

The propagtor can now be written down:

$$L_{RF}(t) = \exp(-i \cdot \theta/\tau w\ t\ \vec{I}_x)$$

$$= \exp(-i \cdot \theta \cdot \vec{I}_x)$$

$$= \exp(+i \cdot \theta/\tau w(t-(2\tau w + \tau s))\vec{I}_x)$$

$$= 1$$

$$= \exp(+i \cdot \theta/\tau w(t-(2\tau w + 2\tau s))\vec{I}_x)$$

$$= \exp(+i \cdot \theta \cdot \vec{I}_x)$$

$$= \exp(-i \cdot \theta/\tau w(t-(4\tau w + 3\tau s))\vec{I}_x)$$

$$= 1$$

each expressed over the appropriate time interval.

Now $H_{int}(t)$ can be calculated by:

$$_{int}(t) = L_{rf}^{-1}(t)\ H_{int}(t)\ L_{rf}(t)$$

$\tilde{H}_{int}(t)$

$= -\Delta\omega(\vec{I}_z \text{ Cos}(\theta/\tau w\ t) + \vec{I}_y \sin(\theta/\tau w\ t))$

$= -\Delta\omega(\vec{I}_z \text{ Cos } \theta + \vec{I}_y \sin\theta)$

$= -\Delta\omega(\vec{I}_z \text{ Cos}(\theta/\tau w(t-(2\tau w + \tau s)))-\vec{I}_y \sin(\theta/\tau w(t-2\tau w + \tau s))))$

$= -\Delta\omega(\vec{I}_z)$

$= -\Delta\omega(\vec{I}_z \text{ Cos}(\theta/\tau w(t-(\tau w + 2\tau s)))-\vec{I}_y \sin(\theta/\tau w(t-(\tau w + 2\tau s))))$

$= -\Delta\omega(\vec{I}_z \text{ Cos } \theta - \vec{I}_y \sin\theta)$

$= -\Delta\omega(\vec{I}_z \text{ Cos}(\theta/\tau w(t-(4\tau w + 3\tau s)))+\vec{I}_y \sin(\theta/\tau w(t-(4\tau w + 3\tau s))))$

$= -\Delta\omega(\vec{I}_z)$

The cyclic time dependence of $H_{rf}(t)$ has been imposed upon H_{int} making it $H_{int}(t)$. The zero order average Hamiltonian ($\bar{H}^{(0)}$) can be calculated over the cycle time as:

$$H^{(0)} = \tau_c^{-1} \int_0^{\tau c} \tilde{H}_{int}(t^1)\,dt^1$$

$$\bar{H}^{(0)} = \frac{-\Delta w}{\tau c} \int \vec{I}_z \cos(\theta/\tau w\, t) - \vec{I}_y \sin(\theta/\tau w\, t))dt$$

$$+ L(\vec{I}_z \cos\theta + \vec{I}_y \sin\theta)dt$$

$$+ \int(\vec{I}_z \cos(\theta/\tau w[t - (2\tau w + \tau s)])$$

$$-(\vec{I}_y \sin(\theta/\tau w[t - (2\tau w + \tau s)]))dt$$

$$+ L(\vec{I}_z)dt$$

$$+ \int(\vec{I}_z \cos(\theta/\tau w[t - (3\tau w + 2\tau s)])$$

$$-\vec{I}_y \sin(\theta/\tau w[t - (3\tau w + 2\tau s)]))dt$$

$$+ \int(\vec{I}_z \cos\theta - \vec{I}_y \sin\theta)dt$$

$$+ \int(\vec{I}_z \cos(\theta/\tau w[t - (4\tau w + 3\tau s)])$$

$$+(\vec{I}_y \sin(\theta/\tau w[t - (4\tau w + 3\tau s)]))dt$$

$$+ L(\vec{I}_z)dt$$

again, each is over the appropriate time interval.

After considerable algebraic rearrangement we obtain:

$$\bar{H}^{(0)} = \frac{-\Delta w}{\tau c} \cdot 4 \cdot [2(\tau w/\theta)\sin(\theta/2) + \tau s \cos(\theta/2)] \times \cos(\theta/2) \cdot \vec{I}_z$$

APPENDIX B. ^{31}P CHEMICAL SHIFT TENSOR IN DNA

The object here is to determine the ^{31}P CS tensor in the frame of the fiber (FF) (XYZ). This is defined in Figure B-1. The $\vec{Z}$-axis is parallel to the fiber axis, the $\vec{Y}$-axis is perpendicular to the fiber axis and along a radial line through the phosphorus atom. The $\vec{X}$-axis is tangential to the radial circle formed by the locus of the phosphorus atoms.

Hertzfeld *et al.* (1978) have determined the ^{31}P CS tensor for barium diethyl phosphate (BDEP), a model substance. The principle values of DNA and the orientation of BDEP will be used. The principle values are +79.5, +17.5 and -109.8 ppm from 85% H_3PO_4 (isotropic shift = -5.47 ppm). These values are reasonably close to those found in DNA (+83, +25, -110 ppm and isotropic = -0.67 ppm). The tensor given in a molecular frame (MF; xyz) shown in Figure B-2. The plane drawn in Figure B-2 is defined by the O_3-P-O_4 plane and the $\vec{x}$-axis is defined to be along the O-P-O bisector. The $\vec{z}$-axis is normal to the plane and the $\vec{y}$-axis is orthogonal to both forming a right-handed system. The CS tensor in its PAS can be rotated into this xyz frame using the two rotation matricies in Hertfeld *et al.* (1978). The tensor in the xyz frame is:

Figure B-1. Fiber frame of DNA.

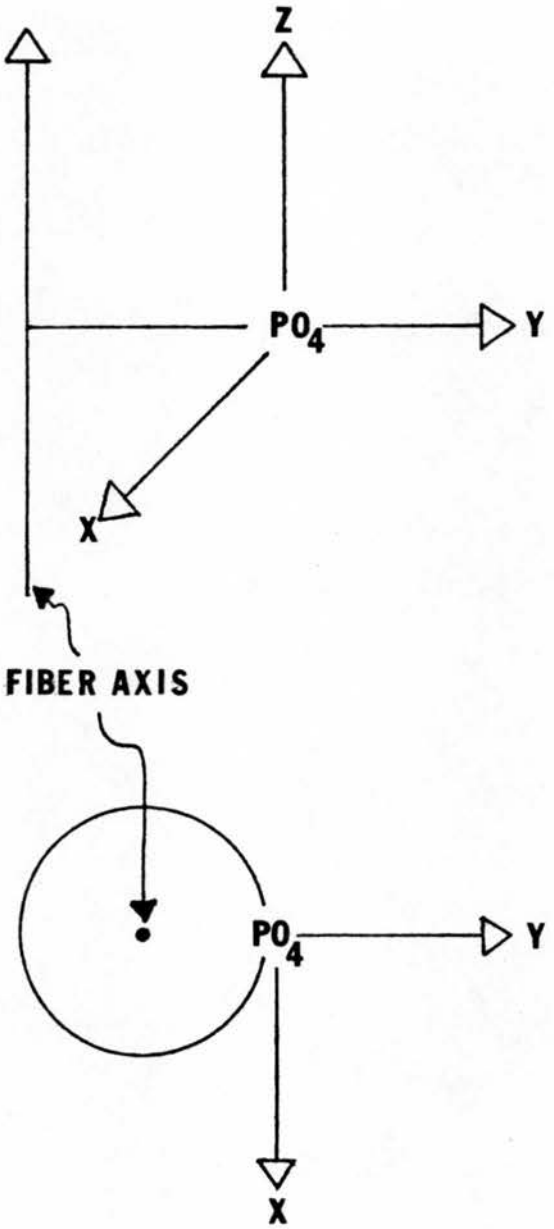

$$\sigma_{xyz} = \begin{matrix} +26.6 & + 1.4 & - 9.8 \\ + 2.4 & -108.3 & +17.8 \\ - 9.8 & +17.8 & +79.7 \end{matrix}$$

It can be seen that the tensor fits naturally into this frame. While it is not diagonal it is almost so. Also, the tensor is symmetric (as it should) and the trace is the same as the xyz tensor (these two tests will be applied at every step as a check of mathematical errors). σ_{11} = +83 is approximately along $\vec{z}$, σ_{22} = +25 is close to $\vec{x}$ and σ_{33} = -110 is close to $\vec{y}$.

The next step is to determine the orientation of this MF in the FF using atomic coordinates obtained from x-ray diffraction data, and determine the rotation matrix needed to take MF into FF. The atomic coordinates used are obtained from (Langridge *et al.*, 1960) Model 3. The coordinates are given in terms of cylindrical coordinates shown in Figure B-3. r is the radial distance from the ten-fold screw axis, ϕ is the twist from the dyad axis and z is the distance projected along the ten-fold screw axis. The coordinates are given as:

Atom	r(Å)	ϕ	z(Å)	as defined in Figure B-2
P	9.05	58.8	-1.36	P
O_1	8.88	62.9	0.04	O_1
O_2	9.14	65.3	-2.45	O_4
O_3	10.33	54.2	-1.18	O_2
O_4	7.85	52.3	-1.43	O_3

Figure B-2. Phosphate molecular frame.

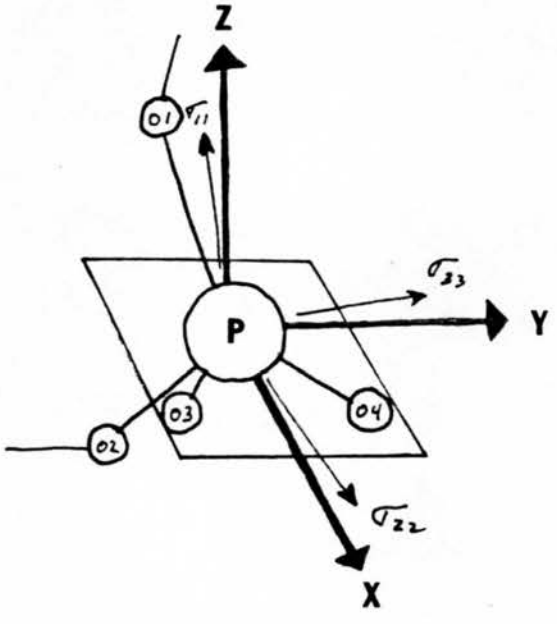

First, these are converted to cartesian coordinates with an origin congruent with the cylindrical coordinates and axes defined as in Figure B-3. Next, the origin is translated to the phosphorus atom. The coordinates are then given as:

Atom	x(Å)	y(Å)	z(Å)
P	0	0	0
O_1	-0.64	0.17	1.40
O_2	-0.87	0.56	-1.09
O_3	-1.35	0.64	0.18
O_4	0.11	-1.53	-0.07

Now, the xyz frame can be elaborated. Since the origin is at (0, 0, 0) any point P (x_p, y_p, z_p) can be thought of as a (direction) vector. To get the $\vec{x}$-axis previously defined as the bisector of O_2-P-O_4, we need only take the arithmetic mean of the O_2 and O_4 direction vectors to get the bisector vector. $\vec{x}$ = (-0.449, -0.573, -0.685). From the coordinates of the O_2, O_4 and P atoms a plane can be defined. A plane is defined by the general equation: $ax + by + cz + d + 0$. From the coordinates the coefficients can be determined as a = 1, b = 0.106, c = -0.744, and d = 0. The normal to this plane is the $\vec{z}$-axis and can be determined easily. $\vec{z}$ = (0.799, 0.085, -0.595). Now by definition $\vec{z} \times \vec{x} = \vec{y}$, so: $\vec{y}$ = (-0.399, 0.814, -0.420) and we have defined the xyz system in terms of XYZ. The last step is to generate the tensor which takes xyz into XYZ and apply it to the σxyz to get σXYZ. The rotation matrix is:

Figure B-3. Geometry of Watson-Crick structure in cylindrical coordinates.

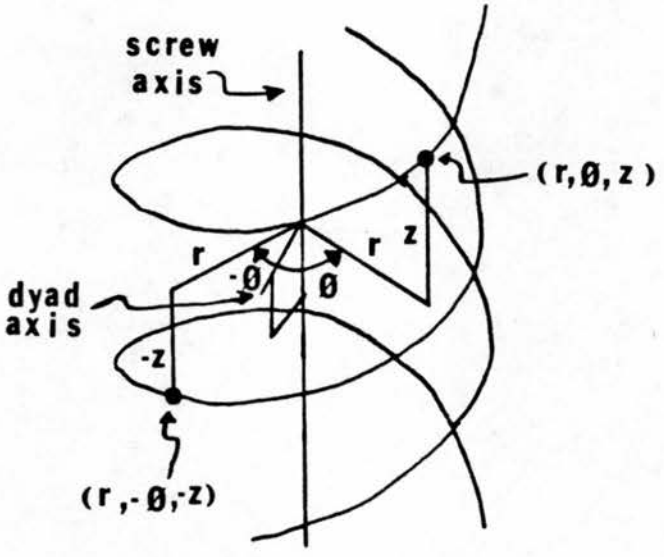

$$R = \begin{bmatrix} -0.449 & -0.399 & 0.799 \\ -0.573 & 0.814 & 0.085 \\ -0.685 & -0.420 & -0.595 \end{bmatrix}$$

And the final tensor $\sigma_{XYZ} = R\sigma_{xyz}R^{-1}$

$$\sigma_{XYZ} = \begin{bmatrix} +35.2 & +63.1 & -46.2 \\ +63.1 & -60.3 & +31.0 \\ -46.2 & +31.0 & +23.3 \end{bmatrix}$$

With the knowledge of the shielding tensor in the fiber frame it is an easy matter to perform manipulations (i.e., time averages over certain types of motion) to determine structure and dynamics. This will now be applied to the ^{31}P NMR spectra obtained from (Poly-A-(Poly-U)$_2$ in solution. There is considerable evidence that the AU_2 molecule is stiffer than or DNA so it is very likely that the axially symmetric pattern observed is due to rapid rotation about the fiber axis of the nucleic acid molecule ($\vec{z}$ axis). To perform the time average of the static tensor it is only necessary to use the spatial average of three sites (Andrew, 1956) so the following matrix equation is solved:

$$\sigma_{Ave} = 1/3\left[R(0)\sigma_{xyz}\ R^{-1}(0) + R(120^{o})\sigma_{xyz}\ R^{-1}(120^{o}) + R(240^{o})\sigma_{xyz}\ R^{-1}(240^{o})\right] \qquad \text{(B-1)}$$

where

$$R(\alpha) = \begin{bmatrix} \cos\alpha & \sin\alpha & 0 \\ -\sin\alpha & \cos\alpha & 0 \\ 0 & 0 & 1 \end{bmatrix}$$

The average tensor obtained is:

$$\sigma_{Ave} = \begin{bmatrix} -12.6 & 0 & 0 \\ 0 & -12.6 & 0 \\ 0 & 0 & +23.3 \end{bmatrix}$$

which agrees very well with the experimental data shown in Figure B-1.

Figure B-4. ^{31}P NMR (60.9 MHz) spectra of Poly-A-(Poly-U)2 in solution.

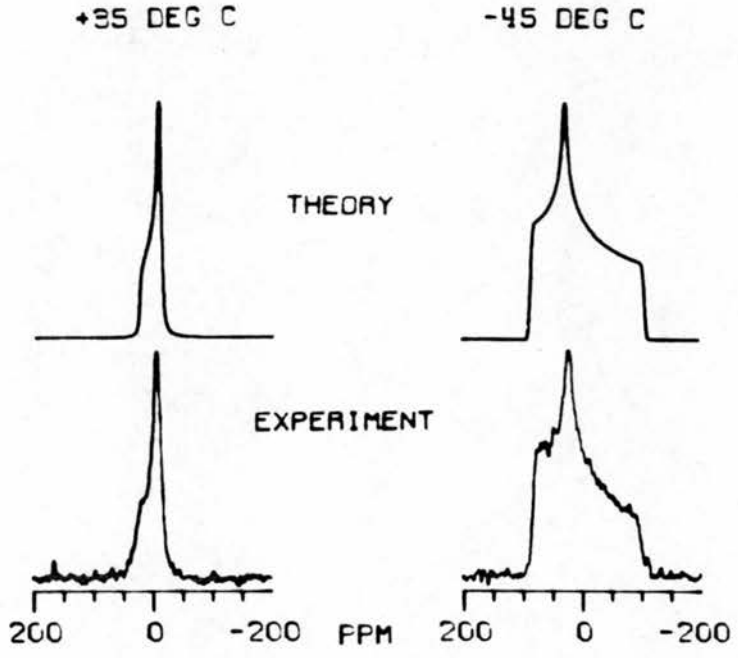

APPENDIX C. PROBE RF DESIGN

IF IT DOESN'T FIT, FORCE IT; IF IT BREAKS
THEN IT NEEDED REPLACING ANYWAY.

MURPHY

C.1. RATIONALE

The probe is where the action is in a solid state spectrometer. Basically the probe is a transducer which converts electrical energy into magnetic energy and back. This is not a tall order except when it must do so at two different frequencies and be able to detect 10^{-12} watts of nuclear induction. This is not difficult except that there must be 10^{3} watts of decoupling power present at the other (proton) frequency at the same time. In many high resolution experiments this state of affairs must be maintained for as much as one second. This can be likened to detecting the splitting of a single uranium atom (10^{-4} erg) in the presence of a blow from an elephant gun (10^{10} erg).

From this description it can be seen that double resonance probes must possess the following attributes:

1) high power handling capability
2) high Q factor for efficiency in electrical to

magnetic energy conversion and visa versa

3) high isolation between the two frequencies

The reasons for the desirability of high Q and power handling are actually the same. The resistive losses present in a tuned circuit are where the power is dissipated as heat and inefficiency in generating large RF fields occurs. Similarly these same resistive losses are where the precious nuclear signal is buried under thermal noise and lost to the experimenter.

Coil Q's are kept high by the use of large gauge wire, usually AWG #16 to 20. Silver plating is sometimes used to improve the Q in VHF circuitry by virtue of the lower resistive losses. However, at least in our hands, other losses in the circuitry are sufficiently large that we have observed no difference. The same is true for bare or tinned copper wire. Our probe Q's typically range from 150 to 300.

Once the inductor has been selected (on the basis of probe geometry and operating frequency) its electrical properties must be measured. A good model of an inductance well into VHF frequencies is shown in Figure C-1. It consists of a pure inductance in parallel with a (large) resistance representative of losses and a small capacitance also in parallel due to inturn capacitance. These parameters are most conveniently measured with a Vector Impedance meter (HP #4815A) but a simple Ham radio noise bridge can be used by those with more modest budgets. It is also necessary to have a very high Q (much larger than

Figure C-1. Electrical model of probe inductor.

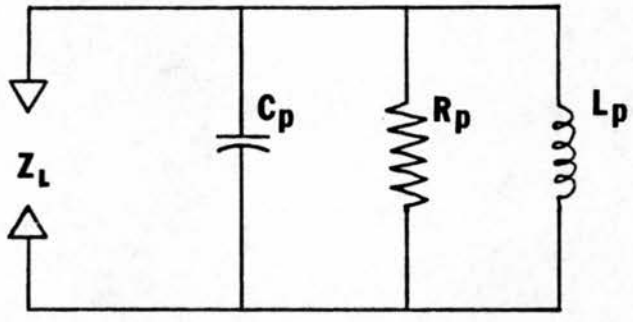

expected coil Q's) capacitor, C_{ext}. The self resonant high impedance of the coil must first be measured (f_o). Then the high impedance resonance of the coil capacitor combination is measured (f_{ext}) along with the resonant impedance at this frequency ($X_{r,ext}$). The model parameters can then be determined using the following relationships:

$$(2\pi f_{ext})^2 = 1/(L(c_{ext}+c_p))$$

$$(2\pi f_o)^2 = 1/(Lc_p)$$

$$r_p = X_{r,ext}$$

Unless the coil is unusually large or has many closely spaced turns the value of c_p will be very small ($\leq$ 2 pfd) and can be neglected, however, it is crucial that f_o, the self resonant frequency of the coil is higher than the frequency to which the coil will be tuned or it will be impossible to tune it with the circuits described in the next section.

C.2. L-Match Circuitry

It is a well known fact in the RF community that maximum power is transferred from a source to a load when the impedances of both are equal to each other and to the characteristic impedance of the transmission line connecting them. This is usually 50 + j0Ω. The probe circuitry functions to efficiently transform the complex impedance of the inductor to the characteristic system impedance. This process is

Figure C-2. L-match circuitry.

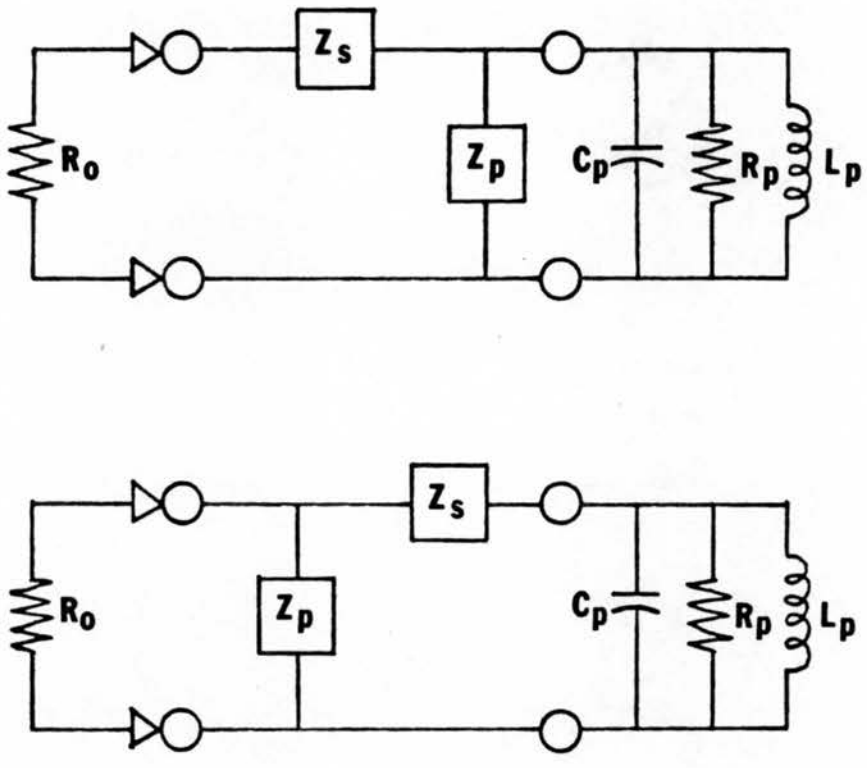

commonly called tuning and matching.

L-matching circuits are a class of simple two element circuits which can transform a complex impedance, such as that presented by an inductor to a pure resistance necessary to couple to the rest of the system. The two forms of these circuits using generalized impedances are shown in Figure C-2. The unspecified impedances can, in principle, be inductors, capacitors or resistors. Resistors are avoided except in special circumstances because anything but a pure reactance will dissipate energy and cause losses. For the same reason capacitors are favored over inductors since they are available with high Q and consequently have lower losses. So choosing both Z_p and Z_s to be capacitors the two circuits are functionally equivalent in that they can tune and match the same range of inductors. In practice the only difference between them is the resultant values of capacitors and in most cases one set will be experimentally more practical.

For concreteness consider the following inductor used for a ^2H probe at 38 MHz (8.5T field): 6 turns of #16 bare copper wire, 10 mm ID x 15 mm long. The electrical characteristics were measured at 38 MHz: $L = 0.23\ \mu H$, $X_L = +56\Omega$, $C_p < 2$ pfd, $R_p = 8900\Omega$ and $Q = 160$. To couple this to a $50 + j0\Omega$ system it is necessary to simultaneously cancel out the inductive reactance of $+56\Omega$ (tuning) and transform the parallel resistance of 8900Ω to 50Ω (matching). It is easy to see that the inductive reactance could be cancelled by placing a 75 pfd capacitor ($X_c = -56\Omega$ @ 38 MHz) in parallel with it, however, there is

no simple way of transforming the pure resistance remaining to 50 + j0Ω without incurring large losses. The L-match circuit in Figure C-2a achieves this function by partially cancelling the X_L with Z_p, transforming the remaining parallel combination to its equivalent series form where the series resistance is found to be 50Ω then cancelling the remaining series reactance with Z_s. This is shown in detail in Figure C-3.

A similar analysis is applicable for Figure C-2b except that it is convenient to use the series representation for the inductor since the first operation is summing with a series capacitor.

C.3. Probe Breakdown

It was seen in the previous section that the 50Ω system impedance was either up-converted to a large resistance (8900Ω) in one circuit or down-converted to a small resistance (0.35Ω) in the other given a probe Q of 160. Since the power delivered to the probe from the final power amplifiers must be dissipated in a resistance the voltage-current relationships can be analyzed easily with an eye towards understanding electrical breakdown of the probe.

The probe previously described converted the 50Ω to 0.35Ω. One Kw_{rms} of RF power is commonly applied to this probe in order to develope 2 μsec π/2 pulse widths. Using Ohm's Law it can be seen that

Figure C-3. Tuning and matching a sample inductor.

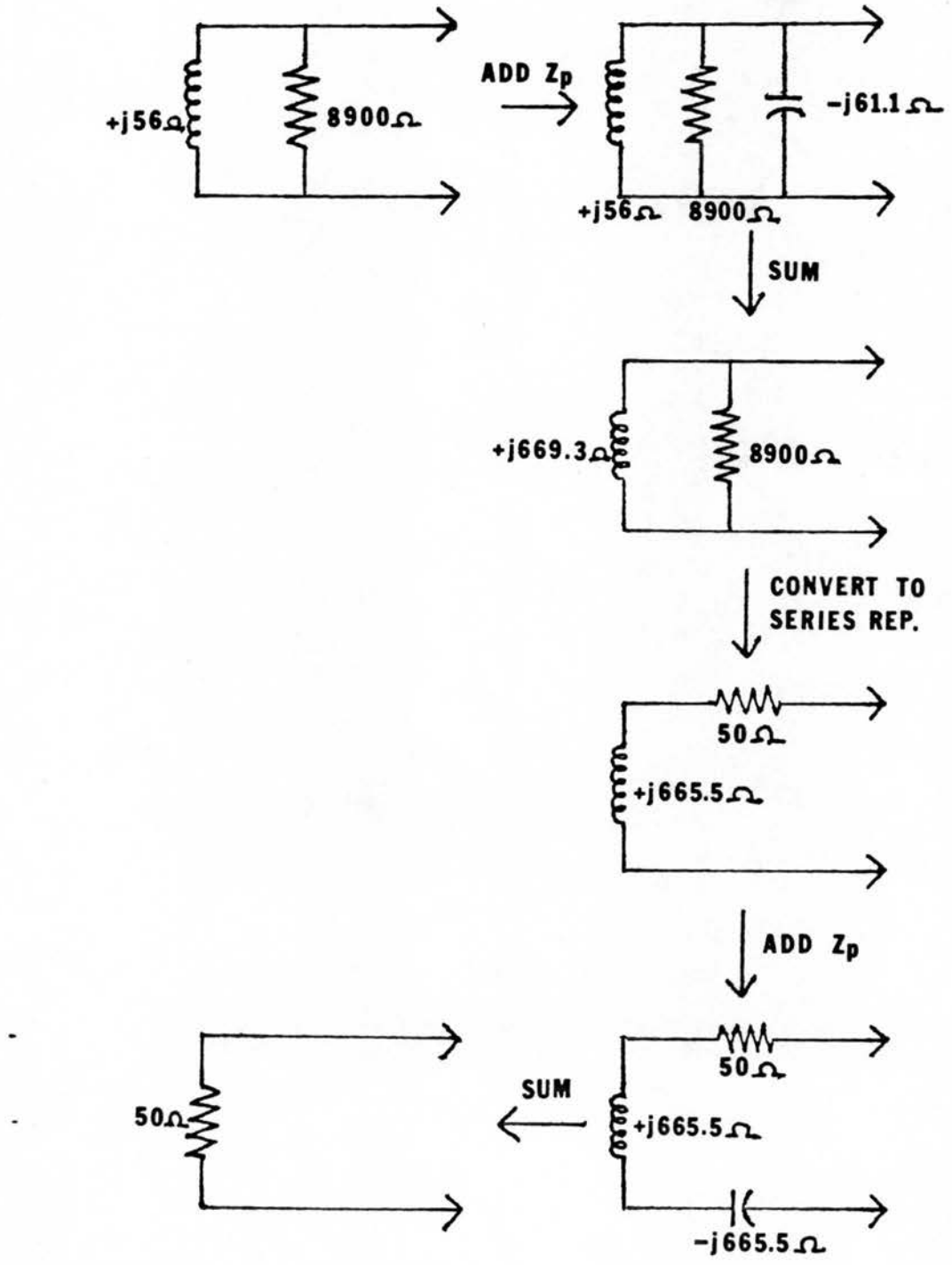

the voltage across the resistance is only 26 V_{peak} but the current flowing through is 75 A_{peak}. The capacitor Z_p is in parallel with this resistance and is an intimate part of the recirculating tank circuit hence the same current is flowing through it. This well exceeds the current carrying capabilities of all non-magnetic capacitors of any reasonable size. For this reason this capacitor must actually consist of several fixed capacitors in parallel with a variable one in order to share the RF current load otherwise the high current density will "punch-through" the dielectric of the capacitor, permanently destroying it.

In the alternate form of the circuit, 50Ω is up-converted to 8900Ω and now the voltage-current relationships are very different. The voltage across the resistance is 4.2 Kv_{peak} and only 0.5 A_{peak} flowing through it. Now the potential for "arcing" by ionization of the surrounding air is great. Since Z_p is much smaller than Z_s in this circuit, it is the latter capacitor which bears the brunt of the voltage. It can be fortified by breaking the required capacitance up into 2-4 approximately equal capacitors in series so that each must only bear a fraction of the total voltage.

In either case it is simple to determine if a probe is breaking down. As always the most definitive test is the spin response. A (liquid) sample is placed in the coil and the probe tuned. The power to the probe is reduced to only a few hundred watts and the π pulse width is determined by nulling the FID. The power is gradually in-

Figure C-4. Synthetic equations for the L-match circuits.

SERIES-PARALLEL EQUIV. CIRCUTS

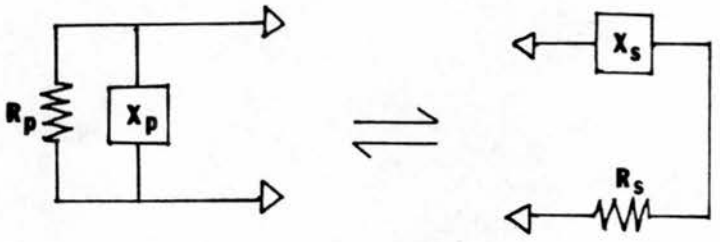

$$Q=R_p/X_p=X_s/R_s$$

$$R_p=R_s(1+Q^2)$$
$$X_p=X_s(1+1/Q^2)$$

$$R_s=R_p/(1+Q^2)$$
$$X_s=X_p/(1+1/Q^2)$$

HIGH-CURRENT L-MATCH

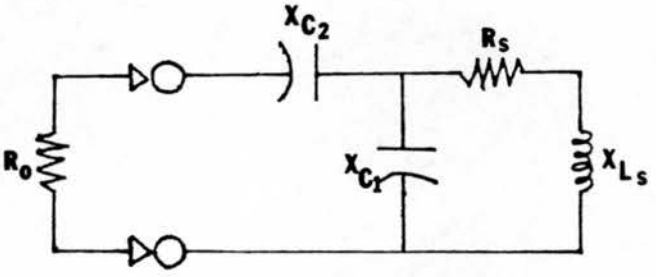

$$X_{C2}=\sqrt{R_oR_s(1+Q_L^2)-1}$$

$$1/X_{C1}=1/X_{Ls}-1/(X_{C2}(1+(R_o/X_{C2})^2))$$

HIGH-VOLTAGE L-MATCH

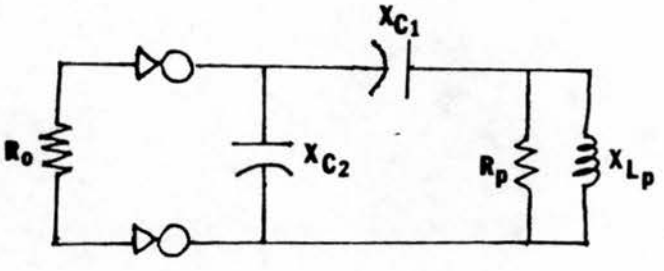

$$X_{C2}=\sqrt{R_oR_p/(R_oQ_L^2-R_p)}$$

$$X_{C1}=X_{Lp}-X_{C2}/(1+(R_o/X_{C2})^2)$$

creased and the π pulse width is seen to get shorter. At some point the pulse width will become catastrophically long and possibly a cracking noise can be heard from the probe. If there is any doubt a directional coupler can be placed in the line between the probe and final power amplifier. The forward/reflected voltage ratio will drop to unity when there is breakdown occurring. At this point some reasonable intuition and careful (!) observation of the open tuned probe should reveal the offending member.

In our laboratory porcelain ceramic fixed capacitors (ATC Ceramic Capacitors, Huntington Station, New York) and copper/silver plated teflon dielectric variable capacitors (Polyflon Capacitors, New Rochell, New York) are used because of their non-magnetic nature, high power capability and high circuit Q.

The final form of the L-match circuits and their synthetic equations are shown in Figure C-4.

The circuit in Figure C-4b has often been called "parallel match-series tune" but it can be seen by a rearrangement of the synthetic equations that the tune/match functions are not so neatly segregated. This is also true for the so-called "series match-parallel tune" circuit of Figure C-4b. We prefer to use the functionally more accurate titles used in the labelling of Figure C-4 namely "high-voltage" and high-current" since this is truly the distinction between the circuits and leads to greater insight into their operation.

C.4. Double Resonance Tuning

The utility of single coil-double tuned probes does not need to be amplified on here. In our laboratory virtual grounds are generated by quarter wavelength transmission lines as in Figure C-5. The object here is to generate two 2-terminal impedances which are equivalent to "good" inductors (as defined in the previous section) at each respective frequency. The high frequency analysis for this circuit is simple. The open $\lambda/4$ line looks like a small inductor and the open line appears as a small capacitor. The equivalent circuit is then two inductors in series with a capacitor in parallel. The effect of the second "virtual" inductor is to lower the efficiency of the LF circuit through the loss of filling factor and to raise the value of inductance that must be tuned and matched. While this may be somewhat inconvenient the presence of the parallel capacitance may, under certain circumstances, be disastrous since the L-Match circuitry can only operate on inductive reactance (in fact, only a limited range of inductors). If the capacitive reactance is smaller than the inductive reactance then the parallel circuit of the two will be dominated by the smaller and the effective impedance presented to the L-Match network will be capacitive. Previously the only alternative would be to decrease the size of the inductor until the total inductive reactance is less than the capacitive reactance. This usually results in a non-

Figure C-5. Virtual grounds generated by coaxial lines for double tuning a probe.

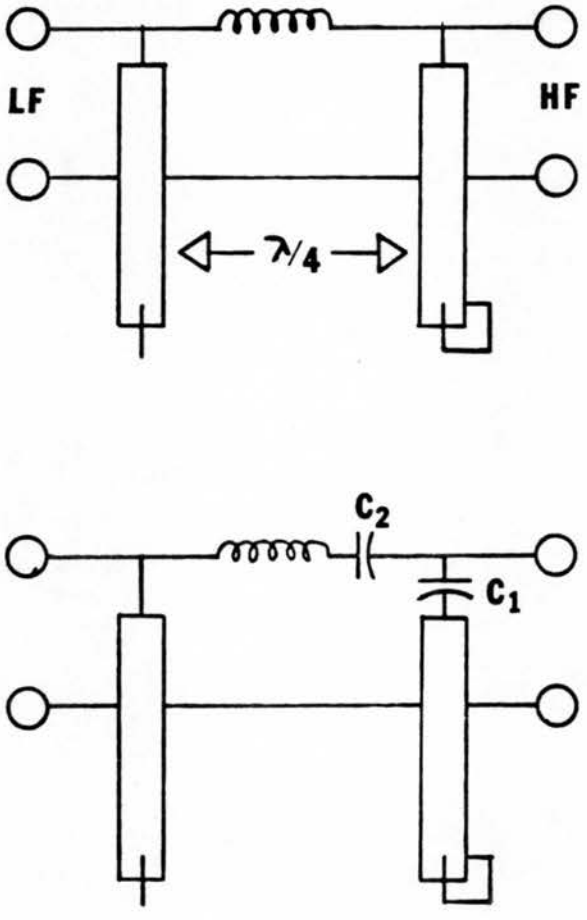

optimal coil geometry or volume. The approach that we've taken is to place a capacitor in series with the closed line (Cl in Figure C-3) with a reactance that is equal to (with opposite sign) the inductive reactance presented by the line at the low frequency. This resonated with the line cancelling out the inductance leaving in its place a small resistance representative of the high Q combination. The effect of this capacitor on the high frequency performance is negligible since it is in series with a high impedance resonant circuit.

This addition makes many more coil sizes available to the experimenter. While it seems that changes in the absolute frequency do not lead to any severe problems some ratios of the high and low frequencies lead to a situation where the low frequency port still appears capacitive. This is true of ^{31}P-^{1}H double tuned probes even when the closed line capacitor is used. Once again a trick is available. A capacitor (C-2 in Figure C-5) is now placed on series with the sample inductor which serves to cancel out some inductive reactance of the sample coil again making the net inductive reactance smaller than the open line capacitive reactance. However, the choice of capacitor is now more critical since it usually does not take much capacitance to resonate with the inductor at the high frequency! It is better to start with a large capacitor first and check to see if the impedance at both ports is inductive at the respective frequencies. Then each side is tuned according to the previous prescription.

APPENDIX D. SPECTROMETER CONSTRUCTION

"NEVER TURN YOUR BACK ON THESE MACHINES OR
THEY'LL BITE YOU IN THE ASS."

RYBACZEWSKI

In this Appendix some practical details for the construction of spectrometers for doing High Resolution NMR in solids are given. As a sort of disclaimer it should be said that the nuclear moments are the final arbiters of any spectrometer design or modification. The would-be NMR spectroscopist would be well advised to enter into this work with an armful of test samples of varying difficulty with well known NMR spectral parameters and to use them liberally because no type of electronic measurement is more sensitive to the quirks of the machines as those little spins. Figure D-1 shows a block diagram of our 3.5 T spectrometer.

D.1. DESIGN FACTORS

As always sensitivity is of paramount importance since the observable signal in an NMR experiment is proportional to the population difference of the two spin states. This population difference is related to the Boltzman distribution and is indeed small at room

Figure D-1. Block diagram of Spectrometer.

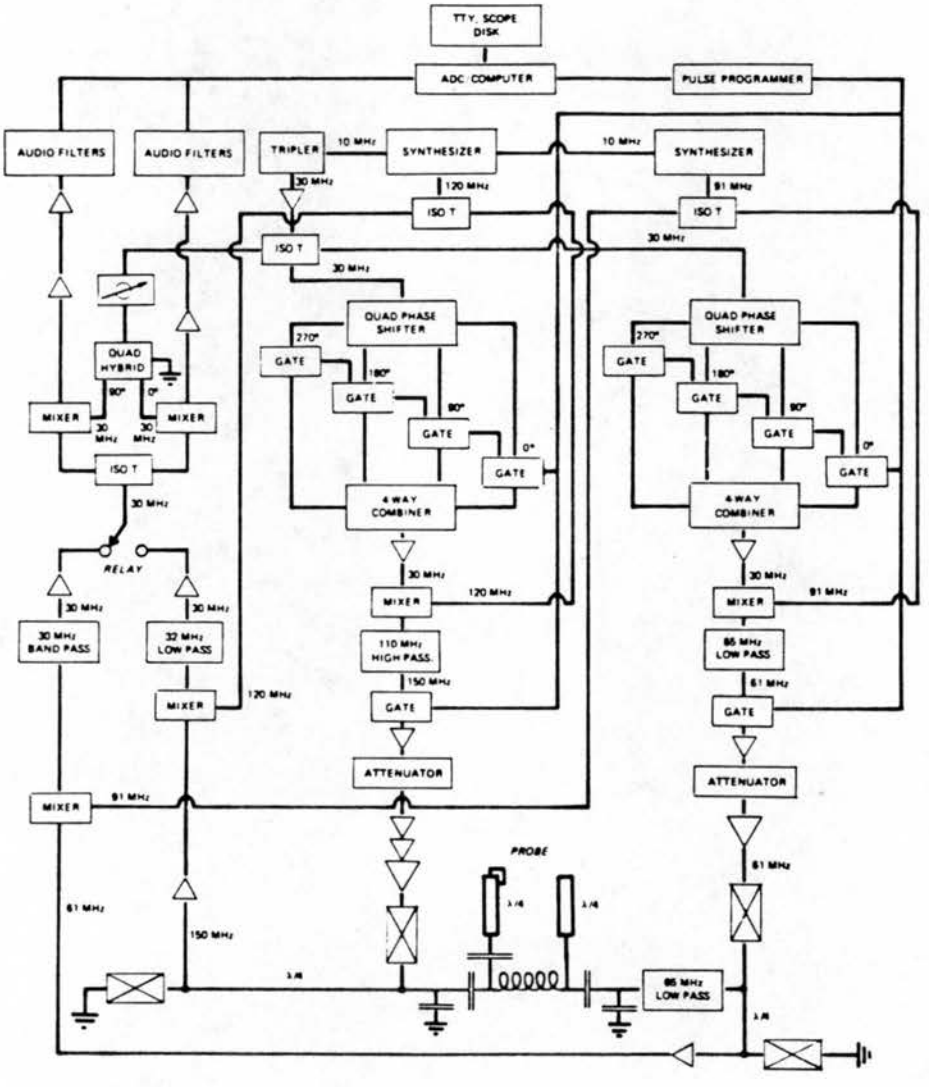

temperatures. This situation is aggravated for biological systems for a number of reasons. Many interesting biomoleculea are difficult to obtain in large quantities necessary and even if they were physiological concentrations can be so low that not much sample could be fit inside a sample coil.

After sample size, sensitivity depends most critically on probe efficiency (Q) and receiver sensitivity. It is important to have a probe Q as high as possible and receiver noise as low as possible while maintaining high gain. Both of these problems are addressed in other sections.

Flexibility in designing and implementing new pulse sequences is dictated primarily by the pulse programmer. Modern spectrometers commonly utilize a particular type known as a timing stimulator. This device consists of a computer type memory which contains the information necessary to define each interval in the experiment in blocks of "words". Each work contains the length of the time interval, usually in increments of the master clocking frequency and which events are to be activated during that interval. The experiment is then performed by moving through the memory and performing each instruction for the time interval that it itself defines. The previously tedious problem of generating new pulse sequences now becomes one of computer programming the timing stimulator.

Broad band operation, while not crucial is important for operational efficiency. In the current spectrometers switching the

observed nucleus is performed by changing the probe, transmit/receive switch, and the setting on a frequency synthesizer.

High power operation is perhaps the most difficult facet of these experiments both in principle and practice. Large amounts of RF energy are needed to decouple protons and also to cover large spectral widths commonly found in deuterium quadrapolar spectra. Several transmitters currently in use in this laboratory have RF outputs which are measured in kilowatts.

D.2. Receivers

Once the nuclear induction has been picked up by the probe it is the responsibility of the receiver to amplify and demodulate it. The receivers for the two spectrometers described here are identical except for the choice of intermediate frequency (30 MHz for 3.5 T and 160 MHz for 5.8 T). The sensitivity is equally good in both, 160 MHz was chosen for improved image rejection at the higher frequencies.

The basic receiver design is superheterodyne with quadrature phase detection of the IF resulting in audio signals sent to the digitizers in the computer. Approximately 10-60 db of audio gain is available. The half power bandwidth is roughly 1 MHz determined by both IF filters and bandwidth limiting of the audio gain stages (Model 51; Analog Devices, Norwood, Massachusetts). Additional audio filtering is available by the use of 6-pole active filters from 0 to 50

KHz. Both Butterworth and Bessel functions are present (Frequency Devices, Haverhill, Massachusetts) however, we tend to prefer the Bessel function. The faster cutoff of the Butterworth filters doesn't seem to be any more advantageous since a sufficiently fast digitization rate prevents the alaising of noise and the transient Bessell response is definitely superior.

The large gain step occurs at the IF (RHG Series ICE; Deer Park, New York) with a range of 30-70 db. It has a noise figure of approximately 4 db. A passive filter is placed in front of the IF amplifier to prevent overloading of the amplifier during the transmitter pulse. No attempt at active gating has been made.

Preceding the IF filter we have the RF preamplifier and converter stages. It can be shown that the first RF preamplifier determines the system noise figure if it has a gain exceeding 20 db. An RHG (Series ICFT) amplifier with 35 db gain and a 2 db noise figure is used here. RF conversion is performed in a standard doubly bananced mixer (SRA-1 Mini Circuits Laboratories, Brooklyn, New York).

One distinctive feature of the 3.5 T receiver is the presence of a broad band terminator (Ham Radio, February, p. 26, 1977) after the mixer. The purpose of this is to present a 50Ω load to the mixer at both the sum and difference frequencies which improves both the mixer's dynamic range and conversion loss. In practice a greater improvement is noted at higher RF frequencies, presumably due to the mixer's increased image sensitivity at the higher sum frequencies.

We commonly characterize the receiver sensitivity by injecting an RF signal from a synthesizer into the input of the RF preamp and measuring how much RF is necessary to give an s/n ratio of 1 at the audio output as measured on a digital RMS reading AC voltmeter. With audio filters set at 50 KHz and a signal offset of 1 KHz the receiver sensitivity measured by this method is -116 dbm.

D.3. TRANSMITTERS

As can be seen in the block diagrams there are essentially two separate high power pulsed transmitters in each spectrometer. RF frequencies are generated by synthesizers (model #5600 Rockland, Nyack, New York) and the IF's are derived from the 10 MHz synthesizer clock. 30 MHz is generated simply by distorting the 10 MHz and filtering off the appropraite harmonic, 90 and 160 MHz are synthesized by phase locked loops synchronized to the same clock. It was necessary to use ECL logic to generate these frequencies reliably. Except in the low side of the 5.8 T console all RF gating and phase shifting is performed at the intermediate frequencies. In the low 5.8 T side this is done directly at the RF frequency. All amplitudes and phases are finely trimable. After the IF is gated it is mixed with the RF ± IF and the appropriate sideband filtered and amplified.

The power amplifiers for the high side of both spectrometers are tuned amplifiers made from commercial ham radio equipment. The

finals in both are tube type devices powered by heavily filtered 3 Kv plate supplies. The final power outputs are 1.6 and 3.0 Kw_{rms} at 150 and 250 MHz, respectively. For a driver at 150 MHz a 150 W 2 meter transistor amplifier (Motorola model MICOR Mobile) is used, however, it has been extensively modified by the addition of biasing networks to each RF transistor to change the operating class from C to B and heavy power supply filtering. This is necessary to linearize the gain (as a function of input power) which allows the use of variable level decoupling. The 250 MHz driver is a commercial unit (Amplifier Research, model #30LM3, Souderton, Pennsylvania) modified by the manufacturer to optimize the performance at 250 MHz.

On both spectrometers the low frequency power amplifier is the same (Amplifier Research, model #200L). This is an extremely rugged broadband (1-200 MHz) 400W (pulsed) linear amplifier which serves all of the nuclei that we are currently interested. Due to the extremely high linear gain these amplifiers have the undesirable characteristic of being noisy. To circumvent this the manufacturer has installed a "blanking" option which lowers the gain (and noise) by removing the screen voltage from the final tubes. The manufacturer has spec'ed this option as 5 μsec to activate and 15 μsec to deactivate, nominal (including transients). While this is perfectly adequate for most experiments there are some, including multiple pulse dipolar averaging experiments which require a shorter time interval. We have developed a simple passive transmitter isolation switch which obviates the need

Figure D-2. Transmitter Switch.

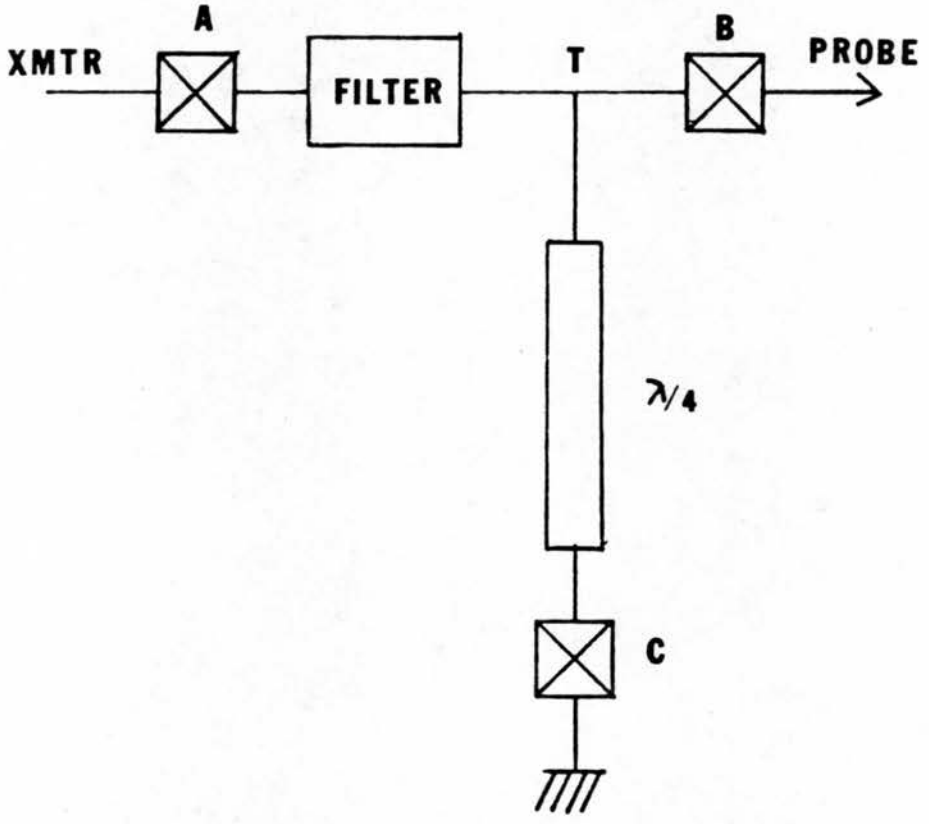

for the blanking. The schematic is shown in Figure D-2. It consists of two sets of series diodes, a Butterworth bandpass filter and a $\lambda/4$ line terminated with a set of diodes to ground. The device must be tuned for each particular frequency and is basically a voltage variable "T" attenuator where the bandpass filter limits the range of RF frequencies from the transmitter under both high and low power conditions, and the $\lambda/4$ line removes residual RF under low but not high power conditions. During the high power RF pulse all three sets of diodes are turned on. Diodes "A" and "B" present a low impedance to the RF which passes through the filter to the probe; since diodes "C" are also turned on the $\lambda/4$ line is shorted to ground and presents a high impedance at point "T" effectively removing the influence of the $\lambda/4$ line. When the amplifier is not driven the diodes are turned off. While the diode sets "A" and "B" are not sufficient to prevent the amplifier noise from getting to the probe, with diodes "C" off the $\lambda/4$ line presents a short to ground at "T" for RF not removed by the filter. Noise suppression with the circuit is greater than 60 db which is fully adequate for limiting noise below detection levels of the normal receiver T/R switch. The insertion loss is about 0.2 db. For maximum efficiency all components, i.e., diodes and filter should be enclosed in separate boxes.

While it is expected that 10 Gauss of ^{1}H irradiation would be adequate for high power proton decoupling we find experimentally that for truly high resolution in ^{13}C MASS as much as 40 Gauss is necessary!

This easily attainable with our current power amplifiers, however, for realization of the sensitivity gain produced by cross-polarization 160 Gauss of ^{13}C irradiation would be necessary for the Hartmann-Hahn match. This problem can be circumvented by the ability to vary the ^{1}H transmitter level from 10 Gauss during the mix pulse to 10-40 Gauss during the acquisition time. This function is generated on our spectrometers by the Two-Level Decoupler. A TTL signal from the pulse programmer selects one of two states of a switch each generating an independently variable voltage controlled from the front panel. The selected voltage is routed to a voltage to current converter which feeds the IF part of a doubly-balanced mixer (SRA-1; Mini-circuits Laboratories, Brooklyn, New York) acting as a current-controlled attenuator. A range of over 30 db in power is available on each of the two channels and the transition time is 5 μsec, maximum.

D.4. Spinners

Magic Angle Sample Spinning (MASS) is one of the last truly powerful black arts praticed on the planet today. A number of designs have been published, most of which can perform or not depending on a surprisingly enormous number of variables. Probably the best advice to one comtemplating construction of this beast is obtain a large quantity of aluminum and Delrin stock, go to the machine shop and vary

every conceivable parameter until optimal performance is obtained and don't try to analyze the errors to deeply. However, once a suitable combination has been found it will be amazing how reliably it will operate.

Two types of spinners have been used on our laboratory namely, Andrew and Veeman. The need for two styles arises from the different optimizations of each mechanism. Probe heads are built with mating hardware that will accommodate either spinning hardware so that the advantages of each may be utilized to the fullest.

Andrew spinners consist of a rotor with a cylindrical sample chamber (10 mm OD) attached to a conical turbine base (19.6 mm Dia max). Our present design is made of Delrin or Kel-F and has a maximum sample capacity of 300 µl. It easily fits into an 11 mm ID RF coil. The stator is made of aluminum, which incidently is not seen to interfere with the RF circuitry, and is mounted in a quick change mounting (Opella *et al.*, 1980a). The fluted rotors spin at 3.5 KHz with 40 PSI of air and have reached 4.5 KHz with higher pressures.

Due to the inability of Andrews spinners to spin liquid samples reliably, Veeman type spinners have been incorporated. The Veeman rotor sports a double bearing design which gives it more stability and bearing air can be adjusted independently for optimization. This also enables the rotors to spin at slow speeds, i.e., 500 Hz. In principle the Veeman spinners should be capable of speeds on the order of 5-6 KHz although we have not as yet been able to realize this. Sensitivity

is inherently greater than the Andrew design because of larger sample volumes and improved RF filling factor.

APPENDIX E. CRYSTAL STRUCTURE OF $MePO_3H_2$

The determination of the crystal structure of $MePO_3H_2$ was undertaken as a check on the technique suggested in Chapter VIII. To do this the coordinates of the phosphorous atoms were needed to calculate a parameter which has been called the "lattice sum". This is the sum of all interatomic distances each raised to the minus sixth power. The sum is taken out to some limit and convergence is usually quick because of the high power. This sum is used in the calculation of the second moment (see Equation VIII-3). The limit used here was 16 Å and the calculation included 160 internuclear distances. Convergence was complete. The crystal data is as follows:

$$CH_3PO_3H_2,\ M_w = 96.01$$

$$\text{cell volume} = 839.50\ \text{Å},\ Z = 8$$

$$D_c = 1.519,\ D_m = 1.486$$

The other parameters are seen in the computer printout.

This structure has the interesting property that atoms, (1) and (2), of the unit cell are related by $\frac{1}{2}x$. This structure is presently being reworked to determine if some systematic error exists. However, it is unlikely that there will be a drastic change in the phosphorous coordinates since there is excellent agreement between the calculated and experimental second moments.

METHYL PHOSPHONIC ACID

RUN ON 15-FEB-81 AT 15:27:25

DIRECT CELL PARAMETERS

A	B	C	ALPHA	BETA	GAMMA
15.329000	5.836000	9.889000	90.000	108.389	90.000
		COSINE	0.00000000	-0.31546801	0.00000000

RECIPROCAL CELL PARAMETERS

A*	B*	C*	ALPHA*	BETA*	GAMMA*
0.068746	0.171350	0.106564	90.000	71.611	90.000
		COSINE	0.00000000	0.31546804	0.00000000

SYMMETRY TRANSFORMATIONS

NO.	TRANSFORMED X	TRANSFORMED Y	TRANSFORMED Z
1	0.000000 1. X 0. Y 0. Z	0.000000 0. X 1. Y 0. Z	0.000000 0. X 0. Y 1. Z
2	0.000000 -1. X 0. Y 0. Z	0.000000 0. X -1. Y 0. Z	0.000000 0. X 0. Y -1. Z
3	0.000000 1. X 0. Y 0. Z	0.500000 0. X -1 Y 0. Z	0.500000 0. X 0. Y 1 Z
4	0.000000 -1. X 0. Y 0. Z	0.500000 0. X 1. Y 0. Z	0.500000 0. X 0. Y -1. Z

NO.	ATOM	X	Y	Z	B11	B22	B33	B12	B13	B23	TYPE
1	P1	0.089408	0.135018	0.892940	0.008713	0.029366	0.018251	-0.000603	0.008188	0.001123	1.
2	O11	-0.006273	0.293458	0.376356	0.009447	0.033722	0.022833	-0.000937	0.009174	-0.029445	1.
3	O12	0.097501	0.445488	0.247655	0.014529	0.059683	0.022761	0.022157	0.023289	0.022481	1.
4	O13	0.880361	0.429951	0.499628	0.007919	0.053419	0.031794	-0.002825	0.010168	-0.040620	1.
5	C11	0.174289	0.142904	0.446647	0.006811	0.042435	0.026531	0.009094	0.013257	0.008727	1.
6	P2	0.589784	0.131791	0.695799	0.008479	0.033820	0.016802	-0.005266	0.009750	-0.004444	1.
7	O23	0.496410	0.286069	0.112829	0.006876	0.041535	0.019359	-0.003541	0.003962	0.022435	1.
8	O21	0.595342	0.062705	0.848628	0.013051	0.059509	0.014303	-0.012755	0.005066	0.018477	1.
9	O22	0.384289	0.081224	0.377620	0.007277	0.052742	0.023206	0.009646	0.008491	-0.013200	1.
10	C21	0.692337	0.168236	0.217373	0.006266	0.056853	0.031163	0.006707	0.010509	0.009466	1.
11		0.000000	0.000000	0.000000	0.040000	0.000000	0.000000	0.000000	0.000000	0.000000	7.
12	CENTER	0.500000	0.500000	0.500000	0.040000	0.000000	0.000000	0.000000	0.000000	0.000000	7.

NO.	ATOM	X	Y	Z	RMSD 1	RMSD 2	RMSD 3
1	P1	0.089408	0.135018	0.892940	0.224708	0.284449	0.305888
2	O11	-0.006273	0.293458	0.376356	0.179899	0.318260	0.357610
3	O12	0.097501	0.445488	0.247655	0.248776	0.274255	0.441782
4	O13	0.880361	0.429951	0.499628	0.233718	0.289301	0.425444
5	C11	0.174289	0.142904	0.446647	0.223965	0.281730	0.352385
6	P2	0.589784	0.131791	0.695799	0.233940	0.261554	0.309469
7	O23	0.496410	0.286069	0.112829	0.214371	0.265280	0.351771
8	O21	0.595342	0.062705	0.848628	0.220501	0.308455	0.415714
9	O22	0.384289	0.081224	0.377620	0.232079	0.303826	0.354761
10	C21	0.692337	0.168236	0.217373	0.244214	0.314366	0.378351
11		0.000000	0.000000	0.000000	0.040000	0.040000	0.040000
12	CENTER	0.500000	0.500000	0.500000	0.040000	0.040000	0.040000

ORTHONORMAL REFERENCE VECTORS BASED ON CRYSTAL AXES

X VECTOR	Y VECTOR	Z VECTOR
0.652353E-01	0.0000000E+00	0.2163725E-01
0.0000000E+00	0.1713500E+00	0.0000000E+00
0.0222479E+00	0.0000000E+00	0.1045640E+00

POST-FACTOR TRANSFORMATION MATRIX

0.1532900E+02	0.0000000E+00	0.0000000E+00
0.0000000E+00	0.5836000E+01	0.0000000E+00
-0.3119663E+01	0.0000000E+00	0.9384027E+01

Figure E-1. ORTEP plot of Methylphosphonic acid unit cell.

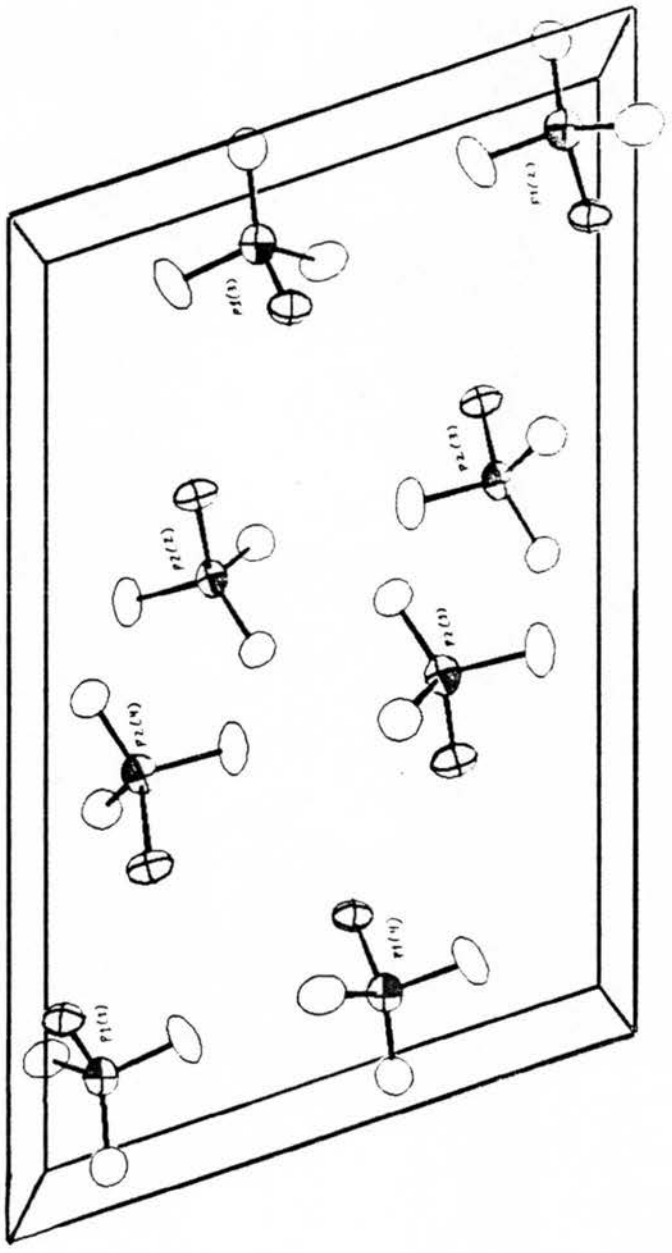

INDEX

AMMONIUM CHLORIDE 115

BROWNIAN DIFFUSION 7

CAPACITOR 152-164

CHEMICAL SHIFT ANISOTROPY 2, 7, 9, 25, 27, 34, 35, 38, 41, 45-48, 58, 65, 69, 74, 79, 83, 85

CORRELATION TIME 4, 41, 44, 50, 65, 74, 83

CORRELATION TIME, ANISOTROPIC 76

CORRELATION TIME, ISOTROPIC 42, 49

DECOUPLING, HETERONUCLEAR 14, 22, 34, 36, 40, 58, 65, 103, 108, 173

DECOUPLING, HOMONUCLEAR 27, 111, 113

DIALYSIS 32, 57, 73, 82, 116

DIFFRACTION 2

DIFFRACTION, NEURTON 80, 128

DIFFRACTION, X-RAY 29, 54, 63, 125, 144

DIFFUSION COEFFICIENT 48, 69

DIPOLAR SPECTRUM 113, 116

ENERGY, ACTIVATION 43, 44

ESCHERICHIA COLI 53, 56, 92, 95, 115

FIBER AXIS 142

FIBER FRAME 148

FIELD STRENGTH 13, 32, 38, 52, 67, 79

HAMILTONIAN, AVERAGE 10, 103, 113
HAMILTONIAN, CHEMICAL SHIFT 23, 27, 101, 110
HAMILTONIAN, DIPOLAR, HETERONUCLEAR 14, 27, 111
HAMILTONIAN, DIPOLAR, HOMONUCLEAR 10, 14, 23, 89, 110
HAMILTONIAN, TOTAL SPIN 3, 90, 110
HAMILTONIAN, QUADRAPOLAR 85
HAMILTONIAN, ZERO ORDER 103, 137
HARTMANN-HAHN MATCH 13
HELIX 30, 49, 54, 98
INDUCTOR 153-164
INTERACTION STRENGTH 80, 83, 90, 113
MAGIC ANGLE 13, 27, 34, 48, 58, 61, 65, 78, 111
MEDIA, GROWTH 56, 110
MOMENT, SECOND 25, 27, 90, 106, 113, 177
MULTIPLE PULSE 110
ORBITALS, ELECTRONIC 7
PEDISTAL 103
PHENOL 115
PROBE RINGING 15, 20
PROBE TUNING AND MATCHING 151-164
PURINE 81, 82
SCALING FACTOR 105, 110, 128
SPECTRAL DENSITY FUNCTION 8, 9, 35, 42

SPIN LOCKING 13

SPIN LOCKING, AT THE MAGIC ANGLE 113

T_1 11, 20, 80

T_{1P} 23, 110

T_2 20, 23, 28, 35, 67, 91, 92

T_{IS} 13

TOGGLING FRAME 105

TRANSMISSION LINE 162

REFERENCES

Abragam, A. (1961) "The Principles of Nuclear Magnetism", Oxford.

Akasaka, K. (1974) Biopolymer 13, 2273.

Akasaka, K., Yamada, A. & Hatano, H. (1977) Bull. Chem. Soc. Japan 50, 2858.

Akutsu, H., Satake, H. & Franklin, R. M. (1980) Biochemistry 19, 5264.

Andrew, E. R. (1956) "Nuclear Magnetic Resonance", Cambridge.

Andrew, E. R. & Berkson, R. (1950) J. Chem. Phys. 18, 159.

Andrew, E. R. & Newing, R. A. (1958) Proc. Phys. Soc. (London) 72, 959.

Andrew, E. R., Bradbury, E. & Eades, R. G. (1958) Nature 182, 1659.

Arnott, S. (1970) Prog. Biophys. & Mol. Biol. 21, 267.

Arnott, S. & Hukins, D. W. L. (1972) Biochem. Biophys. Res. Comm. 47, 1504.

Bachovchin, W. W. & Roberts, J. D. (1978) J. Amer. Chem. Soc. 100, 8041.

Barkley, M. D. & Zimm, B. H. (1979) J. Chem. Phys. 70, 2991.

Barnes, R. G. & Bloom, J. W. (1972) J. Chem. Phys. 57, 3082.

Beck, E., Sommer, R., Averswald, E. A., Kurz. C., Zin, B., Osterburg, G., Schaller, H., Sugimato, K., Sugisaki, H., Okamato, T. & Takanami, M. (1978) Nucleic Acids Res. 5, 4495.

Benyajati, C. & Worcal, A. (1976) Cell 9, 393.

Bloch, F. (1958) Phys. Rev. 111, 841.

Bloomfield, V. A., Crothers, D. M. & Tinaco, I. (1974) "Physical Chemistry of Nuclei Acids", Harper & Row, New York.

Bolton, P. H. & James, T. L. (1979) J. Phys. Chem. 83, 3359.

Bolton, P. H. & James, T. L. (1980a) J. Amer. Chem. Soc. 102, 25.

Bolton, P. H. & James, T. L. (1980b) Biochemistry 19, 1388.

Bovey, F. A. (1972) "High Resolution NMR of Macromolecules", Chapter XV, Academic Press, New York.

Bracewell, R. (1965) "The Fourier Transform and its Applications", McGraw-Hill, New York.

Buchner, P., Maurer, W. & Rutejours, H. (1978) J. Mag. Res. 29, 45.

Calvo, C. (1968) Inorg. Chem. 7, 1345.

Campbell, R. F., Meirovitch, E. & Freed, J. H. (1979) J. Phys. Chem. 83, 525.

Carr, H. Y. & Purcell, E. M. (1954) Phys. Rev. 94, 630.

Coelingh, J. P., Monfoort, C. J., Rozijn, T. H., Leuven, J. A. G., Schiphof, R., Steyn-Pane, E. P., Brounitzer, G., Schrank, B. & Rukfur, A. (1972) Biochem. Biophys. Acta. 282, 1.

Coelingh, J. P., Rozijn, T. H. & Monfoort, C. H. (1969) Biochem. Biophys. Acta. 188, 353.

Cotler, R. I. & Lilley, D. M. J. (1977) FEBS lett. 82, 63.

Crick, F. H. C. & Klug, A. (1975) Nature 255, 530.

Cross, T. A. & Opella, S. J. (1979) J. Supramol. Struct. 11, 139.

Cross, T. A. & Opella, S. J. (1980a) Biochem. Biophys. Res. Comm. 92, 478.

Cross, T. A. & Opella, S. J. (1980b) Biochemistry 20, 290.

Cross, T. A., DiVerdi, J. A., Wise, W. B. & Opella, S. J. (1979) In "NMR and Biochemistry", Dekker, New York.

Davanloo, P., Armitage, I. M. & Crothers, D. M. (1979) Biopolymers 18, 663.

Day, L. A. & Wiseman, R. L. (1978) "The Single Stranded DNA Phages", CSH Laboratory, Cold Spring Harbor, New York.

Day, L. A., Wiseman, R. L. & Marzic, C. J. (1979) Nucleic Acids Res. 7, 1393.

Deeley, C. M. & Richards, R. E. (1954) J. Chem. Soc. 3637.

DiVerdi, J. A. & Opella, S. J. (1981) Biochemistry 20, 280.

Doppler-Bernardi, F. & Felsenfeld, G. (1969) Biopolymers 8, 733.

Dreitlen, J. & Kessemeier, H. (1961) Phys. Rev. 123, 835.

Early, T. A. & Kearns, D. R. (1979) PNAS (USA) 76, 4165.

Edsall, J. T. (1953) Proteins 1 (Part B), 549.

Edzes, H. T., Rupprecht, A. & Berendsen, H. J. C. (1972) Biochem. Biophys. Res. Comm. 46, 790.

Ellett, J. D. & Waugh, J. S. (1969) J. Chem. Phys. 51, 2851.

Evans, W. A. B. & Powles, J. G. (1967) Proc. Phys. Soc. (London) 92, 1046.

Falk, M., Hartman, K. A. & Lord, R. C. (1963) J. Amer. Chem. Soc. 85, 391.

Farrar, T. & Becker, E. (1971) "Pulse and Fourier Transform NMR" Academic Press, New York.

Finch, J. T. & Klug (1976) PNAS (USA) 73, 1897.

Franklin, R. E. & Gosling, R. G. (1953) Acta. Cryct. 6, 673.

Freeman, R. & Morris, G. (1978) Bull. of Mag. Res. 1. 1.

Frey, M. N., Koetzle, T. F., Lehmann, M. S. & Hamilton, W. C. (1973) J. Chem. Phys. 59, 915.

Gall, C. M., DiVerdi, J. A. & Opella, S. J. (1981) J. Amer. Chem. Soc. In the Press.

Genest, D. & Wahl, P. (1978) Biochem. Biophys. Acta. 521, 502.

Gorenstein, D. G. (1975) J. Amer. Chem. Soc. 97, 898.

Gorenstein, D. G. & Kar, D. (1975) Biochem. Biophys. Res. Comm. 65, 1093.

Gorenstein, D. G., Findley, J. B., Monii, R. K., Luxon, B. A. & Kay, D. (1976) Biochem. 15, 3795.

Gorter, C. J. & Broer, L. J. (1942) Physica IX, 591.

Griffin, R. G. (1976) J. Amer. Chem. Soc. 98, 851.

Gutowsky, H. S., Kistiakowsky, G. B., Pake, G. E. & Purcell, E. M. (1949) J. Chem. Phys. 17, 972.

Haeberlen, U. (1976) "High Resolution NMR in Solids", Academic Press, New York.

Haeberlen, U. & Waugh, J. S. (1968) Phys. Rev. 175, 453.

Haeberlen, U. & Waugh, J. S. (1969) Phys. Rev. 185, 420.

Haeberlen, U., Ellett, J. D. & Waugh, J. S. (1971) J. Chem. Phys. 55, 53.

Hanlon, S., Glonek, T. & Chan, A. (1976) Biochemistry 15, 3869.

Hartmann, S. R. & Hahn, E. L. (1962) Phys. Rev. 128, 2042.

Herskovits, T. T., Singer, S. T. & Geiduschek, E. P. (1961) Arch. Biochem. Biophys. 94, 99.

Herzfeld, J. & Berger, A. E. (1980) J. Chem. Phys. 73, 6021.

Herzfeld, J., Griffin, R. G. & Haberkorn, R. A. (1978) Biochemistry 17, 2711.

Hester, R. K., Ackerman, J. L., Neff, B. L. & Waugh, J. S. (1976) Phys. Rev. Lett. 36, 1081.

Hester, R. K., Ackerman, J. L., Cross, V. R. & Waugh, J. S. (1975a) Phys. Rev. Lett. 16, 993.

Hester, R. K., Cross, V. R., Ackerman, J. L. & Waugh, J. S. (1975b) J. Chem. Phys. 63, 3606.

Hogan, M. E. & Jardetzky, O. (1979) PNAS (USA) 76, 6341.

Hull, W. E. & Sykes, B. D. (1975) J. Mol. Biol. 98, 121.

Ikeda, R., McDowell, C. A. & Nakamura, D. (1979) J. Mag. Res. 35, 193.

Jeener, J. & Broekaert, P. (1967) Phys. Rev. 157, 232.

Jelinski, L. W. & Tonchin, D. A. (1980) J. Mol. Biol. 138, 255.

Kallenbach, N. R. & Berman, H. M. (1977) Q. Rev. Biophys. 10, 137.

Kallenback, N. R., Applyby, D. W. & Bradley, C. H. (1978) Nature 272, 134.

Klevon, L., Armitage, I. M. & Crothers, D. J. (1979) Nucleic Acids Res. 6, 1607.

Kornberg, R. D. (1977) Ann. Rev. Biochem. 46, 931.

Langridge, R., Marvin, D., Seeds, W., Wilson, H., Hooper, C., Wilkins,

M. & Hamilton, L. (1960) J. Mol. Biol. 2, 38.

Lee, M. & Goldburg, W. (1965) Phys. Rev. 140A, 1261.

Levy, G. C. & Liether, R. L. (1979) "Nitrogen-15 NMR Spectroscopy", Wiley, New York.

Linder, M., Höhener, A. & Ernst, R. R. (1980) J. Chem. Phys. 73, 4959.

Llinas, M., Wuthrich, K., Schwatzer, W. & von Phillipsborn, W. (1975) Nature 257, 817.

Lutter, L. C. (1978) J. Mol. Biol. 124, 391.

Makowski, L. & Caspar, D. L. D. (1978) "The Single Stranded DNA Phages", pp. 627-644, CSH Laboratory, Cold Spring Harbor, New York.

Mariam, Y. H. & Wilson, W. D. (1979) Biochem. Biophys. Res. Comm. 88, 861.

Marvin, D. A. (1978) "The Single Stranded DNA Phages", pp. 683-704, CSH Laboratory, Cold Spring, New York.

Marvin, D. A. & Hohn, B. (1969) Bacteriol. Rev. 33, 172.

Marvin, D. A. & Wachtel, E. J. (1975) Nature 253, 19.

Marvin, D. A., Wiseman, R. L. & Wachtel, E. J. (1974) J. Mol. Biol. 82, 121.

Marvin, D. A., Pigram, W. J., Wiseman, R. L., Wachtel, E. J. & Marvin, F. J. (1974) J. Mol. Biol. 88, 581.

Marushige, Y. & Marushige, K. (1974) Biochem. Biophys. Acta. 340, 498.

Mehring, M. (1976) "High Resolution NMR Spectroscopy in Solids", Springer-Verlag, Berlin.

Meiboom, S. Gill, D. (1958) Phys. Rev. 29, 688.

Meselson, M. & Stahl, F. W. (1958) PNAS (USA) 44, 671.

Migchelsen, C., Berendsen, H. & Rupprecht, A. (1968) J. Mol. Biol. 37, 235.

Munowitz, M. G., Dobson, C. M., Griffin, R. G. & Harrison, S. C. (1980) J. Mol. Biol. 141, 327.

Munowitz, M. G., Griffin, R. G., Bodenhausen, G. & Huang, T. H. (1981) J. Amer. Chem. Soc. 103, 2529.

McDonald, C. C., Phillips, W. D. & Penman, S. (1964) Science 144, 1234.

McDonald, W. S. & Cruickshank, D. W. S. (1967) Acta. Cryct. 22, 43.

McGhee, J. D. & Felsenfeld, G. (1980) Ann. Rev. Biochem. 49, 1115.

McGhee, Y. H. & von Hippel, P. H. (1975) Biochemistry 14, 1281.

Neidle, S., Berman, H. U. & Shiek, H. S. (1980) Nature 288, 129.

Newman, J., Swinney, H. L. & Day, L. A. (1979) J. Mol. Biol. 593.

Opella, S. J. & DiVerdi, J. A. (1981) "Biochemical Structure Determination by NMR", Marcel Dekker, New York.

Opella, S. J. & Frey, M. H. (1979) J. Amer. Chem. Soc. 101, 5854.

Opella, S. J. & Waugh, J. S. (1977) J. Chem. Phys. 66, 4919.

Opella, S. J., Frey, M. H. & Cross, T. A. (1979) J. Amer. Chem. Soc. 101, 5856.

Opella, S. J., Frey, M. H. & DiVerdi, J. A. (1980a) J. Mag. Res. 37, 165.

Opella, S. J., Wise, W. B. & DiVerdi, J. A. (1981) Biochemistry 20, 284.

Opella, S. J., Yesinowski, J. P. & Waugh, J. S. (1976) PNAS (USA) 73, 3812.

Opella, S. J., Cross, T. A., DiVerdi, J. A. & Sturm, C. F. (1980b) Biophys. J. 32, 531.

Ostroff, E. D. & Waugh, J. S. (1966) Phys. Rev. Lett. 16, 1097.

Pake, G. E. (1948) J. Chem. Phys. 16, 327.

Patel, D. J. (1979a) Biopolymers 18, 553.

Patel, D. J. (1979b) Acc. Chem. Res. 12, 118.

Patel, D. J. & Canuel, L. (1976) PNAS (USA) 73, 674.

Pines, A., Gibby, M. G. & Waugh, J. S. (1973) J. Chem. Phys. 59, 569.

Powles, J. G. & Strange, J. H. (1963) Proc. Phys. Soc. 82, 6.

Rhim, W-K., Elleman, D. D. & Vaughan, R. W. (1973) J. Chem. Phys. 58, 1972.

Rill, R. L., Hillard, P. R., Bailey, J. T. & Levy, G. C. (1980) J. Amer. Chem. Soc. 102, 418.

Robinson, B. H., Lerman, L. S., Beth, A. H., Fusch, H. L., Dalton, L. R. & Auer, C. (1980) J. Mol. Biol. 139, 19.

Rybaczewski, E. F., Neff, B. L., Waugh, J. S. & Sherfinski, J. S. (1977) J. Chem. Phys. 67, 1231.

Sarles, L. R. & Cotts, R. M. (1958) Phys. Rev. 111, 853.

Schaefer, J. & Stejskal, E. O. (1976) J. Amer. Chem. Soc. 98, 1031.

Schaefer, J., Stejskal, E. O. & McKay, B. A. (1979) Biochem. Biophys. Res. Comm. 88, 274.

Sedat, J. & Manuelidies, L. (1978) Cold Spring Harbor Symp. Quart.

Biol. XLII, 331.

Shen, C-K., Ikoku, A. & Hearst, J. E. (1979) J. Mol. Biol. 127, 163.

Shindo, H. (1980) Biopolymers 19, 509.

Shindo, H., McGhee, J. D. & Cohen, J. S. (1980a) Biopolymers 19, 523.

Shindo, H., Wooten, J. B., Pheiffer, B. H. & Zimmerman, S. B. (1980b) Biochemistry 19, 518.

Siminovitch, D. J., Rance, M. & Jeffery, K. R. (1980) FEBS Lett. 112, 79.

Slichter, C. P. (1978) "Principles of Magnetic Resonance", Springer-Verlag, Heidelberg,

Slicther, C. P. & Holton, W. C. (1961) Phys. Rev. 122, 1701.

Smith, M. G. (1966) Methods of Enzymology XIIA, 545.

Smith, I. C. P., Hennings, H. J. & Deslauriers, R. (1975) Acc. Chem. Res. 8, 306.

Sobell, H. M., Tsai, C. C., Gilbert, S. G., Jain, S. C. & Sakare, T. D. (1976) PNAS (USA) 73, 3068.

Spiess, H. W. (1978) "Dynamic NMR Spectroscopy", Springer-Verlag, West Berlin.

Stark, R. E., Haberkorn. R. A. & Griffin, R. G. (1978) J. Chem. Phys. 68, 1996.

Stejskal, E. O. & Schaefer, J. (1975) J. Mag. Res. 18, 560.

Stejskal, E. O., Schaefer, J. & Waugh, J. S. (1977) J. Mag. Res. 28, 105.

Stoll, M. E., Vega, A. J. & Vaughen, R. W. (1976) J. Chem. Phys. 65,

4093.

Suau, P., Bradbury, E. M. & Bradbury, J. P. (1975) Eu. J. Biochem. 97, 593.

Teitelbaum, H. & Englander, S. W. (1975) J. Mol. Biol. 92, 55.

Terao, T., Matsau, S. & Akasaka, K. (1977) J. Amer. Chem. Soc. 99, 6136.

Thomas, G. J. & Murphy, P. (1975) Science 188, 1205.

Toma, F. & Koller, T. (1977) Cell 12, 101.

Urbina, J. & Waugh, J. S. (1974) PNAS (USA) 71, 5062.

Van Vleck, J. H. (1948) Phys. Rev. 74, 1168.

Voet, D. & Rich, A. (1970) Prog. Nuc. Acids. Res. 10, 183.

Wahl, P., Paoletti, J. & LePecq, J.-B. (1970) PNAS (USA) 65, 417.

Watson, J. D. & Crick, F. H. C. (1953) Nature 171, 737.

Waugh, J. S. (1976) PNAS (USA) 73, 1394.

Waugh, J. S. & Huber, L. M. (1967) J. Chem Phys. 47, 1862.

Waugh, J. S., Humphrey, F. B. & Yost, D. M. (1953) J. Phys. Chem. 557, 486.

Waugh, J. S., Huber, L. M. & Haeberlen, U. (1968) Phys. Rev. Lett. 20, 180.

Waugh, J. S., Maricq, M. M. & Cantor, J. (1978) J. Mag. Res. 29, 183.

Yamada, A., Kaneko, H., Akasaka, K. & Hatano, K. (1978) FEBS Lett. 93, 16.

Yamane, T. (1971) Proc. Nuc. Acids. Res. Vol. 2. p. 262, Harper & Row, New York.

Zimmerman, S. B. & Pheiffer, B. H. (1979) PNAS (USA) 76, 2703.